ADVANCING THE STRUCTURAL CHARACTERIZATION OF GP28 AND TRPV1 VSLD MEMBRANE PROTEINS USING ELECTRON PARAMAGNETIC RESONANCE SPECTROSCOPY AND POLYMER NANODISCS

Nancy Chepchumba Rotich

A DISSERTATION

Presented to the Faculty of Miami University in partial
fulfillment of the requirements
for the degree of

Doctor of Philosophy

Department of Chemistry and Biochemistry

The Graduate School
Miami University
Oxford, Ohio

2025

Dr. Gary A Lorigan, Director
Dr. Andrea Kravats, Reader
Dr. Carole Dabney-Smith, Reader
Dr. Kevin Yehl, Reader
Dr. Karthik Vishwanath, Graduate School Representative

Abstract

Membrane proteins are essential for numerous cellular processes yet their structural and dynamic characterization outside the lipid bilayer remains notoriously difficult. These proteins are often challenging to solubilize, inherently unstable, and require environments that closely mimic the native membrane to preserve functional integrity. This dissertation addresses these challenges by integrating site-directed spin labeling (SDSL) and electron paramagnetic resonance (EPR) spectroscopy as well as polymer-based nanodisc systems. This combined approach enabled detailed investigation of the gp28 and TRPV1 Voltage-Sensor-Like Domain (VSLD) and provided new strategies for stabilizing membrane proteins and peptides under native-like conditions.

In the first part of this work, continuous wave and pulsed electron paramagnetic resonance spectroscopic techniques were used to perform different studies on spin-labeled sites. These experiments revealed significant differences in solvent accessibility and conformational flexibility between extracellular loops and transmembrane domains. The findings supported models indicating that the gp28 and TRPV1 VSLD exhibit substantial dynamic behavior with distinct conformational changes. This provided direct experimental evidence for structural information that had previously been inferred largely from computational predictions.

The second part of the study focused on the development and application of polymer-based nanodiscs as alternatives to detergents and liposomes. Both styrene maleic acid (SMA) and a novel class of vinyl ether maleic acid (VEMA) polymers synthesized via RAFT polymerization were investigated. The results demonstrated that polymer charge, molecular weight, and hydrophilic–lipophilic balance play critical roles in nanodisc formation, size, and biomolecular compatibility. These nanodiscs effectively solubilized KCNE1 and membrane-active peptides such as gp28. EPR spectra obtained in polymer nanodiscs closely mirrored those recorded in lipid vesicles confirming that these systems maintain physiologically relevant protein behavior. Collectively, the findings demonstrate the potential of polymer nanodiscs and EPR spectroscopy for advancing membrane protein structural biology. Polymer nanodiscs provide stable, tunable, and scalable membrane mimetic systems while EPR spectroscopy offers site-specific insights into protein structure and dynamics. Together, these approaches expand the toolkit for investigating proteins and peptides that have traditionally been inaccessible with conventional methods. Beyond advancing understanding of gp28 and TRPV1 VSLD, this work establishes a foundation for extending similar methodologies to other ion channels, transporters, and antimicrobial peptides. By combining innovative polymer materials with advanced spectroscopic techniques, the study contributes to the fundamental biochemistry of membrane proteins and supports the development of enabling technologies with applications in drug discovery and biotechnology.

TABLE OF CONTENTS

LIST OF TABLES

LIST OF FIGURES

DEDICATION

To my family and friends: For your unwavering love, patience, and faith in me.

To my parents: Thank you for instilling in me the values of discipline, curiosity, and resilience.

To my mentors and teachers: Your guidance shaped my journey more than you may ever know.

And to every failed experiment and unexpected breakthrough: This work is a testament to persistence and purpose.

ACKNOWLEDGEMENTS

First and foremost, I want to sincerely thank my advisor, Dr. Gary A Lorigan, for allowing me to be a part of his research group and for his constant support and guidance during my research journey. Thanks to his mentorship, I advanced my understanding of chemistry and gained research skills and cultivated vital skills in communication, presentation, collaboration, writing and time management.

To my committee members, Dr. Dabney-Smith, Dr. Kravats, Dr. Yehl and Dr. Vishwanath, thank you for your time, constructive feedback, and the critical perspectives that helped refine this work. I would also like to thank Dr. Rob McCarrick for the time he spent and the patience he exhibited while training and helping me with EPR instrumentation.

To my lab mates and colleagues, Evelyn, Zeeshan, Binaya, Dr. Morris, Dr. Khan, Dr. Stowe, Dr. Bates and all the amazing undergraduate researchers that I worked with; Emily, Julia, Chay and Ben, thank you for the camaraderie, brainstorming sessions, and support through both triumphs and setbacks.

To my Oxford family, especially the Kuranga's; the Friday dinner team and especially Dr. Nafula and Dr. Ngoma who shared similar graduate school challenges, thank you for the laughter, the listening ears, and the adventures that kept me going. You held me up in moments when I felt I could no longer push forward.

To my dear friends and family, my mum and dad who inspired me to pursue further studies after my undergraduate education, thank you for your prayers, unconditional love, and for always reminding me of what truly matters. Finally, I thank God for the strength to persevere. This work is not just the product of one mind but of a community. I carry each of you with me on these pages.

"What lies behind us and what lies before us are tiny matters compared to what lies within us." Ralph Waldo Emerson

Chapter 1

Advancing the Structural Characterization of Membrane Proteins using Polymer Nanodiscs and Electron Paramagnetic Resonance Spectroscopy: Insights from gp28 and TRPV1 VSLD

1.0. Introduction

1.1. Membrane Proteins

Membrane proteins (MPs) are integral or peripheral proteins that are associated with cellular membranes. These two classes of membrane proteins are involved in many cellular functions such as signaling, transport and energy production, emphasizing the significance of these proteins in the cell. Integral proteins are embedded within the membrane's lipid bilayer.[1] [2] The striking characteristic of these proteins is their ability to span the entire membrane permitting interactions with the extracellular as well as intracellular regions.[3,4] This feature allows them to perform a range of roles, such as ion transport, signal transduction, and cell adhesion. The hydrophobic portions of MPs make integral proteins rigidly attach to lipids hence playing a crucial role in maintaining the structural integrity and function of cellular membranes.[5,6]

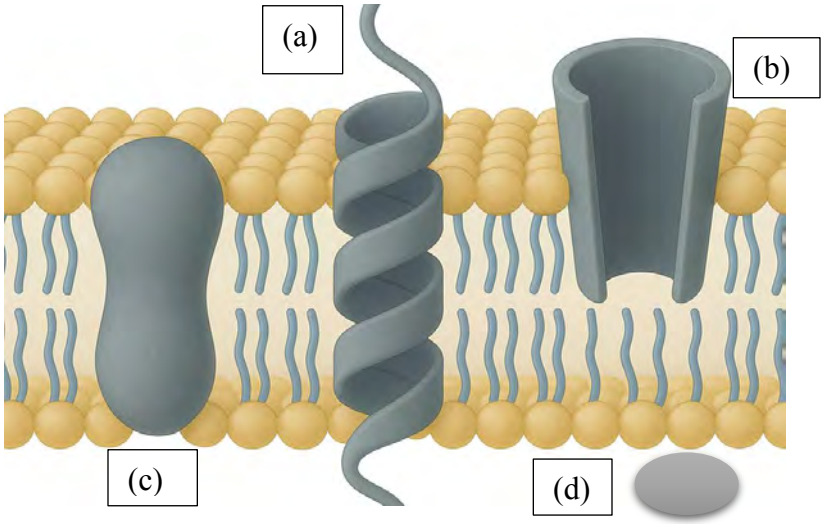

Figure 1. 1: Illustration *of the categorization of membrane proteins based on their interaction with the membrane. (a), (b) and (c) are examples of integral proteins and (d) of a peripheral membrane protein.*

Peripheral proteins are only weakly bound to the lipid bilayer surface and do not penetrate the bilayer as shown in **Figure 1.1**. They are usually associated or connected with integral proteins or the polar heads of the lipids. They may be extracted from the membrane by varying the pH or ionic strength of the membrane.[7] Peripheral proteins are primarily involved in maintaining the cell shape and in signal transduction and they also serve as enzymes or as an anchor for the cytoskeleton.[8] This structural integrity is essential for maintaining cell shape, promoting cellular adhesion, and enabling cell communication. They interact with other proteins, influencing cellular processes and forming complex signaling networks.

The functional importance and biological diversity of membrane proteins (MPs) drive their significance in pharmacology.[9]

Membrane proteins facilitate the movement of ions, small molecules, and larger macromolecules across the lipid bilayer as shown in **Figure 1.2**. This is achieved through various mechanisms, such as passive diffusion, facilitated diffusion, and active transport.[10,11] Specific channel and carrier proteins are essential for maintaining the cell's homeostasis and regulating the concentration of substances within and outside the cell. Ion channels are integral membrane proteins that facilitate the passage of ions across cellular membranes playing crucial roles in various physiological processes.[12,13] Receptor are a type of membrane proteins that bind with specific ligands such as hormones or neuro transmitters causing an activation of intracellular responses.[14] This interaction affects cellular communication and is also involved in immune response, cell proliferation and apoptosis. This helps with their key roles in regulation of an array of cellular activities under normal conditions and in response to various environmental factors.[15]

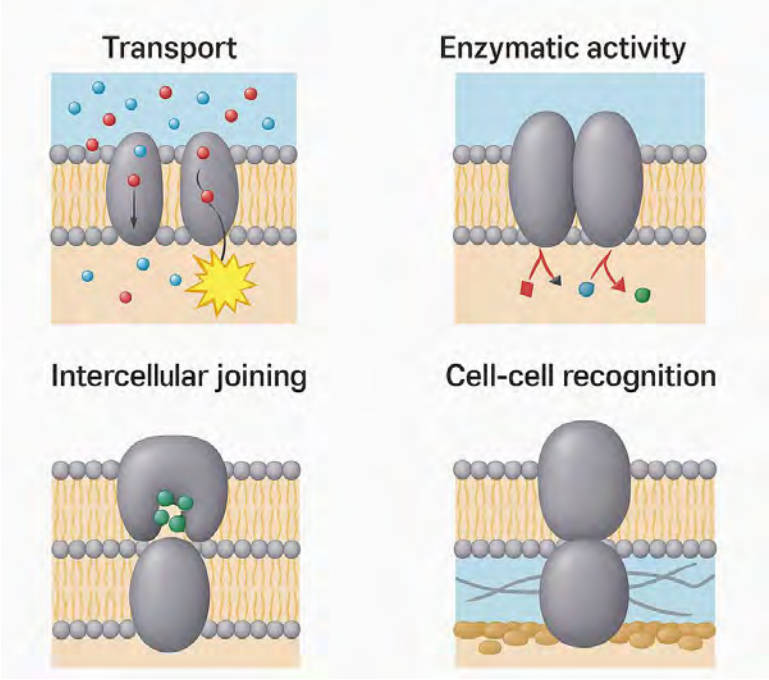

Figure 1. 2: Different functional characteristics of Membrane Proteins (MPs).

Approximately 60% of drug therapies have been developed to specifically target membrane proteins, owing to their critical role in various physiological pathways. [6,16] This targeted approach not only enhances the efficacy of the therapies but also minimizes potential side effects by focusing on the underlying mechanisms of various diseases at the molecular level. The ongoing research and understanding of

membrane proteins continue to pave the way for innovative drug design to improve treatment outcomes across various medical conditions, inspiring researchers to explore the potential of their work in real-world applications.

1.2. Ion Channels

Ion channels are integral membrane proteins that mediate the transport of ions across cell membranes and are involved in various physiological functions. These channels are usually ion selective, allowing particular types of ions such as sodium (Na^+), potassium (K^+), calcium (Ca^{2+}) and chloride (Cl^-) to pass through the membrane of the cell, thereby controlling homeostasis of the cell and the generation of electrical signals and the contraction of muscles and release of neurotransmitters.[12,17]

Ion channels can be classified based on their gating mechanisms. Voltage-gated ion channels open or close in response to changes in membrane potential, while ligand-gated ion channels open in response to the binding of specific molecules, such as neurotransmitters.[18] Other ion channels include mechanically gated channels, which respond to physical deformation of the membrane, and thermally gated channels, which are influenced by temperature changes.[19]

Dysfunction in ion channels can lead to various pathological conditions that significantly impact overall health and well-being, highlighting their importance in maintaining physiological balance and function within the body. When ion channels become dysfunctional, either due to genetic mutations, environmental factors, or other influences, the consequences can be severe and varied resulting in conditions such as cardiac arrhythmias, neurological disorders, and muscular dystrophies. The complex interplay between ion channel activity and physiological health highlights the importance of studying these proteins and the potential for targeted therapies designed to address channel dysfunction and aimed at preventing or treating associated health problems.[20,21]

1.2.1. Transient Receptor Potential Vanilloid 1 (TRPV1)

TRPV1 is a receptor part of the transient receptor potential (TRP) channel family. It is primarily expressed in sensory neurons and is involved in detecting temperature and pain.[22,23] TRPV1 is activated by various stimuli such as capsaicin (the principal pungent ingredient of chili peppers), heat (temperatures above 43°C) and protons ($pH < 6$). Activation of this pathway leads to a large influx of cations including calcium ions. This raised level of intracellular calcium ions is important in many cellular functions.[24,25] Calcium

ions are key mediators in transmitting pain signals within the nervous system. When these cations enter the cells, they can influence the excitability of neurons, leading to heightened sensitivity to stimuli and amplification of pain perception.[26] TRPV1 is also involved in thermoregulation as well as the pathophysiology of various pain-related conditions and diseases.[27]

The structural dynamics of TRPV1 play a critical role in our ability to develop effective modulators aimed at alleviating chronic pain conditions. This understanding is essential not only for identifying how TRPV1 functions at a molecular level, but also for discovering ways to interact with the receptor in a manner that mitigates pain without leading to adverse side effects. By thoroughly investigating the intricate behaviors and conformational changes of TRPV1, researchers can design more targeted therapeutic agents that specifically engage with the receptor's active sites.[28,29] The development of such modulators could revolutionize pain management strategies thus enhancing the quality of life for individuals who currently rely on less effective pain relief options.

1.3. gp28 and pinholin

The emergence of antibiotic-resistant bacteria, commonly called "superbugs," has escalated into a significant public health crisis, necessitating an exploration of alternative therapeutic strategies.[30,31] Bacteriophages have gained huge attention for their efficacy against multidrug-resistant infections.[31] For gram-negative bacteria, three groups of proteins are responsible for cell lysis which are the holins, spanins and endolysins.[32] Holins play a crucial role in the lysis process by forming pores in the bacterial cytoplasmic membrane. This disruption in the membrane potential allows for the accumulation of other lytic proteins. Endolysins are enzymes that cleave the peptidoglycan, weakening the bacterial cell wall and leading to cell death. Spanins are phage lysis proteins that function by disrupting the outer membrane of gram-negative bacteria, facilitating the release of progeny phage from the host cell.[33] They are located at the interface between the inner and outer membranes and play a crucial role in the final stages of the lytic cycle. Together, these proteins coordinate a highly efficient and regulated mechanism for bacterial lysis, which is particularly important for bacteriophages during the infection cycle.[34] Their interactions highlight a sophisticated level of control in microbial ecology and virulence, making them key targets for novel antibacterial strategies.

The bacteriophage-encoded proteins gp28 and pinholin S21 are critical lytic proteins involved in the phage-induced lysis of bacterial cells.[33,35] These proteins enable the release of newly formed phage

progeny by forming pores in the bacterial cell membrane, disrupting the cell's structural integrity.[36] This disruption leads to cell lysis, an essential process for the propagation of bacteriophages. gp28, pinholin and other lytic proteins' activity is an elaborate mechanism used by bacteriophages to guarantee the release of progeny viruses. Pinholins create small lesions in the cytoplasmic membrane. These pores are responsible for activating endolysins before loss of membrane integrity during initial stages of the infection. Pinholin-induced pore formation temporally regulates the subsequent host peptidoglycan degradation and outer membrane permeabilization steps required for lysis in a highly coordinated fashion.[37,38] Thus, pinholin channel formation and its interaction with other lytic proteins are coordinated in bringing about bacterial cell wall lysis. Subsequent biochemical studies have revealed how small hydrophobic peptides such as pinholins are inserted into membranes to create channels that are tight enough to energize the activation of muralytic enzymes without leading to a catastrophic collapse of the proton motive force (pmf).[32]

gp28 is a cationic antimicrobial peptide encoded by the phiKT phage that contributes to the outer membrane permeabilization in the host cell lysis. Its mode of action is like that of antimicrobial proteins (AMPs) which bind to and disrupt bacterial membranes to aid the release of phage progeny.[33,39] gp28's mode of action is much more divergent as it destabilizes the outer membrane (OM) directly through electrostatic interactions with lipopolysaccharides (LPS), which is essential for its use in progeny virion release. This functional difference highlights the distinct evolutionary adaptation of gp28 as a sole OM disrupter in phages that lack spanin complexes. gp28 is in a novel class of phage lysis proteins, named disruptins, which are unrelated to holins, endolysins, or spanins.[35,40] Comparative studies demonstrate that while lysis timing is coordinated by the triggering of active/inactive pinholin pairs, gp28 promotes specificity for OM disruption independently.[36] Functional studies show that gp28 has broad-spectrum antibacterial activity similar to human AMPs such as LL-37. In addition, it prevents the planktonic growth and dissolves biofilms from multi-drug-resistant *P. aeruginosa* strains and contributes to antibiotic sensitivity upon combinational treatment with agents like tobramycin. These results imply the translational potential of gp28-derived peptides for the treatment of antibiotic-resistant infections by exploiting their membrane penetration abilities.[40]

Both gp28 and pinholin illustrate key but mechanistically unique approaches phages use for efficient lysis of bacterial cells and provide attractive models for future development of antimicrobials.[31,41] This

mechanism has significant implications in microbiology and phage therapy, highlighting the potential applications of these lytic proteins in targeting bacterial infections.

1.4. Solid Phase Peptide Synthesis (SPPS)

A solid support resin is functionalized to attach the first amino acid, using a linker that allows for cleavage after synthesis.[42] The next amino acid is activated with a coupling reagent and added to the resin-bound amino acid, forming a peptide bond that links it to the growing peptide chain as shown in **Figure 1.3**.[43] The protecting group on the amino acid's functional group, usually the N-terminus, is removed to expose the amine for the next coupling reaction. Protecting and deprotecting steps are repeated, adding one amino acid at a time until the desired peptide sequence is assembled. After peptide synthesis is complete, the peptide is cleaved from the resin, often using a strong acid that also removes any remaining protecting groups.[44,45] The crude peptide is purified by high-performance liquid chromatography (HPLC) to separate the desired product from side products and impurities. Final characterization of the peptide is done using techniques such as mass spectrometry to confirm its identity and purity.[37,46]

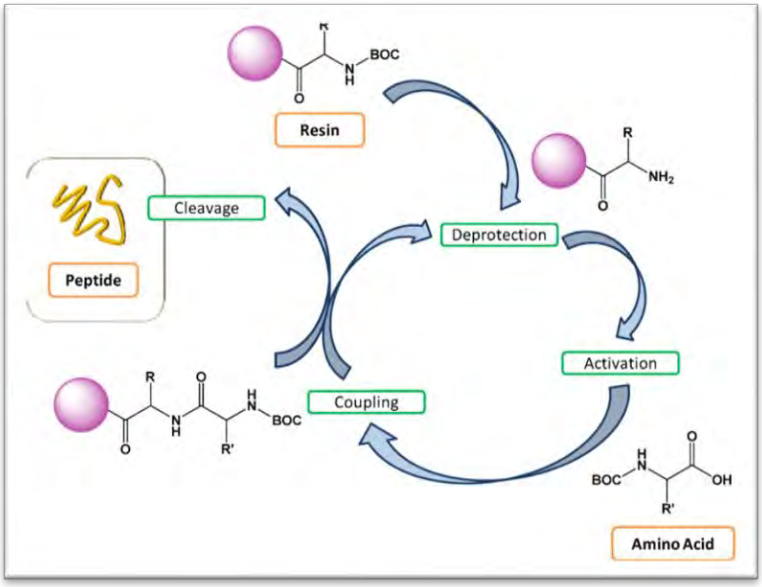

Figure 1. 3: Schematic representation of solid-phase peptide synthesis (SPPS).[43]

1.5. Membrane Proteins: Problems and Solutions

The elucidation of membrane protein structure and function enhances the development of novel therapeutic strategies for various diseases, including cancer, neurological disorders, and cardiovascular conditions.[47] But the amphipathic nature of membrane proteins presents significant challenges for their extraction and purification from biological membranes. The hydrophobic regions of these proteins can aggregate in an aqueous environment and thus makes it difficult to solubilize them in a functional form when removed from the protective lipid bilayer shield.[48,49] The inherent dynamics or conformational flexibility of membrane proteins makes it difficult to study their structures in techniques such as X-ray crystallography and NMR spectroscopy.[50] X-ray crystallography demands well-ordered crystals which are challenging to generate from MPs given their association with lipid bilayers and their tendency to aggregate or denature in the absence of a membrane environment. Nuclear magnetic resonance (NMR) spectroscopy, while powerful in studying the structure and dynamics of proteins in solution, encounters limitations with MPs because of their size, dynamics, and the low solubility of these proteins when extracted from membranes.[46] Electron Paramagnetic Resonance (EPR) spectroscopy has emerged as a powerful tool for studying the structural dynamics of membrane proteins in their native environment, overcoming some limitations of traditional methods like X-ray crystallography and NMR spectroscopy.[51]

1.6. Electron Paramagnetic Resonance

Electron Paramagnetic Resonance (EPR, also known as Electron Spin Resonance (ESR)) is a spectroscopic technique to study systems with one or more unpaired electrons.[52] Among these paramagnetic species are free radicals, organic and inorganic transition metal complexes, and spin-labeled biomolecules. EPR spectroscopy is a crucial tool for studies in chemistry, structural biology, materials science, and biophysics, since it provides information on electronic structure, the molecular dynamics, local environment and spatial distances on the atomic scale.[53]

EPR spectroscopy utilizes the magnetic characteristics of electron spins within a magnetic field. A sample is exposed to a powerful magnetic field leading to spatial separation of the energy levels of unpaired electrons depending on their spins. With the microwave power on, these electrons can shift between different quantum levels. The resultant absorption of microwave power at discrete fields contains specific information about the electronic environment of the unpaired electrons.[53] EPR spectroscopy is rooted in the magnetic properties of unpaired electrons and the steady application of an external magnetic field. At

its most basic level, an EPR system consists of a single unpaired electron spin in a molecular orbital. An electron's spin quantum number, S= 1/2, can only be in one of two magnetic quantum states, M_s= +1/2, or -1/2. These two states degenerate in the absence of a static magnetic field. But, in the presence of a magnetic field, these two states are differentiated as a function of the strength of the magnetic field. The energy difference between the two states, ΔE, may be measured using the equation $\Delta E = g_e\beta_e B_o$ where g_e is the electronic g-factor, β_e is the Bohr magnetron of the electron (joules*Gauss^{-1}) and Bo is the intensity of the static applied magnetic field (Gauss). When resonance occurs, the energy gap (ΔE) is equal to the microwave radiation energy (ΔE). At resonance, the electron transition from ground state to excited state in an external magnetic field can absorb or emit a photon having energy that is quantified as follows: ΔE = hν; whereby h is Planck's constant, and *v* is the photon frequency.[54]

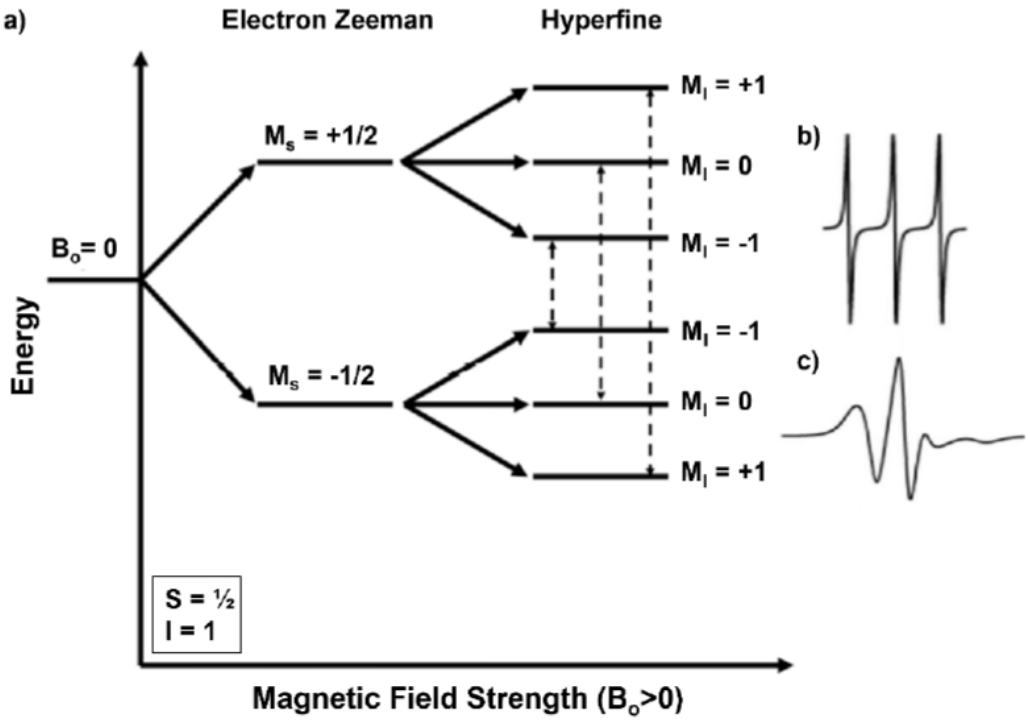

Figure 1. 4: a) Energy diagram of the MTSL spin label with hyperfine interaction with the nitroxide spin label. b) Free spin label spectra. c) Spin labeled incorporated protein spectra.[55]

The nitroxide spin label contains one unpaired electron that is split into two energy levels ($M_s = \pm ½$) in the presence of an external magnetic field by the electron Zeeman effect.[53,55] The energy levels are in addition further divided to several lines by hyperfine interactions with neighboring ^{14}N nucleus following the multiplicity rule 2nI+1, where 'n' is the number of magnetically equivalent nuclei and 'I' is the nuclear

spin. For MTSL, n=1 and I=1 (^{14}N), there are six energy states due to the combined Zeeman and hyperfine interactions. This (in a coordinate system where the magnetic field is zero) permits three possible transitions from the EPR transition rules ($\Delta M_s = \pm 1$ and $\Delta M_I = 0$). A typical three-line EPR spectrum is obtained for a nitroxide spin label, where the lines have a peak at the resonance position and are split by the hyperfine. These three peaks are the low-field-mid-point, mid-point, and high-field peaks at $M_I = +1$, $M_I = 0$, and $M_I = -1$ as shown in **Figure 1.4**.[53]

1.6.1 Site-Directed Spin Labelling (SDSL)

Biomolecules such as membrane proteins are EPR-silent or diamagnetic in nature. Therefore, they have no unpaired electrons in their ground state and only a weak interaction with magnetic fields necessary for EPR detection.[56] The EPR method depends on unpaired electrons for a measurable signal, and this is a major obstacle to studying biologically relevant molecules.[57]

Site-Directed Spin Labeling (SDSL) alleviates this limitation by covalently binding a stable paramagnetic spin label (usually a nitroxide radical) to a specific site, which may involve genetic engineering, for instance incorporating a cysteine residue into the region of interest.[58,59] In order to use these spin labels, site directed mutagenesis must be used to remove native cysteines and place cysteines in sites of interest. This is a relatively mild method and takes into account that mutations made do not disrupt the structure of the protein, or the function if it is crucial to the study. The spin label serves as a local probe of the protein. Its EPR spectrum then provides information about the protein's structure, flexibility and dynamics.[60]

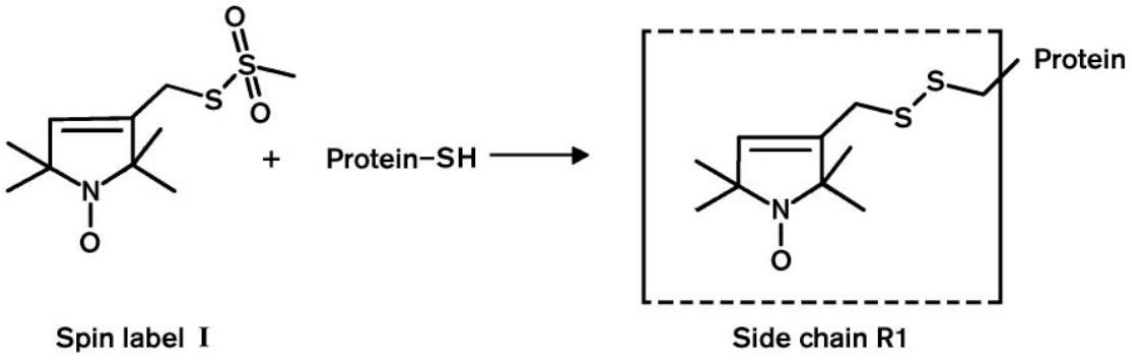

Figure 1. 5: Reaction of the methanethiosulfonate spin label I with cysteine to generate the disulfide-linked nitroxide side chain R1.[60]

There are a variety of spin labels available for use, the most common being nitroxide spin labels such as the ones used in this work, S-(1-oxyl-2,2,5,5-tetramethyl-2,5-dihydro-1H-pyrrol-3-yl)methyl methanesulfonothioate (MTSL) which bind specifically with cysteine through a disulfide bond for MTSL (shown in **Figure 1.5**). The main benefit of SDSL-EPR is its sensitivity to the dynamics and flexibility of proteins in solution or a membrane, providing insight into conformational changes and protein dynamics.[56] Such transitions are frequently a prerequisite for the function of a protein, as many intermolecular biological functioning is based on structural rearrangements. Unlike static methods, such as X-ray crystallography or NMR spectroscopy, which reveal only fixed details, SDSL can report on real-time substrate flexibility, segmental motions, and interactions in the context of a near-native protein.[61] SDSL may be used with a range of biological systems, even with membrane proteins complexes, and may thus extend the range of structural analyses in different environments. Between two localized sites within one protein or between contact interfaces of interacting proteins, inter-spin distances can be measured and a description of the spatial orientation and dynamics of the molecular interface can be obtained.[54] EPR-derived distances can elucidate complex formation, allosteric changes and the ligand binding mechanism. With the extreme sensitivity of EPR spectroscopy and the capability of precise site-specific labeling, SDSL has emerged as a powerful tool for the investigation of biomolecular function and dynamics.[61]

Despite its unique benefits for structural research, there are limitations when using SDSL-EPR. The presence of spin labels may alter the native structure of the protein, but this can be circumvented by careful choice of labeling positions. SDSL-EPR's ability to further inform the understanding of protein dynamics, particularly when combined with complementary approaches like cryo-electron microscopy and molecular dynamics simulations has the potential to offer a more comprehensive discovery of protein dynamics and would, no doubt, increase our knowledge of molecular and functional biology, and aid in the identification of new drug-targets. The recent emergence of new spin labels (e.g., Gd^{3+}, trityl and hydrophilic nitroxides), deuterated lipids and cryogenic stabilization has added to this sensitivity and resolution, and new frontiers in membrane protein research are now possible, for studies of transient states, allosteric modulation, and biologically relevant conformational ensembles of interest in complex membrane proteins.[62,63]

1.6.2 Continuous-Wave Electron Paramagnetic Resonance (CW-EPR)

CW-EPR uses a magnetic field that is varied with a fixed microwave frequency (usually the X-band, ~9.5 GHz) and measures microwave absorption by unpaired electrons during spin flip transitions. CW-EPR

spectra are sensitive monitors of the local dynamics and polarity at the spin-labeled site of spin-labeled membrane proteins.[56] The spectral lineshape depends on the anisotropy of the g-tensor as well as on the hyperfine interaction between the unpaired electron and the nitrogen nucleus of the nitroxide species, resulting in three principal lines (in isotropic motion). From simulations of the line shape, using different models (e.g., Stochastic Liouville Equation (SLE)), a characteristic rotational correlation time (τ_R) can be derived, which is related to the segmental motion of the protein backbone.[64] Narrow, sharp peaks reflect rapid isotropic motion characteristic of solvent exposed or disordered regions, while a signal with a broader, anisotropic profile represents restricted motions typical of transmembrane helices or densely packed tertiary structures.[65] CW-EPR spectroscopy is utilized in mapping the dynamic topological map of membrane proteins and to recognize helical periodicity and secondary structures as well as to observe ligand- or voltage-induced protein conformational transitions.

1.6.3. Power Saturation CW-EPR

Power saturation EPR is an extension of CW-EPR that determines the relaxation pattern of the spin label with external paramagnetic collision partners.[66] The power saturation of the spin-system can be obtained from the EPR signal intensity as a function of increasing microwave power, which is dependent upon the corresponding longitudinal relaxation time (T_1). Relaxation agents like molecular oxygen (O_2, lipid-soluble) or water-soluble species like nickel (II) ethylenediamine diacetic acid (NiEDDA) interact with T_1 via spin exchange, depending on the access of spin label to them.[67] The accessibility parameter Π, which describes the magnitude of change in the power saturation behavior that occurs in the presence of a relaxant vs in its absence, is calculated by comparing the power saturation with and without each relaxant. This parameter can be empirically linked to the depth of the spin-labeled residue in the lipid bilayer through accessibility profiles and hydrophobicity gradients.[67] For instance, O_2, apolar, partitions within the membrane bilayer and reports on transmembrane domains exposed to lipids, while NiEDDA senses exposure to aqueous solvent on each side of the bilayer.[37,67] It is thereby possible to determine which residues are located in the extracellular vs. the intracellular part of the protein membrane. The dual-parameter accessibility plot (Π_{O_2} vs. Π_{NiEDDA}) or the depth parameter Φ ($\Phi = \ln[\Pi_{O_2}/\Pi_{NiEDDA}]$) that exhibits a linear relationship with distance from the bilayer center could be used for quantitative analysis. These methods have been widely used to establish the orientation of α-helices in membrane-spanning.

1.6.4. Electron Spin Echo Envelope Modulation (ESEEM)

ESEEM spectroscopy yields atomic-level information on weak hyperfine couplings between the unpaired electron of the spin label and nearby magnetic nuclei, especially those not resolvable in CW-EPR due to line broadening or overlap. ESEEM employs a series of microwave pulses, typically in a three-pulse ($\pi/2$–τ–$\pi/2$–T–$\pi/2$–τ–echo) to generate spin echoes whose amplitude is modulated by the nuclear Larmor frequencies of nearby nuclei such as hydrogen, nitrogen, or other atoms present within the molecular structure.[37,46] The resulting echo envelope is Fourier transformed to yield frequency-domain spectra. ESEEM is particularly sensitive to weakly coupled nuclei in the 0.1–5 MHz range and can detect solvent-accessible protons or deuterons within ~5–8 Å of the nitroxide. In deuterated buffer (D_2O), ^2H coupling in the ESEEM reveals information about local hydration. This allows water-surface mapping and the differentiation of buried versus exposed sites within transmembrane segments or peripheral loops. ESEEM can also detect ^{31}P or ^{14}N nuclei of the phospholipid headgroups, providing information on lipid-protein interactions and the positioning of residues with respect to the membrane surface.[68]

The possibility of directly probing the local α-helical secondary structures of membrane peptides through ESEEM has been previously illustrated. This strategy is especially useful in membrane proteins; whereby solid-state NMR is time consuming and costly.[69] Integrating EPR with computational methods can also improve structural characterization of membrane proteins by introducing structurally-in/from function generators of power to be exploited for structure determination referred to distance restraints derived from experiment, into molecular model. Such an integrative strategy aids in uncovering the entire ensemble of conformers of proteins, leading to a more complete picture of their structural dynamics.[70]

The simultaneous use of CW-EPR, power saturation, and ESEEM spectroscopy is a powerful approach for structural biology of gp28 and TRPV1 VSLD membrane proteins. For CW-EPR, dynamic and topological profiles are obtained, with power saturation being able to provide information on the membrane depth and orientation; for ESEEM, atomic-resolution information of the local chemical microenvironment. These approaches allow functional and structure-based insights into the behavior of membrane proteins. Over the past years, the combination of these EPR techniques with distance-based measurements such as Double Electron-Electron Resonance (DEER) and molecular dynamics (MD) simulations allow the generation of high confidence structural models in lipid bilayers, without the requirement of crystallization or high protein concentration.[71]

1.7. Membrane mimetic systems

Membrane mimetic systems have emerged as powerful means to study membrane proteins that stabilize them in an environment that closely mimics their natural surroundings. These systems are prepared to mimic the selective permeability, fluidity and structural integrity of biological membranes, which are crucial for cellular homeostasis and intercellular communication. The lipid bilayers or polymeric matrices on which these are based are designed to mimic the wide diversity of lipid compositions and complex organizations that living systems offer.[72]

Lipid-associated detergents were the first group of membrane mimetics and one of the earliest solutions to the solubilization of membrane proteins from cellular membranes. Detergents such as n-Dodecyl-B-D-Maltoside (DDM) in aqueous solutions form micelles associated with the hydrophobic part of the receptor protein so that the protein can be solubilized in the water phase.[73] Micelles have been conveniently employed in structural studies of membrane proteins. In addition, the high curvature of micelles and their inability to replicate the lateral pressure of biological membranes limit the use of micelles in certain structural and functional studies.[74] To overcome the drawbacks of detergent micelles, lipid bilayer-containing systems such as liposomes, bicelles, and nanodiscs were created. These platforms provide a more native-like environment due to the bilayer arrangement that these systems form similar to that of natural membranes, a property that is essential for structural and functional studies of membrane proteins.[75] Liposomes consist of spherical vesicles with lipid bilayers and provides a more dynamic and possibly more physiological relevant system for reconstitution of membrane proteins.[76] Liposomes are customizable for size and lipid composition, providing great flexibility when conducting different studies. Nonetheless, the broad size distribution and instability under some conditions render them less amenable to high-resolution biophysical approaches. Long-chain lipid/short-chain detergent bicelles assume bilayered, disk-like structures. Such systems can be partially aligned in magnetic fields and so are widely applicable in solution NMR and EPR spectroscopy.[77] Bicelles provide enhanced stability over micelles and allow better duplication of a natural bilayer environment, however they continue to share some of the obstacles inherent to detergent-mediated systems and specifically with reported issues on size and temperature sensitivity.[78]

Nanodiscs, as developed in the Sligar laboratory, represent a dramatic advancement in membrane mimetic apparatus. Nanodiscs that are composed of a lipid bilayer and enclosed by membrane scaffold proteins (MSPs) thus offering a natural-like membrane environment.[79] This process still requires the

presence of detergent; thus, proteins that are very sensitive to detergents are still not compatible with this mimetic. A mimetic that does not require the introduction of detergent and ideally keeps the native membrane intact is required.[80]

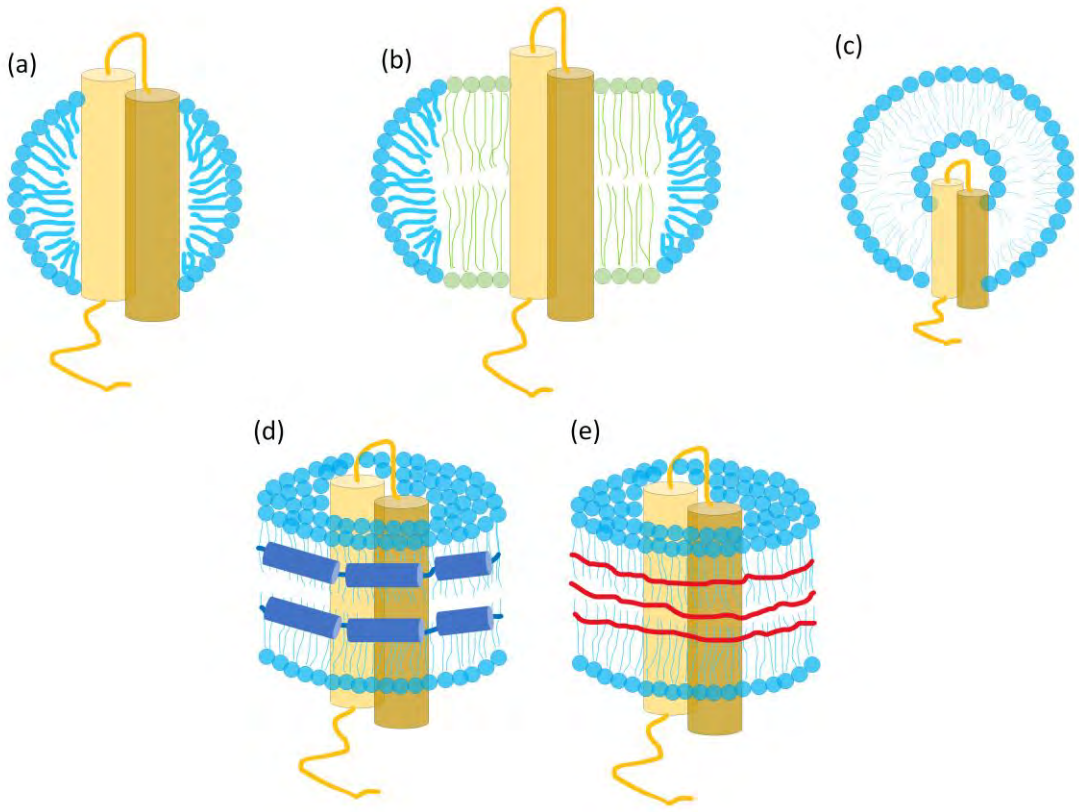

Figure 1.5: Visual depictions of various membrane mimetics: (a) micelle, (b) bicelle, (c) liposome, (d) nanodisc, and (e) SMALP.[33]

1.8. Polymer Supported Bilayer BioMimics: SMALPs and Beyond

The limitations of detergent-based and bilayer mimetics systems have initiated the rise of polymeric membrane mimetics, where Styrene Maleic Acid Lipid Particles (SMALPs) has emerged as one of the most promising breakthroughs.[79] SMALPs are generated from the reaction of SMA (styrene-maleic acid) copolymers with biological membranes, which can extract membrane proteins from their membrane while preserving their native lipid environment.[81] SMA copolymers also provide significant advantages for the stabilization and soluble preparation of membrane proteins in the form of lipid particles without the need for detergents.[82] SMALPs have been particularly successful for EPR spectroscopy, native mass spectrometry, and cryo-EM, all of which can benefit from analysis of the structure and lipid annulus of the membrane protein in a native-like state and a resolution that is not influenced by artifacts.[80]

Although SMA copolymers have emerged as an important new class of membrane mimetics, their usage is not without restrictions. Differences in the Styrene to Maleic Acid ratio, charge densities and polymer sizes affect protein stabilization and subsequently, the biophysical data.[83] Moreover, styrene UV-Vis absorbance interference from the aromatic ring may also distort data quantification when using these systems, requiring polymer-based mimetics alternatives such as Vinyl Ether Maleic Acid (VEMA) derivatives.[78]

VEMA, a polymer that replaces styrene in SMA analogs, is a biological tool that overcomes these impediments as it decreases UV sensitivity, leading to more precise and accurate measurements especially for protein concentration.[84] VEMA-based systems can promote the determination of membrane protein structures more accurately because of the more accurate data acquisition beyond the spectral interference of the styrene part. These changes increase the ease of use of polymeric mimetics in membrane protein studies and enable greater control over the nature of the polymer and its behavior in and with lipid bilayers.[78]

1.9. Conclusion

In conclusion, the combined use of site-specific spin labeling and EPR spectroscopy is a powerful approach for the study of the structural topology of proteins such as gp28 and TRPV1. These strategies have enabled the investigation of dynamic conformations and interactions of proteins that can be informative with their functional mechanism. In membrane mimetic systems, detergents were used to solubilize and help purify membrane proteins initially but now the field has advanced in general towards more complex mimetics: vesicles, bicelles and nanodiscs as well as new polymeric systems: SMA copolymers, SMA derivatives and vinyl ether maleic acid derivatives. The change reflects the increasing need for systems that more accurately mimic the native membrane setting, with improved stability, structural fidelity, and functional relevance for biophysical studies. With further development of these technologies, their potential applications in structural biology and drug development will increase, leading to new developments and applications in the life sciences. Continuous-Wave EPR (CW-EPR), power saturation, and Electron Spin Echo Envelope Modulation (ESEEM) techniques have been utilized very effectively in gaining distinct insight about the structural aspects of gp28 and TRPV1 VSLD membrane proteins at molecular level in this study.

References

(1) Whited, A. M.; Johs, A. The Interactions of Peripheral Membrane Proteins with Biological Membranes. *Chem Phys Lipids* 2015, *192*, 51–59. https://doi.org/10.1016/j.chemphyslip.2015.07.015.

(2) Palsdottir, H.; Hunte, C. Lipids in Membrane Protein Structures. *Biochimica et Biophysica Acta (BBA) - Biomembranes* 2004, *1666* (1–2), 2–18. https://doi.org/10.1016/j.bbamem.2004.06.012.

(3) Gatenby, R. A. The Role of Cell Membrane Information Reception, Processing, and Communication in the Structure and Function of Multicellular Tissue. *Int J Mol Sci* 2019, *20* (15), 3609. https://doi.org/10.3390/ijms20153609.

(4) Nicolson, G. L. The Fluid—Mosaic Model of Membrane Structure: Still Relevant to Understanding the Structure, Function and Dynamics of Biological Membranes after More than 40years. *Biochimica et Biophysica Acta (BBA) - Biomembranes* 2014, *1838* (6), 1451–1466. https://doi.org/10.1016/j.bbamem.2013.10.019.

(5) Levental, I.; Lyman, E. Regulation of Membrane Protein Structure and Function by Their Lipid Nano-Environment. *Nature Reviews Molecular Cell Biology*. 2023. https://doi.org/10.1038/s41580-022-00524-4.

(6) Escribá, P. V.; González-Ros, J. M.; Goñi, F. M.; Kinnunen, P. K. J.; Vigh, L.; Sánchez-Magraner, L.; Fernández, A. M.; Busquets, X.; Horváth, I.; Barceló-Coblijn, G. Membranes: A Meeting Point for Lipids, Proteins and Therapies. *J Cell Mol Med* 2008, *12* (3), 829–875. https://doi.org/10.1111/j.1582-4934.2008.00281.x.

(7) Quinn, P. J.; Chapman, D.; Keith, A. D. The Dynamics of Membrane Structur. *Critical Reviews in Biochemistry* 1980, *8* (1), 1–117. https://doi.org/10.3109/10409238009105466.

(8) Cheng, X.; Smith, J. C. Biological Membrane Organization and Cellular Signaling. *Chem Rev* 2019, *119* (9), 5849–5880. https://doi.org/10.1021/acs.chemrev.8b00439.

(9) Denker, S. P.; Barber, D. L. Ion Transport Proteins Anchor and Regulate the Cytoskeleton. *Curr Opin Cell Biol* 2002, *14* (2), 214–220. https://doi.org/10.1016/S0955-0674(02)00304-6.

(10) Yang, N. J.; Hinner, M. J. Getting Across the Cell Membrane: An Overview for Small Molecules, Peptides, and Proteins; 2015; pp 29–53. https://doi.org/10.1007/978-1-4939-2272-7_3.

(11) Stillwell, W. Membrane Transport. In *An Introduction to Biological Membranes*; Elsevier, 2013; pp 305–337. https://doi.org/10.1016/B978-0-444-52153-8.00014-3.

(12) Alberts B, Johnson A, Lewis J, et al. Molecular Biology of the Cell. 4th Edition. New York: Garland Science; 2002. Ion Channels and the Electrical Properties of Membranes.

(13) Dubyak, G. R. Ion Homeostasis, Channels, and Transporters: An Update on Cellular Mechanisms. *Adv Physiol Educ* 2004, *28* (4), 143–154. https://doi.org/10.1152/advan.00046.2004.

(14) Fletcher, A. The Cell Membrane and Receptors. *Anaesthesia & Intensive Care Medicine* 2023, *24* (5), 298–302. https://doi.org/10.1016/j.mpaic.2023.01.006.

(15) Hotamisligil, G. S.; Davis, R. J. Cell Signaling and Stress Responses. *Cold Spring Harb Perspect Biol* 2016, *8* (10), a006072. https://doi.org/10.1101/cshperspect.a006072.

(16) Gong, J.; Chen, Y.; Pu, F.; Sun, P.; He, F.; Zhang, L.; Li, Y.; Ma, Z.; Wang, H. Understanding Membrane Protein Drug Targets in Computational Perspective. *Curr Drug Targets* 2019, *20* (5), 551–564. https://doi.org/10.2174/1389450120666181204164721.

(17) Alexander, S. P. H.; Mathie, A.; Peters, J. A. Ion Channels. *Br J Pharmacol* 2007, *150* (S1). https://doi.org/10.1038/sj.bjp.0707204.

(18) Bezanilla, F. Voltage-Gated Ion Channels; 2007; pp 81–118. https://doi.org/10.1007/0-387-68919-2_3.

(19) Ranade, S. S.; Syeda, R.; Patapoutian, A. Mechanically Activated Ion Channels. *Neuron* 2015, *88* (2), 433. https://doi.org/10.1016/j.neuron.2015.10.016.

(20) Kullmann, D. M.; Hanna, M. G. Neurological Disorders Caused by Inherited Ion-Channel Mutations. *Lancet Neurol* 2002, *1* (3), 157–166. https://doi.org/10.1016/S1474-4422(02)00071-6.

(21) Steinlein, O. K. Ion Channel Mutations in Neuronal Diseases: A Genetics Perspective. *Chem Rev* 2012, *112* (12), 6334–6352. https://doi.org/10.1021/cr300044d.

(22) Tominaga, M.; Caterina, M. J. Thermosensation and Pain. *J Neurobiol* 2004, *61* (1), 3–12. https://doi.org/10.1002/neu.20079.

(23) Xiao, R.; Xu, X. Z. S. Temperature Sensation: From Molecular Thermosensors to Neural Circuits and Coding Principles. *Annu Rev Physiol* 2021, *83* (1), 205–230. https://doi.org/10.1146/annurev-physiol-031220-095215.

(24) Shuba, Y. M. Beyond Neuronal Heat Sensing: Diversity of TRPV1 Heat-Capsaicin Receptor-Channel Functions. *Front Cell Neurosci* 2021, *14*. https://doi.org/10.3389/fncel.2020.612480.

(25) Pingle, S. C.; Matta, J. A.; Ahern, G. P. Capsaicin Receptor: TRPV1 A Promiscuous TRP Channel; 2007; pp 155–171. https://doi.org/10.1007/978-3-540-34891-7_9.

(26) Frias, B.; Merighi, A. Capsaicin, Nociception and Pain. *Molecules* 2016, *21* (6), 797. https://doi.org/10.3390/molecules21060797.

(27) Straub, R. H. TRPV1, TRPA1, and TRPM8 Channels in Inflammation, Energy Redirection, and Water Retention: Role in Chronic Inflammatory Diseases with an Evolutionary Perspective. *J Mol Med* 2014, *92* (9), 925–937. https://doi.org/10.1007/s00109-014-1175-9.

(28) Brito, R.; Sheth, S.; Mukherjea, D.; Rybak, L.; Ramkumar, V. TRPV1: A Potential Drug Target for Treating Various Diseases. *Cells* 2014, *3* (2), 517–545. https://doi.org/10.3390/cells3020517.

(29) Iftinca, M.; Defaye, M.; Altier, C. TRPV1-Targeted Drugs in Development for Human Pain Conditions. *Drugs* 2021, *81* (1), 7–27. https://doi.org/10.1007/s40265-020-01429-2.

(30) Salam, Md. A.; Al-Amin, Md. Y.; Salam, M. T.; Pawar, J. S.; Akhter, N.; Rabaan, A. A.; Alqumber, M. A. A. Antimicrobial Resistance: A Growing Serious Threat for Global Public Health. *Healthcare* 2023, *11* (13), 1946. https://doi.org/10.3390/healthcare11131946.

(31) Saeed, U.; Insaf, R. A.; Piracha, Z. Z.; Tariq, M. N.; Sohail, A.; Abbasi, U. A.; Fida Rana, M. S.; Gilani, S. S.; Noor, S.; Noor, E.; Waheed, Y.; Wahid, M.; Najmi, M. H.; Fazal, I. Crisis Averted: A World United against the Menace of Multiple Drug-Resistant Superbugs -Pioneering Anti-AMR Vaccines, RNA Interference, Nanomedicine, CRISPR-Based Antimicrobials, Bacteriophage Therapies, and Clinical Artificial Intelligence Strategies to Safeguard Global Antimicrobial Arsenal. *Front Microbiol* 2023, *14*. https://doi.org/10.3389/fmicb.2023.1270018.

(32) Pang, T.; Park, T.; Young, R. Mutational Analysis of the S 21 Pinholin. *Mol Microbiol* 2010, *76* (1), 68–77. https://doi.org/10.1111/j.1365-2958.2010.07080.x.

(33) Rasal, M.; Khan, H. *Probing the Structural Topology, Dynamics, Conformation, And Secondary Structure of Pinholin S 21 And Gp28, Bacteriophage Lytic Proteins, Using Electron Paramagnetic Resonance Spectroscopy*.

(34) Cahill, J.; Young, R. Phage Lysis: Multiple Genes for Multiple Barriers; 2019; pp 33–70. https://doi.org/10.1016/bs.aivir.2018.09.003.

(35) Holt, A.; Cahill, J.; Ramsey, J.; Martin, C.; O'Leary, C.; Moreland, R.; Maddox, L. T.; Galbadage, T.; Sharan, R.; Sule, P.; Cirillo, J. D.; Young, R. Phage-Encoded Cationic Antimicrobial Peptide Required for Lysis. *J Bacteriol* 2022, *204* (1). https://doi.org/10.1128/JB.00214-21.

(36) Holt, A.; Cahill, J.; Ramsey, J.; Martin, C.; O'Leary, C.; Moreland, R.; Maddox, L. T.; Galbadage, T.; Sharan, R.; Sule, P.; Cirillo, J. D.; Young, R. Phage-Encoded Cationic Antimicrobial Peptide Required for Lysis. *J Bacteriol* 2022, *204* (1). https://doi.org/10.1128/JB.00214-21.

(37) Khan, R. H.; Rotich, N. C.; Morris, A.; Ahammad, T.; Baral, B.; Sahu, I. D.; Lorigan, G. A. Probing the Structural Topology and Dynamic Properties of Gp28 Using Continuous Wave Electron Paramagnetic Resonance Spectroscopy. *J Phys Chem B* 2023, *127* (43), 9236–9247. https://doi.org/10.1021/acs.jpcb.3c03679.

(38) Ahammad, T.; Drew, D. L.; Khan, R. H.; Sahu, I. D.; Faul, E.; Li, T.; Lorigan, G. A. Structural Dynamics and Topology of the Inactive Form of S21Holin in a Lipid Bilayer Using Continuous-Wave Electron Paramagnetic Resonance Spectroscopy. *Journal of Physical Chemistry B* 2020, *124* (26), 5370–5379. https://doi.org/10.1021/acs.jpcb.0c03575.

(39) Rotich, N. C.; Khan, R. H.; Morris, A.; McCarrick, R.; Baral, B.; Okorafor, E. A.; Faul, E.; Wardrip, L.; Sahu, I. D.; Lorigan, G. A. Probing the Secondary Structure of Membrane-Bound Gp28 Using Electron Spin Echo Envelope Modulation (ESEEM) Spectroscopy. *J Phys Chem B* 2025, *129* (10), 2659–2667. https://doi.org/10.1021/acs.jpcb.4c08270.

(40) Wilkinson, R. C.; Thomas, N. E.; Bhatti, A.; Burton, M. R.; Joyce, N.; Jenkins, R. E. Phage-Encoded Antimicrobial Peptide Gp28 Demonstrates LL-37-Like Antimicrobial Activity Against Multidrug-

Resistant *Pseudomonas Aeruginosa*. *PHAGE* 2025, *6* (1), 12–19. https://doi.org/10.1089/phage.2024.0009.

(41) Puri, B.; Vaishya, R.; Vaish, A. Antimicrobial Resistance: Current Challenges and Future Directions. *Med J Armed Forces India* 2025, *81* (3), 247–258. https://doi.org/10.1016/j.mjafi.2024.07.006.

(42) Backes, B. Solid Support Linker Strategies. *Curr Opin Chem Biol* 1997, *1* (1), 86–93. https://doi.org/10.1016/S1367-5931(97)80113-5.

(43) El-Faham, A.; Albericio, F. Peptide Coupling Reagents, more than a Letter Soup. *Chem Rev* 2011, *111* (11), 6557–6602. https://doi.org/10.1021/cr100048w.

(44) Conda-Sheridan, M.; Krishnaiah, M. Protecting Groups in Peptide Synthesis; 2020; pp 111–128. https://doi.org/10.1007/978-1-0716-0227-0_7.

(45) Isidro-Llobet, A.; Álvarez, M.; Albericio, F. Amino Acid-Protecting Groups. *Chem Rev* 2009, *109* (6), 2455–2504. https://doi.org/10.1021/cr800323s.

(46) Rotich, N. C.; Khan, R. H.; Morris, A.; McCarrick, R.; Baral, B.; Okorafor, E. A.; Faul, E.; Wardrip, L.; Sahu, I. D.; Lorigan, G. A. Probing the Secondary Structure of Membrane-Bound Gp28 Using Electron Spin Echo Envelope Modulation (ESEEM) Spectroscopy. *J Phys Chem B* 2025, *129* (10), 2659–2667. https://doi.org/10.1021/acs.jpcb.4c08270.

(47) Palomar-Alonso, N.; Lee, M.; Kim, M. Exosomes: Membrane-Associated Proteins, Challenges and Perspectives. *Biochemistry and Biophysics Reports*. 2024. https://doi.org/10.1016/j.bbrep.2023.101599.

(48) Zhang, Q.; Cherezov, V. Chemical Tools for Membrane Protein Structural Biology. *Curr Opin Struct Biol* 2019, *58*, 278–285. https://doi.org/10.1016/j.sbi.2019.06.002.

(49) Sadaf, A.; Cho, K. H.; Byrne, B.; Chae, P. S. Amphipathic Agents for Membrane Protein Study; 2015; pp 57–94. https://doi.org/10.1016/bs.mie.2014.12.021.

(50) Puthenveetil, R.; Christenson, E. T.; Vinogradova, O. New Horizons in Structural Biology of Membrane Proteins: Experimental Evaluation of the Role of Conformational Dynamics and Intrinsic Flexibility. *Membranes (Basel)* 2022, *12* (2), 227. https://doi.org/10.3390/membranes12020227.

(51) Bali, A. P.; Sahu, I. D.; Craig, A. F.; Clark, E. E.; Burridge, K. M.; Dolan, M. T.; Dabney-Smith, C.; Konkolewicz, D.; Lorigan, G. A. Structural Characterization of Styrene-Maleic Acid Copolymer-Lipid Nanoparticles (SMALPs) Using EPR Spectroscopy. *Chem Phys Lipids* 2019, *220*. https://doi.org/10.1016/j.chemphyslip.2019.02.003.

(52) El-Faham, A.; Albericio, F. Peptide Coupling Reagents, more than a Letter Soup. *Chem Rev* 2011, *111* (11), 6557–6602. https://doi.org/10.1021/cr100048w.

(53) Conda-Sheridan, M.; Krishnaiah, M. Protecting Groups in Peptide Synthesis; 2020; pp 111–128. https://doi.org/10.1007/978-1-0716-0227-0_7.

(54) Davies, M. J. Detection and Characterisation of Radicals Using Electron Paramagnetic Resonance (EPR) Spin Trapping and Related Methods. *Methods* 2016, *109*, 21–30. https://doi.org/10.1016/j.ymeth.2016.05.013.

(55) Roessler, M. M.; Salvadori, E. Principles and Applications of EPR Spectroscopy in Chemical Sciences. *Chem Soc Rev* 2018, *47* (8), 2534–2553. https://doi.org/10.1039/C6CS00565A.

(56) Klug, C. S.; Feix, J. B. Methods and Applications of Site-Directed Spin Labeling EPR Spectroscopy; 2008; pp 617–658. https://doi.org/10.1016/S0091-679X(07)84020-9.

(57) Torricella, F.; Pierro, A.; Mileo, E.; Belle, V.; Bonucci, A. Nitroxide Spin Labels and EPR Spectroscopy: A Powerful Association for Protein Dynamics Studies. *Biochimica et Biophysica Acta (BBA) - Proteins and Proteomics* 2021, *1869* (7), 140653. https://doi.org/10.1016/j.bbapap.2021.140653.

(58) Sahu, I. D.; Lorigan, G. A. Electron Paramagnetic Resonance as a Tool for Studying Membrane Proteins. *Biomolecules* 2020, *10* (5), 763. https://doi.org/10.3390/biom10050763.

(59) Roessler, M. M.; Salvadori, E. Principles and Applications of EPR Spectroscopy in the Chemical Sciences. *Chem Soc Rev* 2018, *47* (8), 2534–2553. https://doi.org/10.1039/C6CS00565A.

(60) Hubbell, W. L.; Gross, A.; Langen, R.; Lietzow, M. A. Recent Advances in Site-Directed Spin Labeling of Proteins. *Curr Opin Struct Biol* 1998, *8* (5), 649–656. https://doi.org/10.1016/S0959-440X(98)80158-9.

(61) Klug, C. S.; Feix, J. B. Methods and Applications of Site-Directed Spin Labeling EPR Spectroscopy; 2008; pp 617–658. https://doi.org/10.1016/S0091-679X(07)84020-9.

(62) García-Rubio, I. EPR of Site-Directed Spin-Labeled Proteins: A Powerful Tool to Study Structural Flexibility. *Arch Biochem Biophys* 2020, *684*, 108323. https://doi.org/10.1016/j.abb.2020.108323.

(63) Roopnarine, O.; Thomas, D. D. Structural Dynamics of Protein Interactions Using Site-Directed Spin Labeling of Cysteines to Measure Distances and Rotational Dynamics with EPR Spectroscopy. *Appl Magn Reson* 2024, *55* (1–3), 79–100. https://doi.org/10.1007/s00723-023-01623-x.

(64) Kopf, S.; Bourriquen, F.; Li, W.; Neumann, H.; Junge, K.; Beller, M. Recent Developments for the Deuterium and Tritium Labeling of Organic Molecules. *Chem Rev* 2022, *122* (6), 6634–6718. https://doi.org/10.1021/acs.chemrev.1c00795.

(65) Fielding, A.; Concilio, M.; Heaven, G.; Hollas, M. New Developments in Spin Labels for Pulsed Dipolar EPR. *Molecules* 2014, *19* (10), 16998–17025. https://doi.org/10.3390/molecules191016998.

(66) Jeschke, G. Conformational Dynamics and Distribution of Nitroxide Spin Labels. *Prog Nucl Magn Reson Spectrosc* 2013, *72*, 42–60. https://doi.org/10.1016/j.pnmrs.2013.03.001.

(67) Dzuba, S. A. Probing Small-Angle Molecular Motions with EPR Spectroscopy: Dynamical Transition and Molecular Packing in Disordered Solids. *Magnetochemistry* 2022, *8* (2), 19. https://doi.org/10.3390/magnetochemistry8020019.

(68) Marsh, D. *Spin-Label Electron Paramagnetic Resonance Spectroscopy*; CRC Press, 2019. https://doi.org/10.1201/9780429194634.

(69) Dixit, G.; Sahu, I. D.; Reynolds, W. D.; Wadsworth, T. M.; Harding, B. D.; Jaycox, C. K.; Dabney-Smith, C.; Sanders, C. R.; Lorigan, G. A. Probing the Dynamics and Structural Topology of the Reconstituted Human KCNQ1 Voltage Sensor Domain (Q1-VSD) in Lipid Bilayers Using Electron Paramagnetic Resonance Spectroscopy. *Biochemistry* 2019, *58* (7), 965–973. https://doi.org/10.1021/acs.biochem.8b01042.

(70) Malmberg, N. J.; Falke, J. J. Use of EPR Power Saturation to Analyze the Membrane-Docking Geometries of Peripheral Proteins: Applications to C2 Domains. *Annu Rev Biophys Biomol Struct* 2005, *34* (1), 71–90. https://doi.org/10.1146/annurev.biophys.34.040204.144534.

(71) Åhrling, K. A.; Evans, M. C. W.; Nugent, J. H. A.; Ball, R. J.; Pace, R. J. ESEEM Studies of Substrate Water and Small Alcohol Binding to the Oxygen-Evolving Complex of Photosystem II during Functional Turnover. *Biochemistry* 2006, *45* (23), 7069–7082. https://doi.org/10.1021/bi052146m.

(72) Bottorf, L.; Sahu, I. D.; McCarrick, R. M.; Lorigan, G. A. Utilization of 13C-Labeled Amino Acids to Probe the α-Helical Local Secondary Structure of a Membrane Peptide Using Electron Spin Echo Envelope Modulation (ESEEM) Spectroscopy. *Biochimica et Biophysica Acta (BBA) - Biomembranes* 2018, *1860* (7), 1447–1451. https://doi.org/10.1016/j.bbamem.2018.04.001.

(73) Muñoz, V. Conformational Dynamics and Ensembles in Protein Folding. *Annu Rev Biophys Biomol Struct* 2007, *36* (1), 395–412. https://doi.org/10.1146/annurev.biophys.36.040306.132608.

(74) Lindahl, E.; Sansom, M. Membrane Proteins: Molecular Dynamics Simulations. *Curr Opin Struct Biol* 2008, *18* (4), 425–431. https://doi.org/10.1016/j.sbi.2008.02.003.

(75) Zhou, H.-X.; Cross, T. A. Influences of Membrane Mimetic Environments on Membrane Protein Structures. *Annu Rev Biophys* 2013, *42* (1), 361–392. https://doi.org/10.1146/annurev-biophys-083012-130326.

(76) Mineev, K. S.; Nadezhdin, K. D. Membrane Mimetics for Solution NMR Studies of Membrane Proteins. *Nanotechnol Rev* 2017, *6* (1), 15–32. https://doi.org/10.1515/ntrev-2016-0074.

(77) Le Maire, M.; Champeil, P.; Møller, J. V. Interaction of Membrane Proteins and Lipids with Solubilizing Detergents. *Biochimica et Biophysica Acta (BBA) - Biomembranes* 2000, *1508* (1–2), 86–111. https://doi.org/10.1016/S0304-4157(00)00010-1.

(78) Necelis, M.; Columbus, L. M. Investigating Lipid-Lipid and Lipid-Protein Interactions with Bicelles and Nanodiscs. *Biophys J* 2024, *123* (3), 234a. https://doi.org/10.1016/j.bpj.2023.11.1477.

(79) Thoma, J.; Burmann, B. M. Fake It 'Till You Make It—The Pursuit of Suitable Membrane Mimetics for Membrane Protein Biophysics. *Int J Mol Sci* 2020, *22* (1), 50. https://doi.org/10.3390/ijms22010050.

(80) De Angelis, A. A.; Nevzorov, A. A.; Park, S. H.; Howell, S. C.; Mrse, A. A.; Opella, S. J. High-Resolution NMR Spectroscopy of Membrane Proteins in Aligned Bicelles. *J Am Chem Soc* 2004, *126* (47), 15340–15341. https://doi.org/10.1021/ja045631y.

(81) Shah, M. Z.; Rotich, N. C.; Okorafor, E. A.; Oestreicher, Z.; Demidovich, G.; Eapen, J.; Henoch, Q.; Kilbey, J.; Prempeh, G.; Bates, A.; Page, R. C.; Lorigan, G. A.; Konkolewicz, D. Vinyl Ether Maleic Acid Polymers: Tunable Polymers for Self-Assembled Lipid Nanodiscs and Environments for Membrane Proteins. *Biomacromolecules* 2024, *25* (10), 6611–6623. https://doi.org/10.1021/acs.biomac.4c00772.

(82) Sligar, S. G.; Denisov, I. G. Nanodiscs: A Toolkit for Membrane Protein Science. *Protein Science* 2021, *30* (2), 297–315. https://doi.org/10.1002/pro.3994.

(83) Dörr, J. M.; Scheidelaar, S.; Koorengevel, M. C.; Dominguez, J. J.; Schäfer, M.; van Walree, C. A.; Killian, J. A. The Styrene–Maleic Acid Copolymer: A Versatile Tool in Membrane Research. *European Biophysics Journal* 2016, *45* (1), 3–21. https://doi.org/10.1007/s00249-015-1093-y.

(84) Knowles, T. J.; Finka, R.; Smith, C.; Lin, Y.-P.; Dafforn, T.; Overduin, M. Membrane Proteins Solubilized Intact in Lipid Containing Nanoparticles Bounded by Styrene Maleic Acid Copolymer. *J Am Chem Soc* 2009, *131* (22), 7484–7485. https://doi.org/10.1021/ja810046q.

(85) Swainsbury, D. J. K.; Scheidelaar, S.; Foster, N.; van Grondelle, R.; Killian, J. A.; Jones, M. R. The Effectiveness of Styrene-Maleic Acid (SMA) Copolymers for Solubilisation of Integral Membrane Proteins from SMA-Accessible and SMA-Resistant Membranes. *Biochim Biophys Acta Biomembr* 2017, *1859* (10). https://doi.org/10.1016/j.bbamem.2017.07.011.

(86) Burridge, K. M.; Harding, B. D.; Sahu, I. D.; Kearns, M. M.; Stowe, R. B.; Dolan, M. T.; Edelmann, R. E.; Dabney-Smith, C.; Page, R. C.; Konkolewicz, D.; Lorigan, G. A. Simple Derivatization of RAFT-Synthesized Styrene-Maleic Anhydride Copolymers for Lipid Disk Formulations. *Biomacromolecules* 2020, *21* (3). https://doi.org/10.1021/acs.biomac.0c00041.

Chapter 2

Probing the Secondary Structure of Membrane-bound gp28 using Electron Spin Echo Envelope Modulation (ESEEM) Spectroscopy

Nancy C. Rotich †, Rasal H. Khan †, Andrew Morris †, Robert McCarrick †, Binaya Baral †, Evelyn A. Okorafor, Emily Faul, Luke Wardrip, Indra D. Sahu, and Gary A. Lorigan†*

‡Department of Chemistry and Biochemistry, Miami University, Oxford, OH, 45056, USA.

*Natural Science Division, Campbellsville University, Campbellsville, KY, 42718, USA.

This work has been published in *The Journal of Physical Chemistry B* **2025** *129* (10), 2659-2667: Probing the Secondary Structure of Membrane-Bound gp28 Using Electron Spin Echo Envelope Modulation (ESEEM) Spectroscopy. Nancy C. Rotich, Rasal H. Khan, Andrew Morris, Robert McCarrick, Binaya Baral, Evelyn A. Okorafor, Emily Faul, Luke Wardrip, Indra D. Sahu, and Gary A. Lorigan. DOI: 10.1021/acs.jpcb.4c08270. Reproduced with permission.

Abstract

Membrane proteins play a vital role in various cellular functions and are important targets for drug interactions. However, determining their local secondary structure is challenging due to their hydrophobic nature and limited experimental techniques. This study focuses on the use of electron spin echo envelope modulation (ESEEM) spectroscopy, in combination with site-directed spin labeling (SDSL) and ^{2}H-labeled amino acid sidechain (d_{10}-Leu), to study the local secondary structure of a recently discovered phage-encoded lytic protein, gp28. gp28 is a membrane protein with three predicted helices that plays a crucial role in the lysis process of bacteriophages that lack spanins. gp28 is an antimicrobial protein specifically involved in disrupting the outer membrane of the host cell. Through the synthesis of nine constructs of gp28 peptides, we systematically probed the three predicted helices. The local secondary structure of the gp28 protein in POPC/POPG vesicles was investigated using ESEEM spectroscopy. Additionally, the global secondary structure was verified using CD spectroscopy. Subsequently, the ESEEM technique allowed us to determine the local secondary structure within the three predicted alpha helices of gp28 in a membrane. This study revealed the presence of alpha helical structural components in all three predicted helices of gp28. These results not only enhance our comprehension of the local secondary structure of gp28 but also highlight the effectiveness of the ESEEM spectroscopic technique in studying membrane protein systems encoded by bacteriophages.

2.0. Introduction

Membrane proteins play a crucial role in a diverse range of cellular functions, such as transport, signaling, and lysis.[1] Additionally, they serve as targets for more than 50% of small molecule drug interactions.[2,3] However, determining the local secondary structure of membrane proteins has been a persistent challenge for the scientific community. Their hydrophobic nature, poor overexpression yields, and the absence of high-quality crystals have complicated these efforts. [4,5] Traditional methods for structure prediction in protein research have historically established a foundation that contributes to the understanding of protein folding and stability. However, these techniques can be time-consuming and limited in their ability to handle the complexity of certain protein types, particularly membrane proteins.

Currently, AI-based approaches such as AlphaFold have revolutionized the landscape of protein structure prediction.[6,7] AlphaFold employs deep learning algorithms trained on vast datasets of known protein structures, enabling it to predict the three-dimensional arrangements of amino acids with remarkable accuracy and speed. This advancement marks a significant departure from earlier methodologies, allowing researchers to generate reliable structural models for proteins that were previously difficult to study, including membrane proteins. To fully leverage AI predictions in this context, it is essential to integrate these computational models with experimental data, such as cryo-electron microscopy and/or other biophysical techniques. This synergy can enhance the reliability of predictions and provide insights into the conformational dynamics of membrane proteins. By combining computational data with experimental data, researchers can cultivate AI systems that are better equipped to tackle the puzzle of membrane protein folding and function.[8,9]

In the field of structural biology studies, an array of techniques is utilized to comprehend the secondary structures of protein/peptides. These techniques include circular dichroism (CD), X-ray crystallography, solution and solid-state nuclear magnetic resonance (NMR), FT-Raman spectroscopy, ATR FT-IR, computational modeling, and spectral lineshape analysis with electron paramagnetic resonance (EPR) spectroscopy.[11-13] Among these methods, CD is currently the most widely used and easiest spectroscopic technique.[14-15] However, CD data can only provide information about the overall or global secondary structure and cannot offer site-specific details about the nature of the local secondary structure.[16-20]

Obtaining site-specific secondary structural information is crucial for understanding protein packing and interactions within a lipid bilayer environment.[20-25] Additionally, local secondary structural information

is valuable for gaining insights into the function, dynamics, and interactions of proteins.[17] Local secondary structures can be determined using solid-state NMR spectroscopy by analyzing backbone ^{13}C chemical shift assignments and dipolar couplings.[22-28] Although NMR provides very useful structural information, this method requires substantial amounts of isotopic-labeled protein or peptide samples and extended data acquisition time, ranging from days to weeks, while also suffering from low sensitivity.[17,28] EPR spectroscopic methods are complementary to existing biophysical techniques that require smaller amounts of isotopic-labeled protein or peptide samples (from 10 μM) and involve shorter data acquisition times, while still providing high sensitivity.[17,29]

Previously, the Lorigan group successfully employed ESEEM spectroscopy in combination with site-directed spin labeling (SDSL) and ^{2}H-labeled amino acid sidechain to determine the local secondary structure of model membrane proteins/peptides.[20,31] ESEEM spectroscopy, a highly robust pulsed EPR technique, has been proven valuable in studying a wide range of biological systems.[26] This technique has been employed to differentiate between α-helices and β-sheets and the detection of α-helices versus 3_{10}-helices.[30] The advantage of ESEEM spectroscopic techniques over other biophysical structural biology techniques, such as circular dichroism (CD) spectroscopy, lies in its ability to selectively probe the local secondary structure rather than the global secondary structure.[17,30,31] When studying local secondary structures, ESEEM spectroscopy is cost effective and also overcomes the limitations observed in NMR techniques, offering a valuable method to discern subtle but significant differences in the local secondary structure of peptides and proteins.[27,29] This ESEEM approach can be also applied to larger size protein using bacterial overexpression methods.[13,18]

Studying the local secondary structure with ESEEM spectroscopic technique requires a deuterated (^{2}H) amino acid sidechain, such as d_{10}-Leu, and a site-specific nitroxide spin label positioned within four amino acid residues of the deuterated amino acid. In this case, a nitroxide based spin label called S-(1-oxyl-2,2,5,5-tetramethyl-2,5-dihydro-1H-pyrrol-3-yl) methyl methanesulfonothioate (MTSL) is attached to the substituted cysteine side chain via disulfide bond formation. In ESEEM spectroscopy, the detection mechanism involves capturing the weak interactions between the unpaired electron of the spin label and the deuterium nuclei present in the labeled Leu side chain, within a detection limit of 8 Å. It is also possible to employ other deuterated amino acids (e.g., d_{10}-Val) as well.[33,34.]

The distinctive periodicity of helices (e.g. alpha helices, 3_{10}-helices) and the linear arrangement of β-sheets exhibit distinct patterns in the ESEEM spectra as the spin label is incrementally moved away from the d_{10}-

Leu side chain.[17,35] In a helix, when the spin label is positioned 2 amino acids away from the d_{10}-Leu, both the spin label and the d_{10}-Leu are situated on opposite sides of the alpha helix (**Figure 2.1A**), exceeding the 8 Å ESEEM detection limit.[17,30,36] However, as the spin label is moved to positions 3 or 4 amino acids away from the d_{10}-Leu, the helical structure aligns with both labels on the same side of the helix, allowing for the detection of deuterium modulation **(Figure 2.1B**).[18,36] Conversely, when probing a β-sheet, the linear nature of β-sheets positions the spin label within the detection limit when it is 1 or 2 amino acids away from the d_{10}-Leu, facilitating deuterium modulation.[37] Unlike the α-helix, no deuterium modulation is detected at positions 3 and 4 amino acids away from the d_{10}-Leu in a linear β-strand, as the spin label's distance is more than 8 Å distant from the d_{10}-Leu. The application of the ESEEM technique has been mostly limited to modeling small protein segments with known structures.[17,18,30,38] In this study, ESEEM spectroscopic technique was employed to investigate the local secondary structure of a recently discovered antimicrobial membrane protein called gp28 featuring multiple predicted helices.

Phage lysis is a common cell fate, and dsDNA phages in Gram-negative bacteria are extensively studied to elaborate on the molecular details of this process. The lytic process occurs through the canonical holin-endolysin pathway or the pinholin-SAR endolysin pathway, involving three different classes of lysis proteins: holins, endolysins, and spanins.[39–41] The lysis process starts with holins (canonical holins or pinholins) creating holes in the inner cytoplasmic membrane (IM), followed by endolysins degrading the peptidoglycan (PG), and spanins disrupting the outer membrane.[42] The final stage of lysis typically involves spanins for disrupting the outer membrane (OM).[43] However, there are some phages that lack spanins but are still able to complete the lysis process.[43,44] gp28 is the first identified member of a new class of phage proteins termed disruptins, that lack spanin genes offering an alternative mechanism for degrading the OM. It is a cationic antimicrobial peptide (CAMP) with three predicted alpha helices and is produced by φKT to complement lambda lysis defects.[44]

The final stage of lysis typically involves spanins for disrupting the outer membrane (OM).[43] However, there are some phages that lack spanins but are still able to complete the lysis process.[43,44] gp28 is the first identified member of a new class of phage proteins termed disruptins, that lack spanin genes offering an alternative mechanism for degrading the OM. It is a cationic antimicrobial peptide (CAMP) with three predicted alpha helices and is produced by φKT to complement lambda lysis defects.[44]

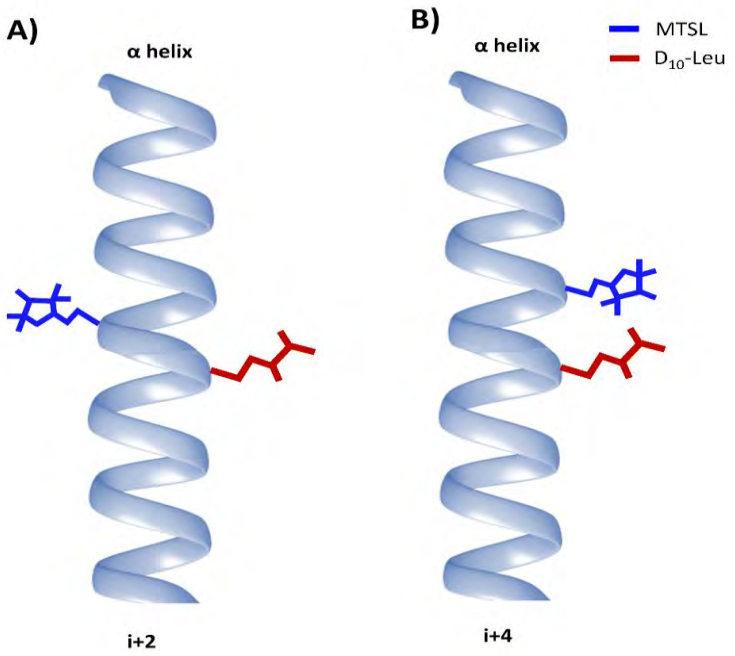

Figure 2. 1: For an alpha helix, A) when the spin label is positioned 2 amino acids away from the d10-Leu, both the spin label and the d10-Leu are situated on opposite sides of the alpha helix, exceeding the 8 Å ESEEM detection limit, B) when the spin label is moved to positions 3 or 4 amino acids away from the d10-Leu, the helical structure aligns with both labels on the same side of the helix, allowing for the detection of deuterium modulation.

The Ry Young group discovered the gp28 peptide and performed various experiments, including biomolecular and functional analyses, along with computational studies. The central focus of these studies was to predict the secondary structure and discern the hydrophobic and hydrophilic regions within the three helices.[44] However, further experiments are needed to validate the presence of the alpha helices as initially predicted by the Ry Young group. To investigate the local secondary structure of gp28, we synthesized gp28 constructs using solid phase peptide synthesis (SPPS) and employed ESEEM spectroscopic technique to study the peptide in a POPC/POPG bilayer membrane.

2.1. Experimental Methods

2.1.1. Peptide synthesis and purification

Solid-phase peptide synthesis was used to generate gp28 constructs using a CEM Liberty Blue Peptide Synthesizer with the Discovery Bio Microwave System which was then cleaved from the solid-phase resin using a trifluoroacetic acid (TFA) cleavage solution.[46,52] A crude peptide was obtained following an optimized cleavage procedure.[36,41] The crude gp28 was purified using reverse-phase high-performance

liquid chromatography (RP-HPLC) on a C4 prep column with a gradient of solvent B (90% acetonitrile/10% water/0.1% TFA). The purified peptides were then collected and lyophilized, and the resulting pure peptides were spin-labeled using MTSL.

Table 1.1: *The primary sequences of gp28 constructs for ESEEM spectroscopic studies. The position of deuterated Leu (d_{10} Leu) is represented by 'i', while the position of cysteine (spin-labeled) substitution is indicated as 'X'. The underlined segments in the primary sequence correspond to the predicted helices by the Ry Young group.*[44]

Wild type gp28:

MSKFK^{5}KY**L**GA^{10}AWDFT^{15}KEHGV^{20}TILRG^{25}VAVL**L**^{30}VGRKV^{35}GRVAN^{40}QSADV^{45}**L**DT VI^{50}KGTKKN^{56}

Helix 1	Leu 8	i-2	MSKFK^{5}**X**Y***i***GA^{10}AWDFT^{15}KEHGV^{20}TILRG^{25}VAVLL^{30}VGRKV^{35}GRVAN^{40}QSADV^{45}LDT VI^{50}KGTKKN^{56}
		i-3	MSKF**X**^{5}KY***i***GA^{10}AWDFT^{15}KEHGV^{20}TILRG^{25}VAVLL^{30}VGRKV^{35}GRVAN^{40}QSADV^{45}LDT VI^{50}KGTKKN^{56}
		i-4	MSK**X**K^{5}KY***i***GA^{10}AWDFT^{15}KEHGV^{20}TILRG^{25}VAVLL^{30}VGRKV^{35}GRVAN^{40}QSADV^{45}LDT VI^{50}KGTKKN^{56}
Helix 2	Leu 30	i+2	MSKFK^{5}KYLGA^{10}AWDFT^{15}KEHGV^{20}TILRG^{25}VAVL***i***^{30}V**X**RKV^{35}GRVAN^{40}QSADV^{45}LDT VI^{50}KGTKKN^{56}
		i+3	MSKFK^{5}KYLGA^{10}AWDFT^{15}KEHGV^{20}TILRG^{25}VAVL***i***^{30}VG**X**KV^{35}GRVAN^{40}QSADV^{45}LDT VI^{50}KGTKKN^{56}
		i+4	MSKFK^{5}KYLGA^{10}AWDFT^{15}KEHGV^{20}TILRG^{25}VAVL***i***^{30}VGR**X**V^{35}GRVAN^{40}QSADV^{45}LDT VI^{50}KGTKKN^{56}
Helix 3	Leu 46	i-2	MSKFK^{5}KY**L**GA^{10}AWDFT^{15}KEHGV^{20}TILRG^{25}VAVL**L**^{30}VGRKV^{35}GRVAN^{40}QSA**X**V^{45}***i***DT VI^{50}KGTKKN^{56}
		i-3	MSKFK^{5}KY**L**GA^{10}AWDFT^{15}KEHGV^{20}TILRG^{25}VAVL**L**^{30}VGRKV^{35}GRVAN^{40}QS**X**DV^{45}***i***DT VI^{50}KGTKKN^{56}
		i-4	MSKFK^{5}KY**L**GA^{10}AWDFT^{15}KEHGV^{20}TILRG^{25}VAVL**L**^{30}VGRKV^{35}GRVAN^{40}Q**X**ADV^{45}***i***D TVI^{50}KGTKKN^{56}

To remove excess spin labels, the spin-labeled peptides underwent another round of purification using RP-HPLC on a C4 semi-prep column with the same gradient and solvent system.[41,47] The purified peptides were subsequently freeze-dried (lyophilized) to obtain solid peptide samples and their purity confirmed by mass spectrometry. Nine variants of gp28 protein were synthesized for comprehensive investigation. Apart from these nine gp28 constructs, the synthesized wild type gp28 peptide without deuterated amino acids was used as a control. Table 1.1 provides an overview of the nine different positions of deuterated and spin-labeled peptides.

2.1.2. Sample preparation for ESEEM spectroscopy

A stock solution of the peptides was prepared using Trifluoroethanol (TFE) at a concentration of 2 mg/mL. The peptides were then reconstituted with buffer solution to facilitate their incorporation into POPC (1-palmitoyl-2-oleoyl-sn-glycero-3-phosphocholine)/POPG (1-palmitoyl-2-oleoyl-sn-glycero-3-phospho-(1'-rac-glycerol) (sodium salt)) vesicles. The desired molar ratio of the peptide to the lipids for POPC/POPG vesicles was set to 1:1000.[36] The 1:1000 protein-to-lipid ratio is often used to ensure that the protein is properly embedded in the lipid bilayer and retains its functional properties. The thin-film method was employed to incorporate the peptides into POPC/POPG (3:1) proteoliposomes.[36,41] Pure spin-labeled peptides dissolved in 2,2,2-Trifluoroethanol (TFE) were mixed with a pre-dissolved POPC/POPG lipid solution in a pear-shaped flask. The organic solvent was gently evaporated by purging with N_2 gas, resulting in a thin uniform film inside the flask. The flask was then placed in a vacuum desiccator overnight to eliminate any residual organic solvent.

To rehydrate the thin film and achieve a final concentration of 200 mM lipid and 200 μM peptide in proteoliposomes, a 20 mM HEPES (4-(2-hydroxyethyl)-1-piperazineethanesulfonic acid) buffer at pH ~7.0 was added to the flask. The lipid film was dispersed from the side wall through vortexing, followed by five freeze-thaw cycles before adding glycerol. A 10% glycerol solution was added to the sample and thoroughly mixed. Glycerol maintains the sample in the buffer system without phase separation for an extended period.[45] This helps to ensure that the liposomes remain intact by stabilizing the lipid bilayer, preventing aggregation, and acting as a cryoprotectant. Its use is particularly important since ESEEM experiments require consistent and functional proteoliposomes. The homogeneity and size of the proteoliposomes were confirmed using dynamic light scattering (DLS) spectroscopy with a ZETASIZER

NANO Series instrument (Malvern Instruments) at 25 °C, using a disposable 40 µL micro cuvette (**Figure 2.2**).[40]

2.1.3. Circular Dichroism (CD) data collection

CD spectra were obtained for gp28 peptides incorporated into proteoliposomes using an Aviv Circular Dichroism Spectrometer (Model 435) and a quartz cuvette with a path length of 1.0 mm.[35] To reduce the concentration of the protein and the vesicles, the gp28 peptides incorporated proteoliposomes samples were diluted ten times with phosphate buffer. The data were collected in the wavelength range of 260 to 190 nm with an average of 5 scans per sample and a bandwidth of 1 nm at a temperature of 25°C.[45]

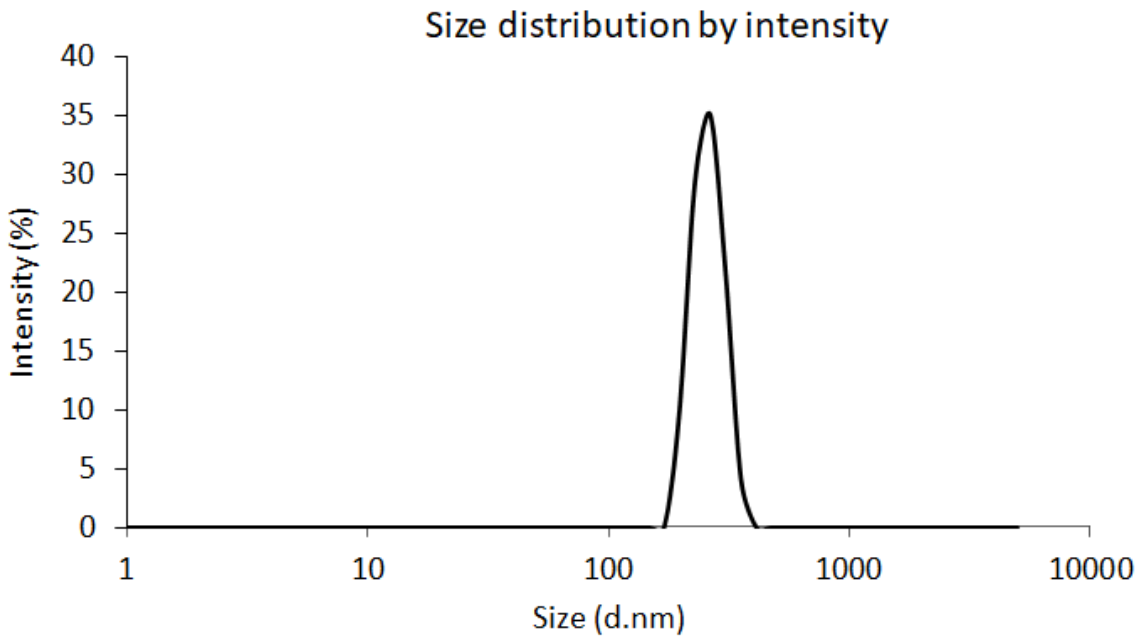

Figure 2. 2: DLS Data: Plotting the signal intensity as a log function of particle diameter for d10-L30 i+3 gp28 incorporated into POPC/POPG vesicles. The size of the vesicles was around 450 nm.

2.1.4. Sample preparation and instrumental setup for CW-EPR and ESEEM Spectroscopy

X-band CW-EPR (~9 GHz) spectra were utilized to determine the spin labeling efficiency, with all samples demonstrating over 85% labeling efficiency. Three-pulse (π/2-τ-π/2-T-π/2) ESEEM measurements were performed using a Bruker ELEXSYS E580 instrument equipped with an ER4118X MS3 resonator using a 200 ns tau value for ^{1}H modulation suppression. The measurements were

conducted at a microwave frequency of approximately 9.269 GHz and a magnetic field of around 3300 G, with a temperature of 80 K and 4-step phase cycling. The spectra were collected with a starting T value of 386 ns with an increase of 12 ns increments for a total of 512 points.[29] The ESEEM data were collected from a 90 μL sample volume incorporated into POPC/POPG vesicles. The time-domain data were fitted using a two-component exponential decay model. The maximum value for the exponential fit and the collected time-domain data were both scaled to one, following established literature procedures.[17,30,48] The scaled ESEEM spectrum was obtained by subtracting the normalized decay curve from the experimental data. Subsequently, Fourier Transformation (FT) was applied to the scaled ESEEM spectra to generate the corresponding frequency domain. The detected deuterium peak appeared at approximately 2.2 MHz, corresponding to the ^{2}H Larmor frequency.

2.2. Results and Discussion

In the cell lysis pathway of bacteriophages lacking spanins, gp28 protein plays a crucial role in the degradation of the outer cell membrane.[44] In this study, both CD spectroscopy and a well-established 3-pulse ESEEM spectroscopic method were employed to investigate the global and local secondary structure of gp28 within the membrane.[17,30] **Figure 2.3** presents representative CD spectra of the wild type gp28 (blue) and spin-labeled construct of gp28 (d_{10}-L30 i+3) (black). The CD spectra were obtained by averaging signals from five scans. The plot shows the mean residue molar ellipticity (MRE) as a function of the incident radiation wavelength. In both cases, double minima at 208 and 222 nm were observed, indicating the presence of a global α-helical secondary structure and the results are consistent with the published data showing that spin-labelling did not alter the global secondary structure of gp28.[17,58]

Once the global secondary structure of the peptides was confirmed, the ESEEM spectroscopic approach was utilized to explore the local secondary structure. In this study, specific positions within the predicted alpha helical regions were chosen for an investigation of the three predicted helices.[44] The position of deuterated amino acid (d_{10}-L) and spin labeling positions (i±n; n=1, 2, 3) were chosen judiciously. For studying helix 1, L8 residue was replaced with d_{10}-L8 (deuterated leucine). Likewise, for helix 2 and helix 3, the L30 and L46 residues were replaced with deuterated leucine, respectively. **Figure 2.4** shows a set of representative ESEEM spectroscopic data for d_{10}-L46 gp28 constructs, indicating the observed modulation in the i-3 and i-4 positions of the time domain, specifically for helix 3. This modulation occurs at a frequency of ~2.2 MHz, corresponding to the ^{2}H Larmor frequency observed in the i-3 and i-4

positions of the spin label, as depicted in **Figure 2.4B**. The presence of the deuterium peak at positions i-3 and i-4, and the absence of the peak at i-2, indicates an α-helical secondary structure for d_{10}-L46 gp28 constructs (**Figure 2.4B**, and **2.5C**).[17,29,31,32,34,50]

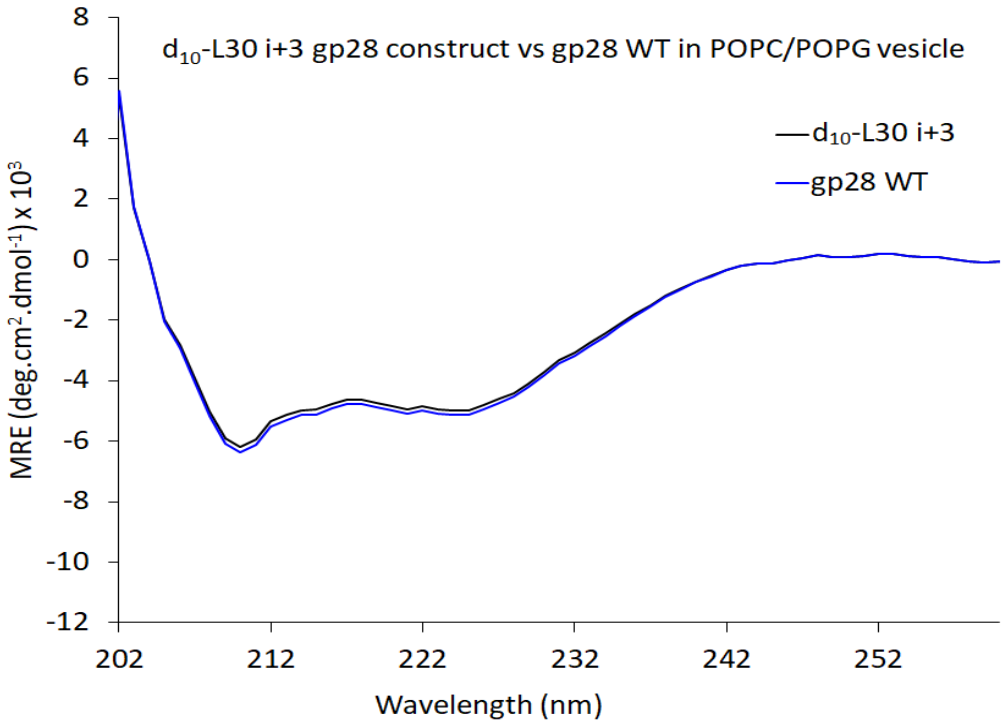

*Figure 2. 3***:** *Circular dichroism spectra of gp28 Wild type (WT) and spin-labeled gp28 (d10-L30 i+3) incorporated into POPC/POPG proteoliposomes.*

Upon confirmation of the presence of an alpha helical structure in helix 3, additional d_{10}-L46 gp28 constructs were prepared with the spin-label in the opposite direction (N□C) of the sequence, namely i+2, i+3, and i+4 (S3). The results obtained for the second set of d_{10}-L46 gp28 constructs corroborate the findings obtained from the first set, thereby confirming the presence of an alpha helical structure (**Figure 2.5C,** and **S2.3**). The pattern observed for d_{10}-L46 gp28 constructs arises from the 3.6 amino acid turn periodicity of α-helices, which aligns the spin label (i±3 and i±4) and deuterated leucine side chain on the same face of the helix, enabling detection of ^{2}H modulation. In contrast, the i±2 position falls on the opposite face of the helix and is beyond the 8 Å detection limit, and thus no ^{2}H modulation was observed for these samples (**Figure 2.5C**, and **S2.3**).[47] Similarly, to check for helix 1, a set of d_{10}-L8 gp28 constructs were used to prepare the corresponding ESEEM samples. The alpha helical pattern can also be observed for the i-2, i-3, and i-4 samples (C□N) of the d_{10}-L8 gp28 (**Figure 2.5A**, and **S2.1**). Additionally, the

presence of an alpha helical secondary structure is clearly discernible for helix 2. As illustrated in **Figure 2.5B**, deuterated L30 exhibits deuterium modulation peaks at the i+3 and i+4 positions, while the i+2 position does not display such modulation. Some minor peaks observed in certain samples may arise from the interaction between the spin label and a small portion of deuterated side chains or unfolded protein.[53] gp28 is a surface peptide and the helical folding for helix 1 might be slightly different while interacting with lipid surfaces that may introduce some minor peaks. Helix 1 might be also exposed to solvents and that can also influence the folding as shown by our previous findings.[58] The peak at approximately 8 MHz may also arise due to the presence of ^{13}P within the solution.

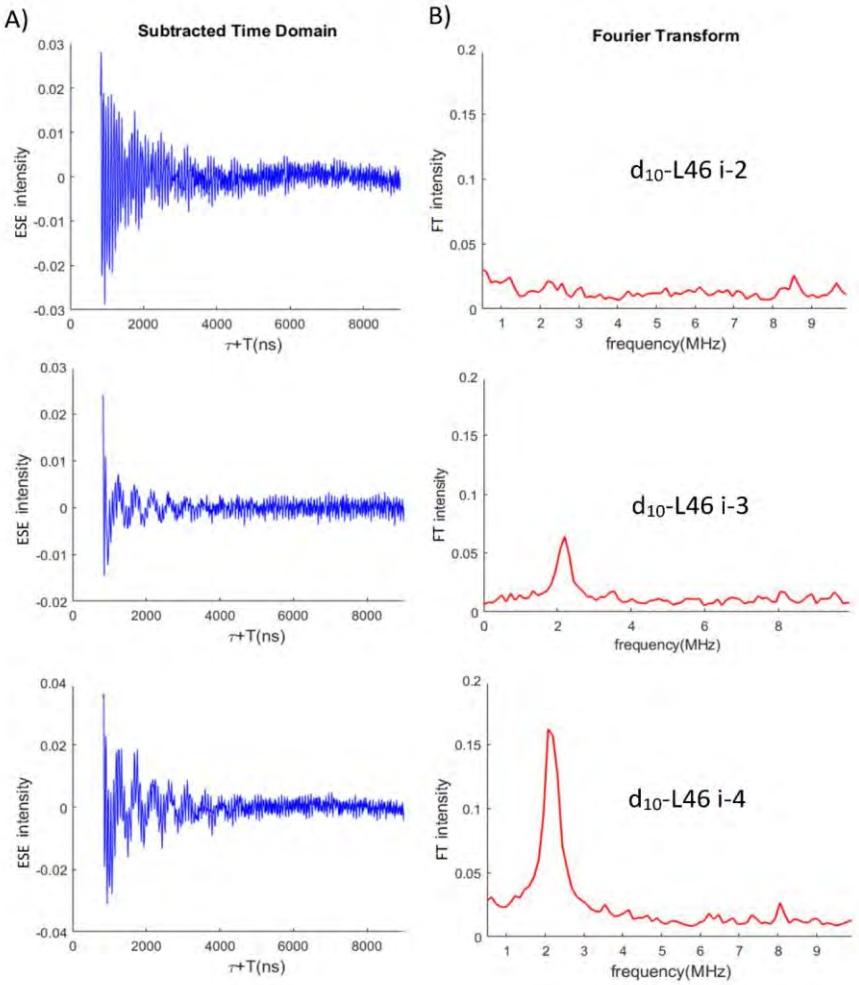

Figure 2. 4: ESEEM data for the gp28 with a deuterated (d_{10}) leucine (Leu) side chain at position 46 in helix 3 incorporated in POPC/POPG liposomes at a protein to lipid ratio of 1:1000. (A) The modulation of deuterium (^2H) observed in the time domain (blue) is reflected by the modulation peaks in the frequency domain intensity (red) (B). ESE: Electron Spin Echo, FT: Fourier Transform.

Additionally, the normalized peak intensities for ^{2}H modulation were analyzed and compared to understand the local helical pattern of gp28 constructs. **Figure 2.6** displays the normalized frequency intensity for all data collected in POPC/POPG vesicles. All the samples had an ESEEM FT ^{2}H peak intensity above the 0.02 level.[31,49]

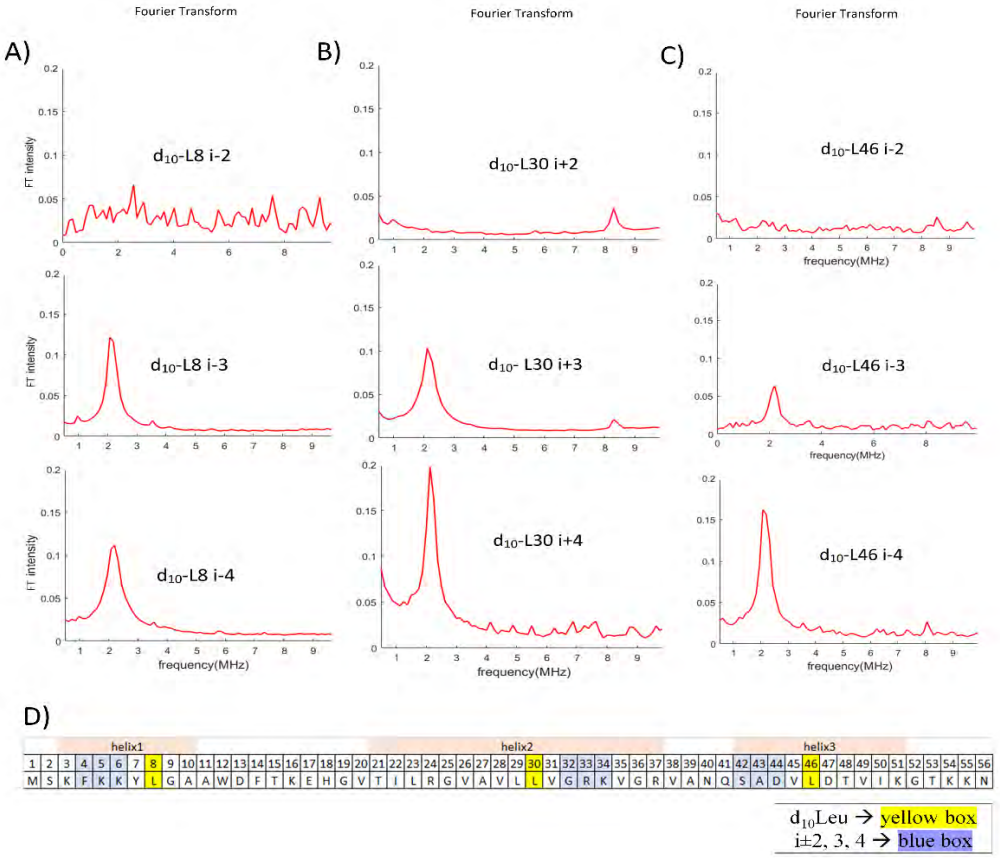

Figure 2. 5: The figure represents ^{2}H frequency domain intensity for all gp28 constructs studied with ESEEM spectroscopy: A) ^{2}H frequency domain intensity for d_{10}-L8 gp28 constructs of helix 1(C→N), B) ^{2}H frequency domain intensity for d_{10}-L30 gp28 constructs of helix 2 (N→C), C) ^{2}H frequency domain intensity for d_{10}-L8 gp28 constructs of helix 3 (C→N). All samples were reconstituted into POPC/POPG vesicles (3:1). D) The primary sequence of gp28 having d_{10}-Leu highlighted in yellow, and spin labeled positions are highlighted in blue. FT: Fourier Transform.

The intensities of the ESEEM ^{2}H peaks ranged from 0.02 to 0.19. The variations in FT peak intensities for the ^{2}H modulation at these positions were pronounced in helix 1 compared to the data for helix 2 and 3. The plot enables the differentiation between the various helices, such as a 3_{10} helix with a 3.1 amino acid turn periodicity or a π helix with a 4.1-4.4 amino acid turn periodicity, by comparing the normalized frequency domain intensities.[38,54,55]

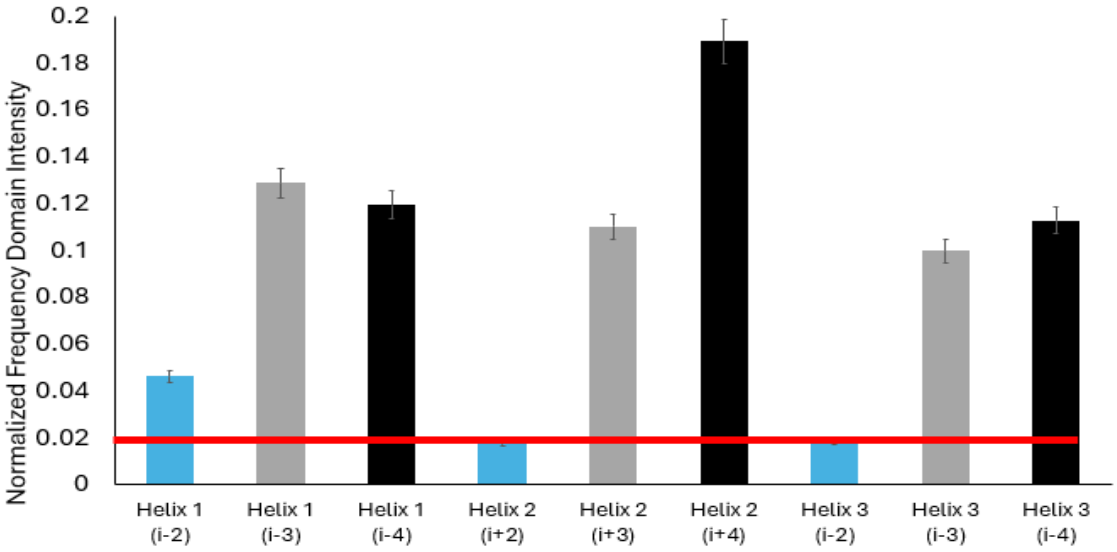

Figure 2. 6: Comparison of normalized FT frequency domain intensity for each gp28 construct in POPC/POPG vesicles at a protein to lipid ratio of 1:1000.

The ESEEM data consistently exhibit greater ^{2}H modulation in both the time domain and frequency domain, particularly evident in samples i ± 4 and i ± 3. Moreover, the ^{2}H modulation in i ± 4 samples consistently shows greater depth compared to i ± 3 samples apart from helix 1. The variations in intensity between positions can be attributed to two primary factors. The first difference arises from the local environment of the helices that influence the mobility and packing of the spin label and d_{10}-Leu side chain. Previous data found that helix 1 could either be completely exposed to the solvent or shows partial electrostatic interaction with lipid head groups, whereas helix 2 and helix 3 clearly interacted with the lipid bilayer.[58] The second factor is the presence of multiple torsion angles in longer side chains, such as leucine, and the fact that MTSL-labeled cysteine also introduces five torsion angles (χ1–5).[46,56,57] This results support the power saturation and molecular dynamics simulation results, which indicated that there is a stable interaction of helix 2 with the phospholipid membrane bilayer, contrasting with helix 1's tendency to remain unstructured and unravel unless supported by contact with the other two helices.[58] These results significantly contribute to our existing knowledge and provide valuable insights into the structural properties of gp28, enabling its application in the study of more complex protein systems using the ESEEM approach.

2.3. Conclusion

Our study of local secondary structures in proteins, particularly gp28 protein, contributes to an understanding of their function, stability, ligand binding sites, and biomolecular interactions. This

knowledge is crucial for protein engineering, conformational study, and gaining evolutionary insights, leading to possible advancements in biotechnological and medicinal applications. In this study, we investigated the local secondary structure of the gp28 protein in POPC/POPG vesicles using the 3-pulse ESEEM spectroscopic method. These findings, which are a significant contribution to the biophysical field, confirm the presence of a global alpha-helical secondary structure for gp28 peptide from CD spectroscopy. The ESEEM approach was then employed to explore the local secondary structure, explicitly focusing on positions within the predicted alpha-helical regions. Our analysis of the ESEEM spectroscopic data confirmed the presence of the α-helical secondary structure for the gp28 constructs for all three helices as suggested by researchers from the Ry Young group.[44,58]

To validate the presence of an alpha-helical structure and investigate the residues incorporated into helix 3, we conducted additional experiments using spin-labeled constructs in the opposite direction. This was particularly important because the predicted length of helix 3 is relatively small. The observed ^{2}H modulation patterns and their Fourier-transformed peaks were consistent with the expected characteristics of α-helices. The comparison of normalized frequency intensity in the POPC/POPG vesicles further supported the differentiation of helices based on their amino acid turn periodicities. These results confirm that all three predicted gp28 helices in POPC/POPG vesicles have an α-helical secondary structure. The findings from this study, combined with our previous investigations, will contribute to a data library that supports the application of the ESEEM approach in studying more complex protein systems.[23,45,47]

2.4. Supporting Information

This section contains all the ESEEM data for the labelled sites of gp28 peptide, frequency and time domain and its corresponding Fourier Transform data.

Supplementary material:

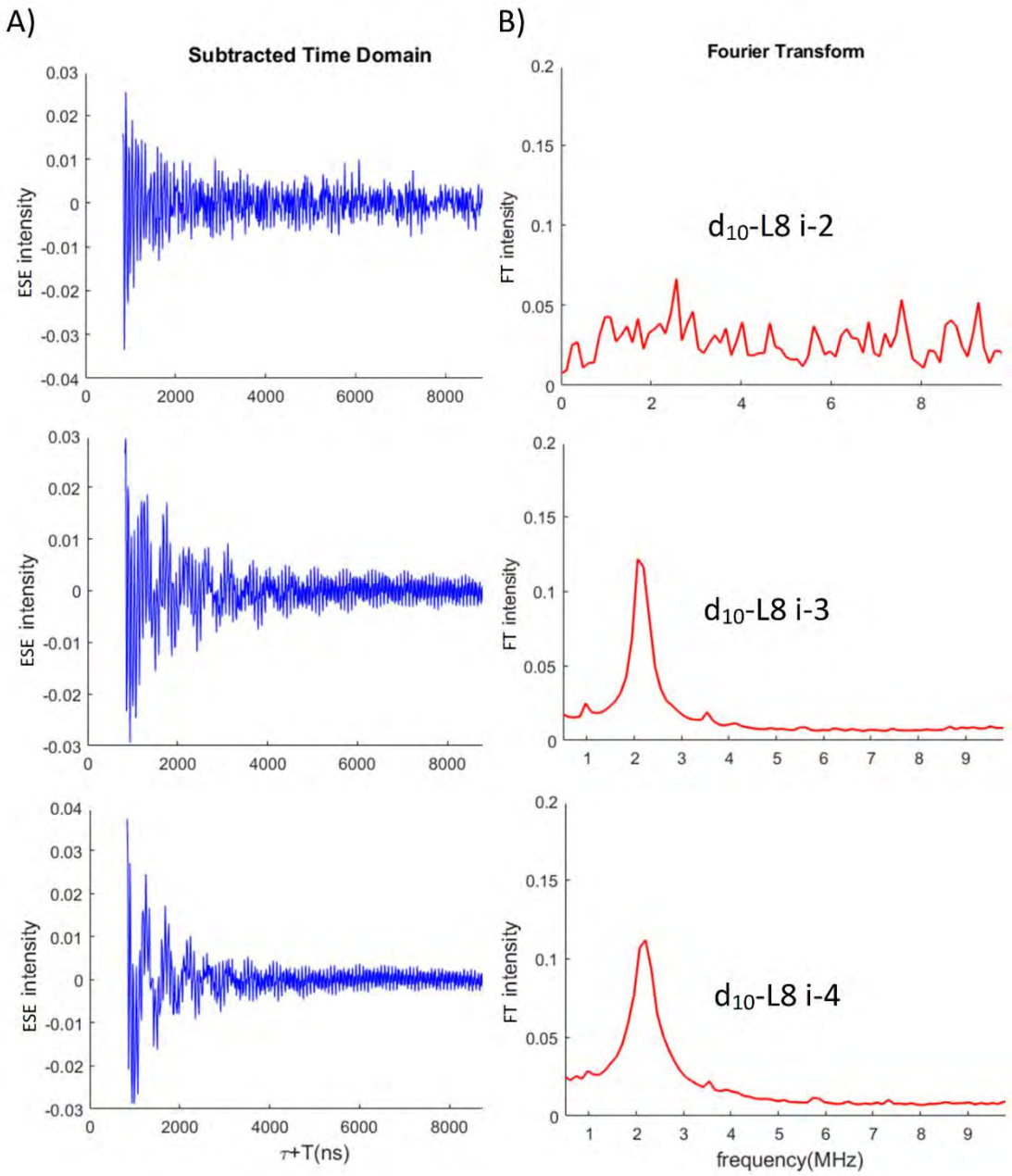

Figure S2.1: *ESEEM data for the gp28 with a deuterated (d_{10}) leucine (Leu) side chain at position 8 in helix 1 for i-2, i-3 and i-4(C→N) incorporated in POPC/POPG liposomes at a protein to lipid ratio of 1:1000. (A) The modulation of deuterium (^2H) observed in the time domain (blue) is reflected by the peaks in the frequency domain intensity (red) (B). ESE: Electron Spin Echo, FT: Fourier Transform.*

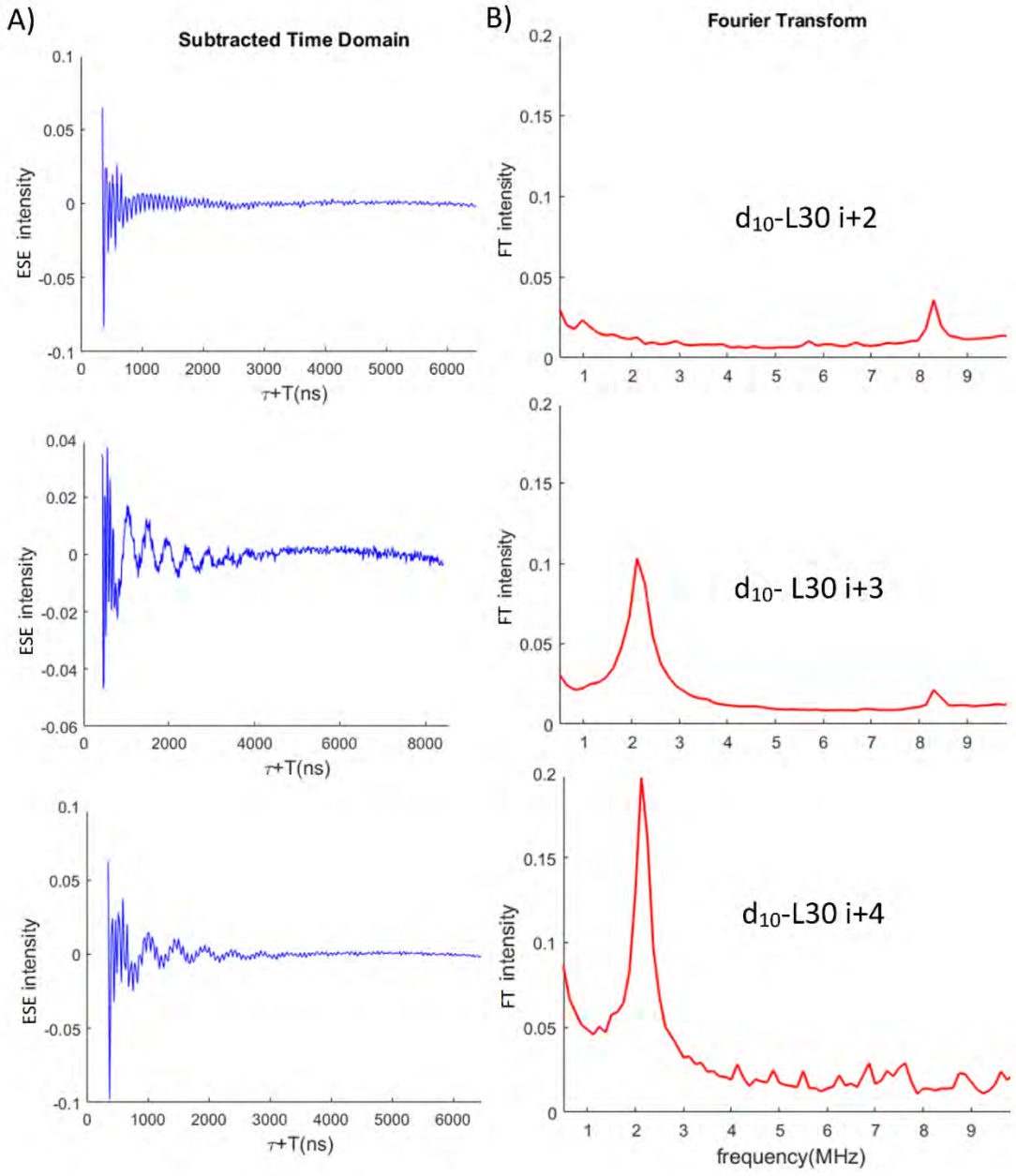

Figure S2.2*: ESEEM data for the gp28 with a deuterated (d10) leucine (Leu) side chain at position 30 in helix 2 for i+2, i+3 and i+4(N→C) incorporated in POPC/POPG liposomes at a protein to lipid ratio of 1:1000. (A) The modulation of deuterium (^{2}H) observed in the time domain (blue) is reflected by the peaks in the frequency domain intensity (red) (B). ESE: Electron Spin Echo, FT: Fourier Transform.*

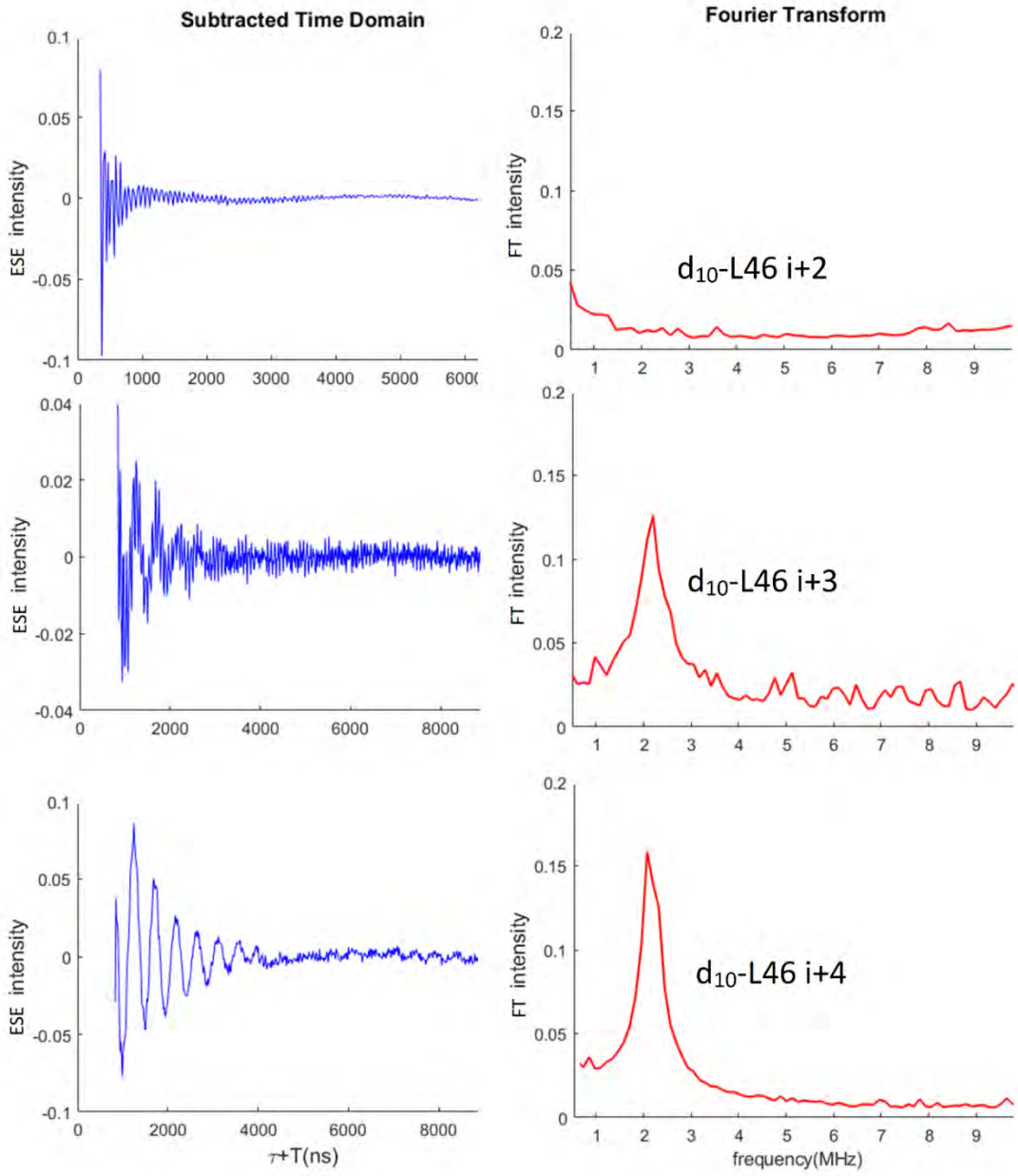

Figure S2.3: *ESEEM data for the gp28 with a deuterated (d_{10}) leucine (Leu) side chain at position 46 in helix 3 for i+2, i+3 and i+4(C→N) incorporated in POPC/POPG liposomes at a protein to lipid ratio of 1:1000. (A) The modulation of deuterium (^2H) observed in the time domain (blue) is reflected by the peaks in the frequency domain intensity (red) (B). ESE: Electron Spin Echo, FT: Fourier Transform.*

Acknowledgments

Gary A. Lorigan would like to acknowledge support from NSF CHE – 2305834 grant and Miami University. Dr. Sahu would also like to acknowledge the support from National Science Foundation NSF MCB-2040917.

References

1. Young, R. Phage Lysis: Three Steps, Three Choices, One Outcome. *J. Microbiol.* **2014**, *52*, 243–258. https://doi.org/10.1007/s12275-014-4087-z.

2. Lappano, R.; Maggiolini, M. G Protein-Coupled Receptors: Novel Targets for Drug Discovery in Cancer. *Nat. Rev. Drug Discov.* **2011**, *10*, 47–60. https://doi.org/10.1038/nrd3320.

3. Tautermann, C. S. GPCR Structures in Drug Design: Emerging Opportunities with New Structures. *Bioorg. Med. Chem. Lett.* **2014**, *24*, 4073–4079. https://doi.org/10.1016/j.bmcl.2014.07.009.

4. Bordag, N.; Keller, S. α-Helical Transmembrane Peptides: A "Divide and Conquer" Approach to Membrane Proteins. *Chem. Phys. Lipids* **2010**, *163*, 1–26. https://doi.org/10.1016/j.chemphyslip.2009.07.009.

5. Huang, C.; Mohanty, S. Challenging the Limit: NMR Assignment of a 31 kDa Helical Membrane Protein. *J. Am. Chem. Soc.* **2010**, *132*, 3662–3663. https://doi.org/10.1021/ja100078z.

6. Chang, L.; Mondal, A.; Singh, B.; Martínez-Noa, Y.; Perez, A. Revolutionizing Peptide-Based Drug Discovery: Advances in the Post-AlphaFold Era. *Wiley Interdiscip. Rev.: Comput. Mol. Sci.* **2024**, *14*, e1693. https://doi.org/10.1002/wcms.1693.

7. Zhao, X.; Yang, V. B.; Menta, A. K.; Blum, J.; Wahida, A.; Subbiah, V. AlphaFold's Predictive Revolution in Precision Oncology. *AI Precision Oncol.* **2024**, *1*, 160–167.

8. Yang, X.; Wang, Y.; Byrne, R.; Schneider, G.; Yang, S. Concepts of Artificial Intelligence for Computer-Assisted Drug Discovery. *Chem. Rev.* **2019**, *119*, 10520–10594. https://doi.org/10.1021/acs.chemrev.9b00328.

9. Kaku, M. *Visions: How Science Will Revolutionize the 21st Century*; Anchor: New York, 2011.

10. Fer, J.; Benison, K. C.; Lloyd, K. G.; Cordero, R. J.; de Campos, C. B.; Yakimov, M. M. Amils, R. Scientific Novelty Beyond the Experiment. *Microb. Biotechnol.* **2023**, *16*, 1131–1173. https://doi.org/10.1111/1751-7915.14222.

11. Hammer, R. P.; McLaughlin, M. L. Amphipathic Control of the 3_{10}-/α-Helix Equilibrium in Synthetic Peptides. *J. Pept. Res.* **2001**, *58*, 108–116. https://doi.org/10.1034/j.1399-3011.2001.00926.x.

12. Millhauser, G. L. 3_{10}-Helices and α-Helices: The Split Personality of Polypeptide Helices. *Acc. Chem. Res.* **1999**, *32*, 1027–1033. https://doi.org/10.1021/ar990010m.

13. Zhang, R.; Sahu, I. D.; Gibson, K. R.; Muhammad, N. B.; Bali, A. P.; Comer, R. G.; Liu, L.; Craig, A. F.; McCarrick, R. M.; Dabney-Smith, C.; et al. Development of Electron Spin Echo Envelope Modulation Spectroscopy to Probe the Secondary Structure of Recombinant Membrane Proteins in a Lipid Bilayer. Protein Sci. 2015, 24, 1707–1713. https://doi.org/10.1002/pro.2795.

14. Khrustalev, V. V.; Barkovsky, E. V.; Khrustaleva, T. A. The Influence of Flanking Secondary Structures on Amino Acid Content and Typical Lengths of 3_{10}-Helices. *Int. J. Proteomics* **2014**, *2014*, 1–10. https://doi.org/10.1155/2014/360230.

15. Smythe, M. L.; Nakaie, C. R.; Marshall, G. R. 3_{10}-Helical Conformation of Alanine-Based Peptides in Aqueous Solution: An Electron Spin Resonance Study. *J. Am. Chem. Soc.* **1995**, *117*, 10555–10562. https://doi.org/10.1021/ja00147a018.

16. Hanson, P.; Millhauser, G.; Formaggio, F.; Crisma, M.; Toniolo, C. ESR Characterization of Hexameric, Helical Peptides Using Double TOAC Spin Labeling. *J. Am. Chem. Soc.* **1996**, *118*, 7618–7625. https://doi.org/10.1021/ja953738s.

17. Toniolo, C.; Polese, A.; Formaggio, F.; Crisma, M.; Kamphuis, J. Circular Dichroism Spectrum of a Peptide 3_{10}-Helix. *J. Am. Chem. Soc.* **1996**, *118*, 2744–2745. https://doi.org/10.1021/ja953738s.

18. Liu, L.; Mayo, D. J.; Sahu, I. D.; Zhou, A.; Zhang, R.; McCarrick, R. M.; Lorigan, G. A.; et al. Determining the Secondary Structure of Membrane Proteins and Peptides via Electron Spin Echo

Envelope Modulation (ESEEM) Spectroscopy. In *Methods in Enzymology*; Elsevier: Amsterdam, 2015; Vol. 564, pp 59–100. https://doi.org/10.1016/bs.mie.2015.06.037.

19. Hubbell, W. L.; López, C. J.; Altenbach, C.; Yang, Z. Technological Advances in Site-Directed Spin Labeling of Proteins. *Curr. Opin. Struct. Biol.* **2013**, *23*, 725–733. https://doi.org/10.1016/j.sbi.2013.06.008.

20. Petratos, K.; Gessmann, R. Three Complete Turns of a 3_{10}-Helix at Atomic Resolution: The Crystal Structure of Z-$(Aib)_{11}$-OtBu. *J. Pept. Sci.* **2003**, *9*, 753–762. https://doi.org/10.1002/psc.490.

21. Marshall, G. R.; Hodgkin, E. E.; Langs, D. A.; Smith, G. D.; Zabrocki, J.; Leplawy, M. T. Factors Governing Helical Preference of Peptides Containing Multiple α, α-Dialkyl Amino Acids. *Proc. Natl. Acad. Sci. U.S.A.* **1990**, *87*, 487–491. https://doi.org/10.1073/pnas.87.1.487.

22. Henzler-Wildman, K. A.; Lee, D. K.; Ramamoorthy, A. Determination of α-Helix and β-Sheet Stability in the Solid State: A Solid-State NMR Investigation of Poly(L-alanine). *Biopolymers* **2002**, *64*, 246–254. https://doi.org/10.1002/bip.10180.

23. Mammi, S.; Rainaldi, M.; Bellanda, M.; Schievano, E.; Peggion, E.; Broxterman, Q. B.; Formaggio, F.; Crisma, M.; Toniolo, C. Concomitant Occurrence of Peptide 3_{10}- and α-Helices Probed by NMR. *J. Am. Chem. Soc.* **2000**, *122*, 11735–11736. https://doi.org/10.1021/ja0023668.

24. Gratias, R.; Konat, R.; Kessler, H.; Crisma, M.; Valle, G.; Polese, A.; Formaggio, F.; Toniolo, C.; Broxterman, Q. B.; Kamphuis, J. First Step Toward the Quantitative Identification of Peptide 3_{10}-Helix Conformation with NMR Spectroscopy: NMR and X-Ray Diffraction Structural Analysis of a Fully Developed 3_{10}-Helical Peptide Standard. *J. Am. Chem. Soc.* **1998**, *120*, 4763–4770. https://doi.org/10.1021/ja973735t.

25. Millhauser, G. L.; Stenland, C. J.; Hanson, P.; Bolin, K. A.; van de Ven, F. J. M. Estimating the Relative Populations of 3_{10}-Helix and α-Helix in Ala-Rich Peptides: A Hydrogen Exchange and High Field NMR Study. *J. Mol. Biol.* **1997**, *267*, 963–974. https://doi.org/10.1006/jmbi.1997.0923.

26. Wu, Y.; Zhao, Y.; Bay, C. W.; Kong, H. A Theoretical Study on the Origin of Cooperativity in the Formation of 3_{10}- and α-Helices. *J. Am. Chem. Soc.* **2001**, *123*, 5313–5319. https://doi.org/10.1021/ja003482n.

27. Karpen, M. E.; Neet, K. E. Differences in the Amino Acid Distributions of 3_{10}-Helices and α-Helices. *Protein Sci.* **1992**, *1*, 1333–1342. https://doi.org/10.1002/pro.5560011013.

28. Ã, N. K. Helix–Helix Interactions and Their Impact on Protein Motifs and Assemblies. *J. Theor. Biol.* **2010**, *264*, 585–592. https://doi.org/10.1016/j.jtbi.2010.02.026.

29. Hong, M. Practical Use of Chemical Shift Databases for Protein Solid-State NMR: 2D Chemical Shift Maps and Amino-Acid Assignment with Secondary-Structure Information. *J. Biomol. NMR* **2013**, *56*, 155–167. https://doi.org/10.1007/s10858-013-9732-z.

30. Drew, D. L.; Ahammad, T.; Serafin, R. A.; Sahu, I. D.; Khan, R. H.; Faul, E.; McCarrick, R. M.; Lorigan, G. A. Probing the Local Secondary Structure of Bacteriophage S21 Pinholin Membrane Protein Using Electron Spin Echo Envelope Modulation Spectroscopy. *Biochim. Biophys. Acta, Biomembr.* **2022**, *1864*, 183836. https://doi.org/10.1016/j.bbamem.2021.183836.

31. Bottorf, L.; Ra, S.; Sahu, I. D.; McCarrick, R. M.; Lorigan, G. A. Utilizing Electron Spin Envelope Modulation to Distinguish between the Local Secondary Structures of an α-Helix and an Amphipathic 3_{10}-Helical Peptide. *J. Phys. Chem. B* **2017**, *121*, 2961–2967. https://doi.org/10.1021/acs.jpcb.7b00626.

32. Liu, L.; Sahu, I. D.; Bottorf, L.; McCarrick, R. M.; Lorigan, G. A. Investigating the Secondary Structure of Membrane Peptides Utilizing Multiple ^{2}H-Labeled Hydrophobic Amino Acids via Electron Spin Echo Envelope Modulation (ESEEM) Spectroscopy. *J. Phys. Chem. B* **2018**, *122*, 1–9. https://doi.org/10.1021/acs.jpcb.7b11890.

33. Sahu, I. D.; McCarrick, R. M.; Lorigan, G. A. Use of Electron Paramagnetic Resonance to Solve Biochemical Problems. *Biochemistry* **2013**, *52*, 5967–5984. https://doi.org/10.1021/bi400834a.

34. Carmieli, R.; Papo, N.; Zimmermann, H.; Potapov, A.; Shai, Y.; Goldfarb, D. Utilizing ESEEM Spectroscopy to Locate the Position of Specific Regions of Membrane-Active Peptides within Model Membranes. *Biophys. J.* **2006**, *90*, 492–505. https://doi.org/10.1529/biophysj.105.062992.

35. Sun, L.; Hernandez-Guzman, J.; Warncke, K. OPTESIM, a Versatile Toolbox for Numerical Simulation of Electron Spin Echo Envelope Modulation (ESEEM) That Features Hybrid Optimization and Statistical Assessment of Parameters. *J. Magn. Reson.* **2009**, *200*, 21–28. https://doi.org/10.1016/j.jmr.2009.05.012.

36. Drew, D. L.; Ahammad, T.; Serafin, R. A.; Sahu, I. D.; Khan, R. H.; Faul, E.; McCarrick, R. M.; Lorigan, G. A. Probing the Local Secondary Structure of Bacteriophage S21 Pinholin Membrane Protein Using Electron Spin Echo Envelope Modulation Spectroscopy. *Biochim. Biophys. Acta, Biomembr.* **2021**, *1864*, 183836. https://doi.org/10.1016/j.bbamem.2021.183836.

37. Zhou, A.; Abu-Baker, S.; Sahu, I. D.; Liu, L.; McCarrick, R. M.; Dabney-Smith, C.; Lorigan, G. A. Determining α-Helical and β-Sheet Secondary Structures via Pulsed Electron Spin Resonance Spectroscopy. *Biochemistry* **2012**, *51*, 7417–7419. https://doi.org/10.1021/bi3010736.

38. Bottorf, L.; Ra, S.; Sahu, I. D.; McCarrick, R. M.; Lorigan, G. A. Utilizing Electron Spin Echo Envelope Modulation to Distinguish between the Local Secondary Structures of an α-Helix and an Amphipathic 3_{10}-Helical Peptide. *J. Phys. Chem. B* **2017**, *121*, 2961–2967. https://doi.org/10.1021/acs.jpcb.7b00626.

39. Cahill, J.; Young, R. Phage Lysis: Multiple Genes for Multiple Barriers. *Adv. Virus Res.* **2019**, *103*, 33–70. https://doi.org/10.1016/bs.aivir.2018.09.003.

40. Park, T.; Struck, D. K.; Dankenbring, C. A.; Young, R. The Pinholin of Lambdoid Phage 21: Control of Lysis by Membrane Depolarization. *J. Bacteriol.* **2007**, *189*, 9135–9139. https://doi.org/10.1128/JB.00847-07.

41. Ahammad, T.; Drew, D. L.; Sahu, I. D.; Serafin, R. A.; Clowes, K. R.; Lorigan, G. A. Continuous Wave Electron Paramagnetic Resonance Spectroscopy Reveals the Structural Topology and Dynamic Properties of Active Pinholin S2168 in a Lipid Bilayer. *J. Phys. Chem. B* **2019**, *123*, 8048–8056. https://doi.org/10.1021/acs.jpcb.9b06480.

42. Young, R. Phage Lysis: Do We Have the Hole Story Yet? *Curr. Opin. Microbiol.* **2013**, *16*, 790–797. https://doi.org/10.1016/j.mib.2013.08.008.

43. Berry, J.; Rajaure, M.; Pang, T.; Young, R. The Spanin Complex Is Essential for Lambda Lysis. *J. Bacteriol.* **2012**, *194*, 5667–5674. https://doi.org/10.1128/JB.01245-12.

44. Holt, A.; Cahill, J.; Ramsey, J.; Martin, C.; O'Leary, C.; Moreland, R.; Maddox, L. T.; Galbadage, T.; Sharan, R.; Sule, P.; Cirillo, J. D.; Young, R. Phage-Encoded Cationic Antimicrobial Peptide Required for Lysis. *J. Bacteriol.* **2022**, *204*. https://doi.org/10.1128/JB.00214-21.

45. Ahammad, T. Probing the Structural Dynamics, Conformational Change, and Topology of Pinholin S21, a Bacteriophage Lytic Protein, Using Electron Paramagnetic Resonance Spectroscopy. Ph.D. Dissertation, Miami University, 2020. https://doi.org/10.1093/nq/s8-VIII.187.68-g.

46. Chandrudu, S.; Simerska, P.; Toth, I. Chemical Methods for Peptide and Protein Production. *Molecules* **2013**, *18*, 4373–4388. https://doi.org/10.3390/molecules18044373.

47. Ahammad, T.; Drew, D. L.; Sahu, I. D.; Khan, R. H.; Butcher, B. J.; Serafin, R. A.; Galende, A. P.; McCarrick, R. M.; Lorigan, G. A. Conformational Differences Are Observed for the Active and Inactive Forms of Pinholin S21 Using DEER Spectroscopy. *J. Phys. Chem. B* **2020**, *124*, 11396–11405. https://doi.org/10.1021/acs.jpcb.0c09081.

48. Bottorf, L.; Sahu, I. D.; McCarrick, R. M.; Lorigan, G. A. Utilization of ^{13}C-Labeled Amino Acids to Probe the α-Helical Local Secondary Structure of a Membrane Peptide Using Electron Spin Echo Envelope Modulation (ESEEM) Spectroscopy. *Biochim. Biophys. Acta, Biomembr.* **2018**, *1860*, 1447–1451. https://doi.org/10.1016/j.bbamem.2018.04.001.

49. Liu, L. Development and Application of a Novel Pulsed EPR Approach for Membrane Protein Local Secondary Structure Characterization. Ph.D. Dissertation, Miami University, 2013. https://doi.org/10.1093/nq/s8-VIII.187.68-g.

50. Deligiannakis, Y.; Rutherford, A. W. Electron Spin Echo Envelope Modulation Spectroscopy in Photosystem I. *Biochim. Biophys. Acta, Bioenerg.* **2001**, *1507*, 226–246. https://doi.org/10.1016/S0005-2728(01)00201-8.

51. Drew, D. L. Investigating the Structure and Dynamic Properties of Bacteriophage S21 Pinholin Using Solid-State Nuclear Magnetic Resonance and Electron Paramagnetic Resonance

Spectroscopy. Ph.D. Dissertation, Miami University, 2021. https://doi.org/10.1093/nq/s8-VIII.187.68-g.

52. Van Doorslaer, S.; Vinck, E. The Strength of EPR and ENDOR Techniques in Revealing Structure-Function Relationships in Metalloproteins. *Phys. Chem. Chem. Phys.* **2007**, *9*, 4620–4638. https://doi.org/10.1039/b701568b.

53. Cieslak, J. A.; Focia, P. J.; Gross, A. Electron Spin-Echo Envelope Modulation (ESEEM) Reveals Water and Phosphate Interactions with the KcsA Potassium Channel. *Biochemistry* **2010**, *49*, 1486–1494. https://doi.org/10.1021/bi9016523.

54. Low, B. W.; Baybutt, R. B. The π-Helix: A Hydrogen Bonded Configuration of the Polypeptide Chain. *J. Am. Chem. Soc.* **1952**, *74*, 5806–5807. https://doi.org/10.1021/ja01142a540.

55. Kumar, P.; Bansal, M. Dissecting π-Helices: Sequence, Structure and Function. *FEBS J.* **2015**, *282*, 4415–4432. https://doi.org/10.1111/febs.13507.

56. Columbus, L.; Kalai, T.; Jeko, J.; Hideg, K.; Hubbell, W. L. Molecular Motion of Spin-Labeled Side Chains in α-Helices: Analysis by Variation of Side Chain Structure. *Biochemistry* **2001**, *40*, 3828–3846. https://doi.org/10.1021/bi002645j.

57. Columbus, L.; Hubbell, W. L. A New Spin on Protein Dynamics. *Trends Biochem. Sci.* **2002**, *27*, 288–295. https://doi.org/10.1016/S0968-0004(02)02095-9.

58. Khan, R. H.; Rotich, N. C.; Morris, A.; Ahammad, T.; Baral, B.; Sahu, I. D.; Lorigan, G. A. Probing the Structural Topology and Dynamic Properties of gp28 Using Continuous Wave Electron Paramagnetic Resonance Spectroscopy. *J. Phys. Chem. B* **2023**, *127*, 9236–9247. https://doi.org/10.1021/acs.jpcb.3c03679.

Chapter 3

A Comparison of the Effect of SMA Derivatives on the Structural Topology and Dynamics of Two Bacteriophage Peptides

Nancy C. Rotich[1], Evelyn A. Okorafor[1], Indra D. Sahu[2,1], Dominik Konkolewicz[1], and Gary A. Lorigan[1].

[1]Department of Chemistry and Biochemistry, Miami University, Oxford, OH, 45056, USA.

[2]Natural Science Division, Campbellsville University, Campbellsville, KY, 42718, USA.

This work has been published in Chem Phys Lipids. 2025 Dec 2;274:105562. doi: 10.1016/j.chemphyslip.2025.105562 :Rotich NC, Okorafor EA, Sahu ID, Shah MZ, Konkolewicz D, Lorigan GA. A comparison of the effect of SMA derivatives on the structural topology and dynamics of two bacteriophage peptides.

3.0 Abstract

Researchers have explored and cultivated suitable membrane mimetics to preserve a physiological solvent condition for membrane protein functions. This involves emulating the properties of lipid bilayers, particularly within the hydrophobic core. Membrane mimetics exist in diverse forms, such as micelles, bicelles, liposomes, and nanodiscs. Polymers, such as styrene-maleic acid (SMA), have been found to offer a potentially suitable means to solubilize membrane proteins without resorting to detergents. It is widely recognized that various membrane mimetics yield distinct structural and dynamic configurations in membrane proteins. Styrene-maleic acid derivatives (SMADs) are of particular significance in this study; they are known for their ability to generate lipid nanoparticles. It has been hypothesized that utilizing SMA derivatives with the same charge as the target membrane protein preserves the protein's structural and dynamic attributes compared to other bilayer membrane mimetics. This study explores the impact of different charges of SMA derivatives on two bacteriophage-encoded peptides explicitly focusing on their influence as charged peptides. Positively charged, neutral, and negatively charged SMA derivatives interactions with pinholin S^{21} and the phage-encoded cationic antimicrobial peptide gp28 lipid vesicles were assessed. These interactions were characterized using dynamic light scattering (DLS) techniques and continuous wave electron paramagnetic resonance (CW-EPR) spectroscopy. From our DLS results we observed a reduction in size from the vesicle control which is consistent with the formation of SMADLPs (styrene maleic acid derivatives lipid nanoparticles). The key outcome was in the identification of how various SMA derivatives affect the interaction gp28 and pinholin membrane peptides which is useful when trying to understand how the different SMA polymers can influence the behavior and stability of protein complexes. For gp28 peptide, CW-EPR spectral analysis indicates no line broadening in its profile, suggesting that binding interactions with SMA derivatives do not significantly disrupt the structural integrity or dynamic behavior of the gp28 peptide. SMA-Pos interaction with pinholin shows some minimal perturbation confirming that it is not as compatible compared to SMA-Neut and SMA-Glu. This study will provide insights into the optimal conditions for studying membrane protein interactions focusing on the structural dynamics of gp28 and pinholin in the presence of different SMA derivatives.

3.1 Introduction

The proteins within the membrane are the link between the cell and the external environment hence play a major role in controlling molecular movements across the membrane and intracellular communication.[1,2] Membrane proteins (MPs) constitute a significant fraction of protein-encoding genes that perform essential functions across all organisms.[3,4] Despite their importance, our understanding of MP folding, stability, and function lags behind that of water-soluble proteins. The scarcity of MP structures in the protein database underscores the challenges of studying these hydrophobic proteins.[5,6] Traditional approaches of solubilizing membrane proteins often involve detergents, which can disrupt native membrane environments.[7–9] Amphipathic polymers have been developed to interact with lipid suspensions by inserting themselves into the bilayer. They interact with the lipid acyl chain using their hydrophobic portion and the lipid head group using their hydrophilic portion.[10] This interaction makes the lipid-protein-polymer mixture soluble, disrupting the bilayer without using detergents.[11,12] An example of amphipathic polymers is Styrene Maleic Acid (SMA) copolymer. In recent years, SMA has emerged as a promising tool for solubilizing and stabilizing membrane proteins.[13–15] SMA extracts proteins in the form of lipid-protein nanodiscs, offering a distinct advantage over detergents, which tend to deplete most or all of the lipids from the immediate environment of membrane proteins.[16–19] This copolymer interacts with lipid samples like liposomes to form SMA lipid nanoparticles (SMALPs).[20] SMA has demonstrated the ability to generate highly pure integral membrane proteins derived from diverse bacterial and eukaryotic sources.[21,22] SMA has also been used to characterize proteins like KCNE1, making it a promising tool for the structural study of membrane proteins.[20,23]

However, there are limitations to the use of SMA in membrane protein solubilization and reconstitution due to the diacidic components they possess. The hydrophobicity of styrene-maleic acid copolymer (SMA) increases when the acids are protonated, and it also binds to divalent metal cations such as calcium and magnesium.[23,24] This affects the structure of the lipid disk. When magnesium concentration exceeds 10 mM or the pH falls below 6, the polymer often precipitates, leading to the disassembly of the SMALPs.[24–26] Unfortunately, most membrane proteins like ATPase, which have enzymatic functions, need magnesium or divalent cations as a cofactor. These limitations have been minimized by derivatizing SMA through a nucleophilic ring opening of RAFT-synthesized styrene maleic anhydride (SMAn) copolymers. [12]

Styrene maleic acid derivatives, commonly called SMADs, are a fascinating class of copolymers with the unique ability to interact with various membrane systems. Their diverse applications in membrane protein research and biotechnological innovations have garnered significant attention. A library of SMA-Derivatives, namely, SMA-Glu, and SMA-AE, both net negatively charged, SMA-Neut, net neutral charged, and SMA-Pos, net positively charged, have been characterized. SMA-Neut and SMA-Pos were proposed to be milder surfactants than the traditional SMA polymer because of their zwitterionic characteristics which mimic surfactants like CHAPSO and DHPC that are used in bicelle membrane mimetic preparation. [12,27] When SMA reacts with glucosamine, it forms SMA-Glu that behaves like alkyl glucosides which is helpful in membrane protein studies.[112] These derivatives are charged polymers that could be utilized in the study of charged membrane peptides and proteins. This study explores a hypothesis that states that protein dynamics and functionality are preserved when overall protein charge matches that of the polymer belt. [12,29]

To fully appreciate the role of SMADs, we must first examine the effect of their interactions with membrane proteins and systems. These interactions are influenced mainly by the charge of the SMADs themselves, which can be positive, neutral, or negative, and how these charges interact with membrane proteins that are similarly classified. The charge-dependent interactions between SMA derivatives and membrane systems highlight the strategic decision-making involved in designing experiments and applications. Each scenario involving positively, neutrally, or negatively charged entities demands a tailored approach. The choice of SMA derivative charge is not merely a matter of preference but a decision that can significantly impact the outcome of membrane protein studies.

In this study, gp28 and pinholin which are charged antimicrobial peptides at pH 7, were reconstituted into nanodiscs with these charged polymers to assess this hypothesis and hence contribute to the screening library of which polymers preserve a more native environment of differently charged peptides/ proteins. The bacteriophage-encoded proteins gp28 and pinholin represent critical components of phage-mediated bacterial lysis, each contributing uniquely to the disruption of host bacterial membranes. The emergence of antibiotic-resistant bacteria, commonly referred to as "superbugs," has escalated into a significant public health crisis, necessitating the exploration of alternative therapeutic strategies. Among these, bacteriophages have garnered considerable attention for their potential to combat multidrug-resistant infections.[30]

Pinholin is a type of holin that forms pores in the cytoplasmic membranes of bacteria to release endolysins that hydrolyze the cell wall and induce cell death.[31,32] During the lytic cycle, pinholin accumulates in the bacterial membrane. Pinholin S^{21} is encoded by the S^{21} gene of phage Φ21, which produces two proteins: the 68-amino acid pinholin ($S^{21}68$) and the 71-amino acid antiholin ($S^{21}71$). Active pinholin is a specific type of protein that plays a crucial role in the lifecycle of bacteriophages, especially during the lytic cycle. [33–35] This protein is responsible for forming pores in the membranes of bacterial cells. When the phage infects a bacterium, the active pinholin triggers the depolarization of the bacterial membrane, leading to increased permeability. Once the pores are formed, they facilitate the release of newly assembled phage progeny from the bacterial cell, allowing the virus to spread to new hosts and propagate its lifecycle effectively. In contrast, the inactive variant of pinholin is a non-functional protein that does not have the ability to create pores in the bacterial membrane. This inactive form fails to trigger the necessary changes in membrane dynamics that would lead to bacteriolysis. As a result, the bacterial cell remains intact, preventing the release of phage progeny. Pinholin activity is tightly regulated to prevent premature cell lysis. It often works in conjunction with other phage proteins to ensure efficient release of viral progeny.[35]

The existence of this inactive pinholin variant can be critical in the regulation of viral replication and lysis, offering a mechanism by which the phage can control its lifecycle based on environmental conditions or host resistance.[36] The pinholin proteins, whether in their active or inactive forms, are characterized by the presence of two transmembrane domains (TMDs).[37,38] These domains are integral structures that typically integrate into the lipid bilayer of the cytoplasmic membrane. In their inactive state, pinholins generally exist as dimers.[39] In this arrangement, both TMDs are firmly inserted into the lipid bilayer, establishing a stable configuration that prevents pore formation. For the transition to the active state, a critical event occurs: TMD1 must be displaced from its position within the lipid bilayer. This displacement is crucial because it initiates the structural rearrangements necessary for pore formation, allowing the pinholin to perform its biological function. The precise mechanisms and conformational changes involved in the displacement of TMD1 are essential for understanding how pinholins operate at the molecular level, ultimately leading to the formation of pores in the membrane, which can facilitate various processes such as phage-induced cell lysis.[40]

gp28 peptide, a phage-encoded cationic antimicrobial peptide (AMP), plays a distinct role in bacteriophage lysis. gp28 is structurally characterized by its alpha-helical conformation and cationic properties, enabling membrane disruption through direct interactions with lipid bilayers. Recent studies

demonstrate its dual functionality as both an outer membrane (OM) disruptor in phage lysis and an antimicrobial agent against gram-negative pathogens like *Pseudomonas aeruginosa***.**[41] Unlike pinholins that form pores to trigger endolysin release, gp28 operates independently of holin-endolysin systems in certain phages, such as phiKT, where it complements peptidoglycan degradation by holins (e.g., gp29) and endolysins (e.g., gp27). Unlike traditional spanins, gp28 is strongly membrane-associated and resistant to removal by denaturing agents such as urea, indicating a robust interaction with the lipid bilayer.[42] This positions gp28 within a newly identified class of phage lysis proteins termed "disruptins," distinct from previously known holins, endolysins, or spanins.[43–45] Functionally analogous studies demonstrate that gp28 exhibits broad-spectrum antibacterial activities similar to human AMPs like LL-37. Specifically, it inhibits planktonic growth and disrupts biofilms formed by multidrug-resistant Pseudomonas aeruginosa strains while enhancing antibiotic susceptibility when combined with agents such as tobramycin.[41] These findings suggest translational potential for gp28-derived peptides in combating antibiotic-resistant infections by leveraging their membrane-targeting properties. These two peptides were selected based on their distinct charge profiles to explore how different environments affect peptide stability. We aim to correlate changes in peptide EPR structure with different SMA charge profiles, providing valuable insights into how charges modulate peptide–polymer interactions in membrane mimetics.

KCNE1 is a negatively charged membrane protein that regulates potassium channels, especially KCNQ1, by altering their function. It plays a key role in controlling potassium ion flow, crucial for heart rhythm and electrical activity in cells.[46] Mutations in KCNE1 can lead to heart conditions like long QT syndrome and arrhythmias.[47] KCNE1 was used as the membrane protein control, given its previous structural studies with these different SMA derivative polymers. Utilizing KCNE1 allows for a comparative analysis of the interactions between the membrane protein and the various SMA derivatives.[48] Previous studies have shown that KCNE1 integrates well within synthetic polymer matrices, facilitating insights into structural dynamics.

This investigation aims to further elucidate the functional implications of these interactions, focusing on how the distinct properties of each SMA variant influence gp28, pinholin, and KCNE1's stability and activity in a membrane-like environment. Membrane-bound proteins and peptides are essential in the assessment of lipid bilayer mimetics effectiveness. KCNE1, pinholin and gp28 are ideal model proteins and peptides as they are small to moderate in size and thus can be studied in different lipid environments.

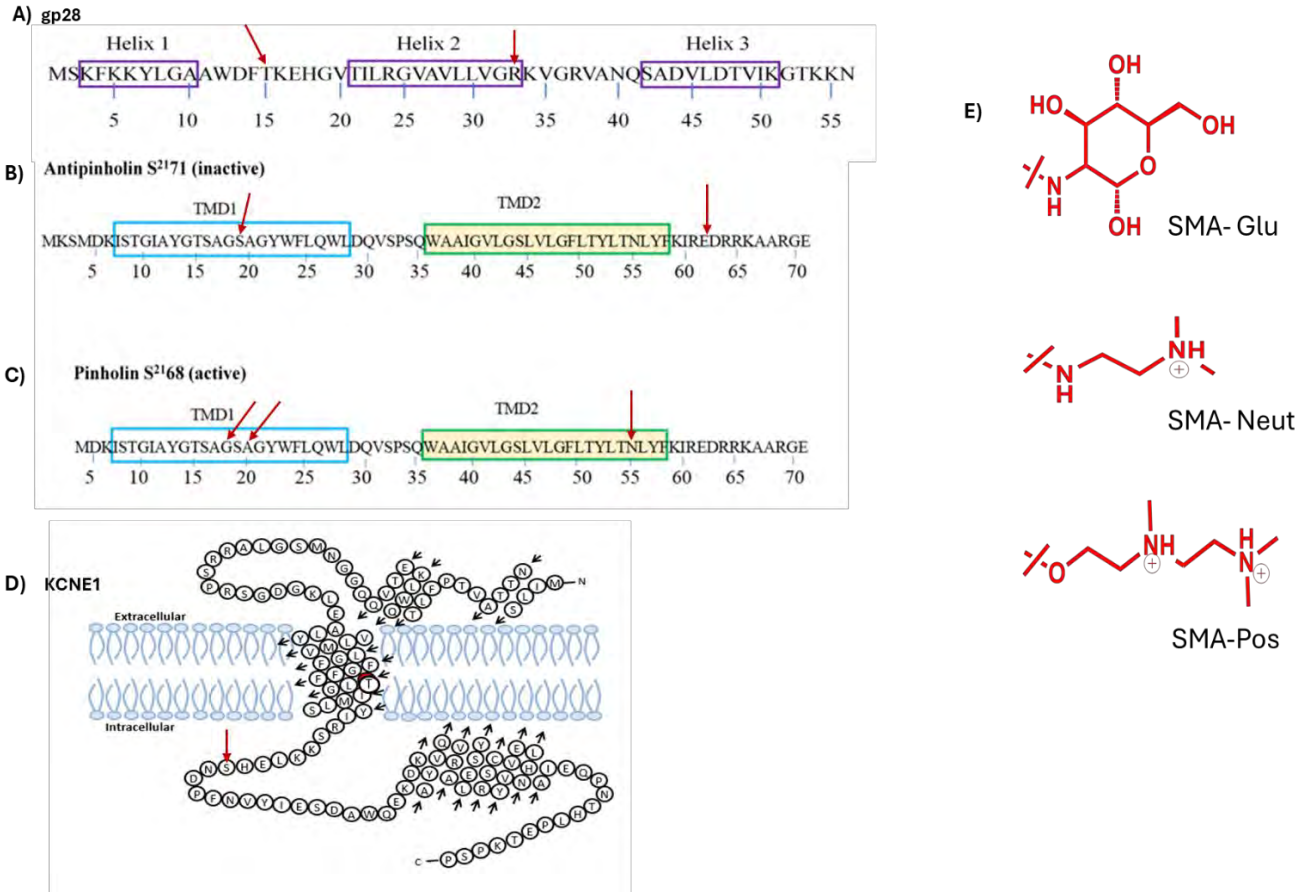

Figure 3. 1: A) gp28 amino acid sequence with helices highlighted in purple. B) Inactive pinholin amino acid sequence (TMD 1 & TMD 2 are highlighted). C) Active pinholin amino acid sequence. D) KCNE1 protein amino acid sequence. E) A summary of Styrene Maleic Acid polymers synthesized from the functionalization of SMAnh, referred to as SMADs. This includes SMA-Glu (poly(styrene-co-maleic anhydride d-glucosamine)), SMA-Neut (poly(styrene-co-maleic anhydride N,N-dimethylethylenediamine)), and SMA-Pos (poly(styrene-co-maleic anhydride 2-{[2-(dimethylamino)ethyl]methylamino} ethanol). The red arrows indicate the mutated amino acid residues that were used in this study.[49]

Polymer screening using styrene-maleic acid (SMA) derivatives is a key step when working with membrane protein systems. Screening these different polymers with different charges helps in the identification of the most effective SMA derivatives for efficient solubilization of membrane proteins without compromising their functionality. Each membrane protein may require specific properties in a polymer for optimal extraction or solubilization.[9] By screening various SMA derivatives, researchers can find the right combination of hydrophobicity, charge, and molecular weight that works best for a given protein system. This process also helps in improving the purity and stability of the proteins, as some polymers are better at protecting membrane proteins from denaturation. Once solubilized with the ideal SMA derivative, the proteins can be analyzed for their structure, function, and interactions, without

interference from the solubilization process. Polymer screening ensures that the membrane proteins remain stable and functional making subsequent research and analysis more effective.[10]

Understanding these interactions is particularly crucial in the field of drug discovery and development. Membrane proteins are frequent targets for pharmaceuticals, and maintaining their structural integrity during study is vital for accurate drug binding and efficacy assessments.This study explores the charge-dependent interactions of three different Styrene Maleic Acid Derivatives: SMA-Glu, SMA-Neut, and SMA-Pos with membrane proteins, offering a robust platform for such studies using their charge properties to allow for precise manipulation of protein-polymer interactions to ensure optimal protein stability and functionality.

3.2 Methodology

3.2.1 Peptide Synthesis

Solid-phase peptide synthesis was used to make gp28 and pinholin peptides using a CEM peptide synthesizer, which was then cleaved from the solid-phase resin using a trifluoroacetic acid (TFA) cleavage solution following established protocols.[38] A crude peptide was obtained following an optimized cleavage procedure. The crude peptides were purified using reverse-phase high-performance liquid chromatography (RP-HPLC) on a C4 prep column with a gradient of solvent B (90% acetonitrile/10% water/0.1% TFA) in a similar manner reported previously.[39] The purified peptides were then collected and lyophilized, and the resulting pure peptide was spin-labeled using MTSL spin label. To remove excess spin labels, the spin-labeled peptide underwent another round of purification using RP-HPLC on a C4 semi-prep column with the same gradient and solvent system. The purified peptides were subsequently freeze-dried (lyophilized) to obtain solid peptide samples. Spin-labeling efficiency was calculated to be 80–90% by using a CW-EPR calibration curve.

3.2.2 Vesicle Sample Preparation/ Formation of SMADLPs:

A stock solution of the peptides was prepared using Trifluoroethanol (TFE) at a concentration of 2 mg/mL. Three different lipids commonly used for studying membrane proteins were used to characterize the formation of homogeneous vesicles and SMADLPs. One vesicle sample was composed of POPC, another was composed of a mixture of POPC and POPG at a molar ratio of 3:1 (POPC: POPG) and the third was

composed of DMPC. The desired molar ratio of the peptide to the lipids for the vesicles was set to 1:1000. In each of the samples, powdered lipids were dissolved in a 2-(4-(2-Hydroxyethyl)piperazin-1-yl)ethanesulfonic acid (HEPES) buffer (20 mM HEPES, 100 mM NaCl, pH 7.0) and brought to a final concentration of 100 mM. The mixture was then vortexed vigorously for one minute and followed by at least 5 freeze/sonication cycles to obtain a homogeneous milky solution. The vesicle solutions were then frozen with liquid nitrogen and placed in a freezer overnight (-20˚C). Dynamic light scattering was used to confirm and analyze the size of vesicles the next day. The protein-lipid complex was incorporated into SMA-polymer following previously published protocols.[50] Styrene-maleic acid derivatives were dissolved in the same buffer (20mM HEPES, 100mM NaCl pH 7), brought to a final concentration of 5% (m/v) and sonicated at 40 ˚C until the solution went clear. SMA derivatives samples were synthesized according to a previously published method.[12] Then the vesicles were titrated with different SMA derivatives polymers by adding them in the solution dropwise, obtaining the weight ratios of 2:1. The nanodisc solution was mixed via slight rotation at room temperature overnight. The protein-SMAD-polymer solution was equilibrated overnight at 4 °C. The resulting solution was centrifuged at 40,000xg for 30 minutes to remove the non-solubilized protein. The supernatant was further concentrated to the desired volume and concentration for DLS and CW-EPR spectroscopic measurements.

3.2.3 Dynamic Light Scattering (DLS)

DLS measurements were performed on a Zetasizer nano series (Malvern Instruments) at 25 °C in disposable 40 μL micro cuvettes. Data was collected for 20 s and averaged for 10 scans. The size distribution in radius is shown on a log scale using Igor Pro (WaveMetrics).

3.3 CW-EPR Measurements

EPR experiments were conducted at the Ohio Advanced EPR Laboratory. CW-EPR spectra were collected at X-band on a Bruker EMX CW-EPR spectrometer using an ER041xG microwave bridge and ER4119-HS cavity coupled with a BVT 3000 nitrogen gas temperature controller. Each spin-labeled CW-EPR spectrum was obtained by averaging the signals from 40 field scans, each lasting 42 seconds with a central field of 3318 G and sweep width of 100 G, modulation frequency of 100 kHz, modulation amplitude of 1 G, and microwave power of 10mW at room temperature. The center linewidth (ΔH) of the EPR data was determined using a previously outlined method in literature.[51]

3.4 Results & Discussion

3.4.1 Dynamic Light Scattering (DLS) Results

The average size of our peptide (gp28 V31) in 3:1 molar ratio of POPC:POPG multilamellar lipid vesicle sample which is our control was about 1000 nm and the average size of the vesicle: SMAD nanodisc was a range of 5nm to about 100 nm as shown from DLS analysis in **Figure 3.2**. The reduction in size observed from the vesicle control to SMADLPs, as well as the homogeneity of the SMADLPs particle size is consistent with the formation of SMADLPs. SMA-Glu and SMA-Neut nanodiscs are larger in size (> 50 nm) when compared to SMA2:1 and SMA-Pos (<10 nm).

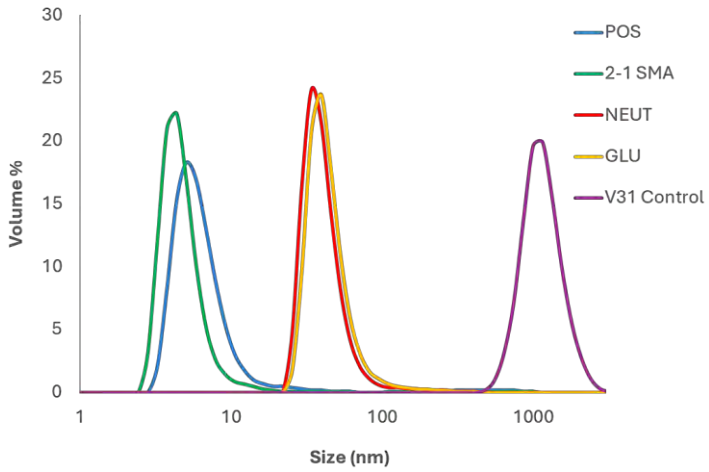

Figure 3. 2: Representative DLS volume-weighted distributions of the hydrodynamic nanoparticle diameter before and after the addition of 2:1 SMA_Glu (yellow), SMA_Neut (red), SMA_Pos (blue) and the vesicle control (purple). The peptide was incorporated in 3:1 POPC: POPG lipid.

This shows that the SMA derivatives exhibit more uniform and consistent particle sizes as well as improved size control when needed due to optimizations in synthesis processes or modifications that enhance stability and functionality. This also confirms that the choice of amphiphilic polymer, its specific formulation, and the solubilization procedure can all have a substantial effect on both the solubilization efficiency and the size of the resulting lipodiscs.[25,51] Substituted polymers with reduced charge, including those that are zwitterionic, tend to produce larger discs, presumably due to reduced repulsive forces. These findings are significant for various scientific and technological applications that rely on precise control over particle or molecule sizes. Given their small size, these nanodiscs might be particularly effective for examining the early stages of processes that involve the oligomerization of peptides in membranes.[24,52]

3.4.2 CW-EPR Spectroscopic Results

Continuous wave-electron paramagnetic resonance (CW-EPR) line shape analysis was used to confirm the effect of the interaction of these polymers on different membrane-bound proteins and peptide complexes. CW-EPR spectroscopy gives insights into the structural and dynamic characteristics of membrane proteins by line shape analysis of the spin-labeled molecules within various membrane-mimicking environments, which is useful in confirming the compatibility of the membrane-bound proteins and peptides, and SMADs.

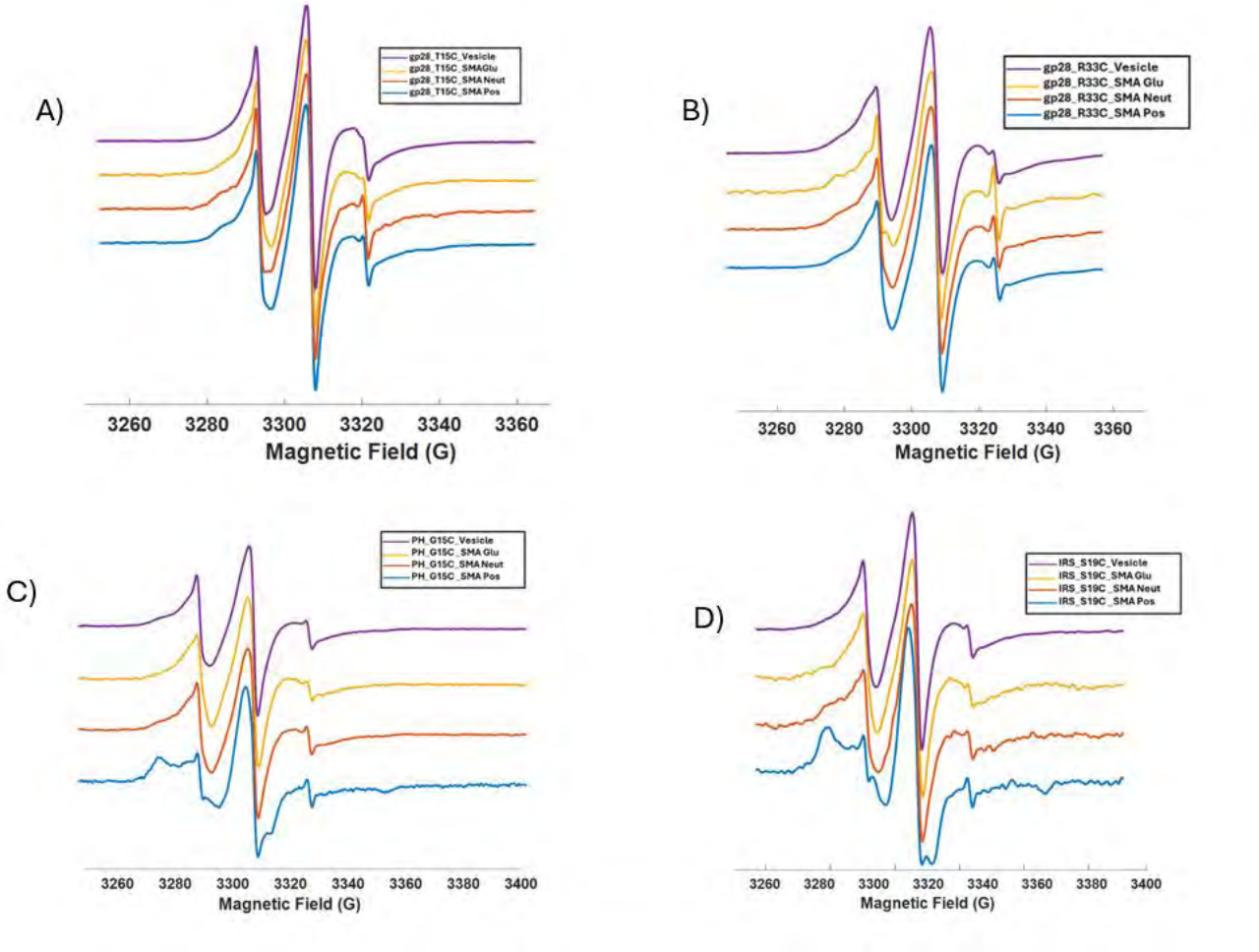

Figure 3. 3: CW-EPR spectra data for A) T15C and B) R33C mutants of gp28, and C) G15C and D) IRS_S19C mutants of pinholin, incorporated into MLVs vesicles (purple) and SMALPs formed by 2:1 SMA_Glu (yellow), SMA_Neut (red), and SMA_Pos (blue). The IRS pinholin mutants represent the inactive (IRS) form of pinholin. The black arrow denotes the mobile spectral component, while the green arrow indicates the rigid component.

As shown **in Figures 3.3** & **3.4**, the lineshape of the peptide vesicles was used as the control. The analysis of gp28 showed no disruption of the lipid bilayer structure, as the SMADs lineshapes resemble that of the control, suggesting that the interactions between the SMAD polymers and the gp28 constructs do not interfere with the protein's structural integrity. From **Figure 3.3B**, it was observed that SMA-Glu caused a very slight modification of the slow/rigid component in the spectra of gp28 R33C which is likely a charge effect or could be due to the fact it is in a region that is embedded in the lipid membrane (helix 2) whereas gp28 T15C is in the solvent exposed region as seen in **Figure 3.3A**. Peripheral membrane proteins have been suggested to associate with the cell membrane by inserting the hydrophobic residues of their amphipathic helix into the cell membrane. This insertion enables a stable association with the membrane, allowing these proteins to fulfill their functions without becoming fully embedded.[61] The limited extent of broadening implies that the conformational characteristics of gp28 are largely preserved, indicating that its functionality remains intact even in the presence of SMA derivatives.

To further explore the interaction between peptide charges and polymer charges on gp28, we introduced pinholin, another lytic peptide that is neutral or slightly cationic depending on the position of the spin-labeled mutant or its reconstitution as well as the type involved either the active or inactive species. In the active pinholin, TMD1 is exposed to the surface and interacts with the solvent, while TMD2 remains embedded in the membrane.[53] In the inactive pinholin, both TMD1 and TMD2 are buried inside the membrane, maintaining a more closed, inactive conformation.[53] This difference in positioning is crucial for the functional activation of pinholin. Two distinct spectral components were observed in some of the EPR spectra, especially from the interaction of the active and inactive pinholin vesicles and the SMA-Pos and SMA-Neut derivatives. SMA-Pos is noted to introduce a pronounced rigid and mobile component in all the mutants studied as shown in **Figures 3.3C, 3.3D, 3.4A**, **3.4B** and **3.4C** for G15C, A17C, IRS-S19C, IRS-N55C and E62C. SMA-Pos lipodiscs caused a larger perturbation than the other derivatives during reconstitution due to charge–charge interaction between the slightly neutral or negatively charged peptide and the cationic polymer.

To further explore our observations, the transmembrane protein KCNE1 S74C was studied (**Figure 3.4D**). No perturbation of protein dynamics occurred when using SMA-Neut which has the lowest charge density compared with SMA-Pos or SMA-Glu. KCNE1 S74C has a calculated charge between −1 and 0 at pH 7.[51] The lineshape of the reconstituted mutant S74C shows minimal amplification of the slow/rigid component of the EPR spectra like that of pinholin when these transmembrane proteins were reconstituted

into nanodiscs with SMA-Pos and SMA-Glu. This confirms our results suggesting that the interactions with SMA seem to be more dependent on the hydrophobic properties of the peptide/ protein and the polymer's amphiphilic nature. Previous studies note that whereas the protein charge dominates in large proteins, in peptides, it is the SMA charge that dominates.[7] For peptide and polymer nanodiscs, the mechanism involves the formation of a high-density peptide or polymer belt surrounding the lipid bilayer instead of a continuous belt as in protein-based nanodiscs. Hence, the peptide/polymer nanodiscs are highly dynamic as a result of an exchange of lipids between nearby nanodiscs.[7] These variations in line shape provide insights into the mobility and rotational freedom of the spin-labeled residues within the proteins, indicating a biochemically relevant environment that supports functional conformational dynamics thus reinforcing its utility for the study of various membrane-associated processes.

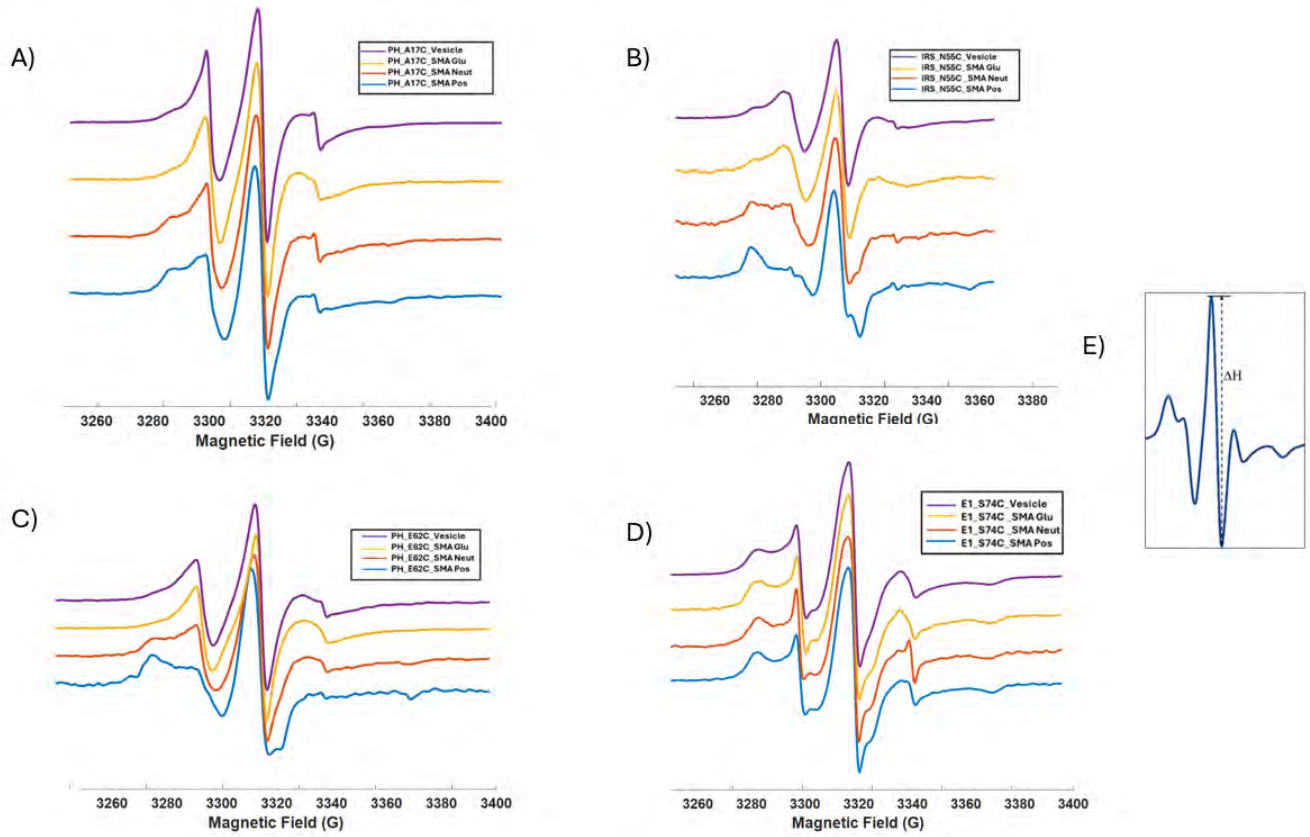

Figure 3. 4: CW-EPR spectral data for A) A17C mutant, B) IRS_N55C mutant of pinholin and C) E62C mutant of pinholin and D) S74C mutant of KCNE1 incorporated into vesicles (purple) and SMALPs formed by 2:1 SMA_Glu (yellow), SMA_Neut (red), and SMA_Pos (blue). The IRS pinholin mutations represent the inactive pinholin vesicles. E) Central linewidth (ΔH) used to calculate the inverse central linewidth ($\Delta H0^{-1}$) in Figure 3.5.

The method proved effective for characterizing not only small peptides but also larger membrane proteins, which often face challenges in traditional solubilization approaches. Through systematic alterations in peptide /protein composition and polymer interactions, optimal conditions were established, highlighting the potential for tailoring the nanodisc environment to suit specific experimental needs. Thus, the combination of CW-EPR and SMADLPs emerges as a potent approach for studying protein-lipid interactions and the functional characterization of membrane proteins.

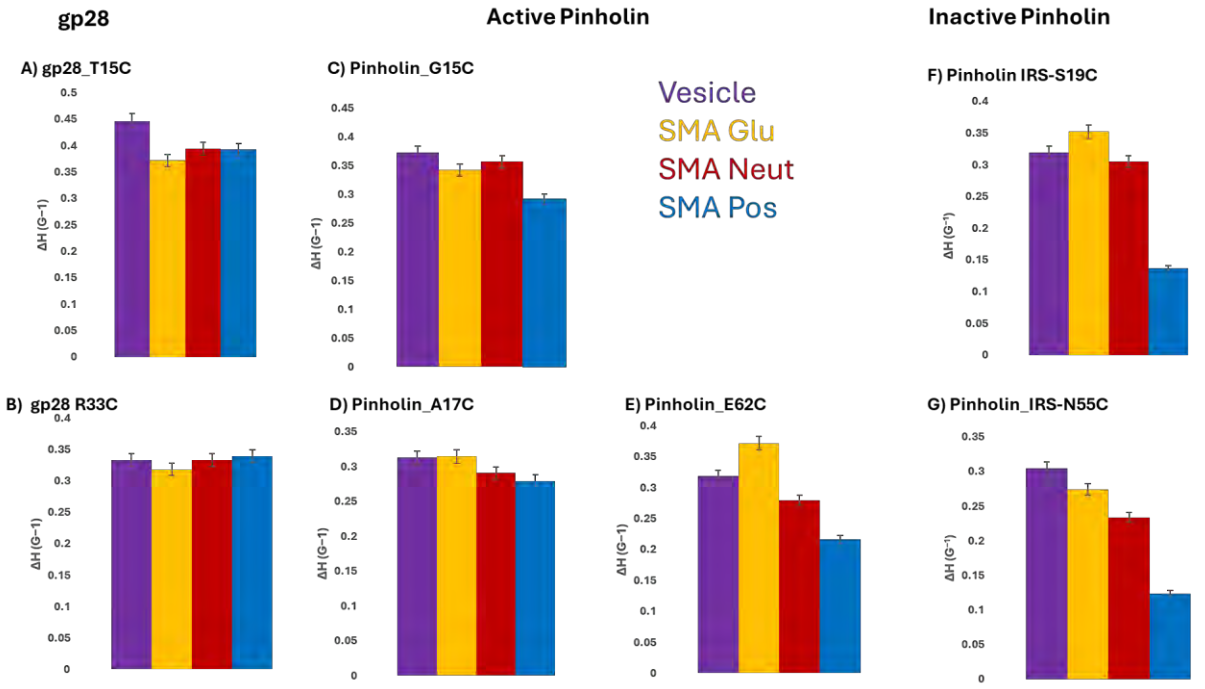

Figure 3. 5: The inverse central linewidth was plotted against the different SMA derivatives for all spin-labeled gp28/ pinholin variants. gp28 and pinholin vesicles (purple), 2:1 SMA_Glu (yellow), SMA_Neut (red) and SMA_Pos (blue). A) gp28 T15C B) gp28 R33C C)Pinholin G15C D)Pinholin A17C E)Pinholin E62C, F)Pinholin IRS-S19C and G) Pinholin IRS-N55C. Figures 5C, D, and E are from the active variant, while F and G are mutants from the inactive variants. Error bars represent the standard error of mean for two replicates. These values are calculated from the corresponding CW-EPR spectra in Figure 3.4.

To further probe the dynamic behavior of the different peptide vesicles in the presence of SMA derivatives, the inverse central linewidth ($\Delta H0^{-1}$) was utilized to analyze our data. The central-line width is the width of the peak-to-peak splitting of the first derivative.[54,56] As shown in **Figure 3.5**, the inverse central linewidth was plotted against the different SMA derivatives for all spin-labeled gp28 and pinholin variants. A higher value of this inverse central linewidth parameter indicates greater mobility. The spin interaction between the SMA derivatives at gp28 sites were more mobile than at the same sites in pinholin. The inverse central linewidth varies between 0.4 G^{-1} to 0.5 G^{-1} for gp28 samples and 0.2 G^{-1} to 0.4 G^{-1} for

the pinholin mutants. There was less variability in the motion of gp28 mutants with the addition of SMADs among the three derivatives. SMA-Pos was less mobile in pinholin variants in comparison to gp28 mutants. Inactive pinholin had the least mobility and a noticeable pattern from the interaction of the IRS-S19C and IRS-N55C samples with SMA-Pos. Overall, the difference between the spin-label environments in pinholin with SMA-Pos was more pronounced. This suggests that in this system, the spin label attached to the pinholin peptide has more restricted motion. This result indicates that pinholin might be more sensitive to its environment and reduced lipid binding affected its local structural perturbation. These observed motional differences could be due to the relationship of the polymer belt's charge density to the membrane protein's charge density.

gp28 which is mostly a surface or solvent exposed protein and pinholin that has both solvent exposed and trans-membrane domains were successfully reconstituted by the different SMA derivatives and although they exhibit different interactions, this study confirms the utility of the SMA copolymers as an alternative method for biological membrane reconstitution. The minor broadening observed for the gp28 data suggests that the SMA derivatives do not interact significantly with the protein itself; however, it may increase the solvent's viscosity, causing these minor broadenings. It is essential to note that the specific effects of polymer belt charge on protein incorporation into nanodiscs can vary based on several factors, including the magnitude of the charges involved, the overall composition of the nanodiscs, and the surrounding environmental conditions such as pH and ionic strength.[55] These conditions affect the solubility and charge state of SMA derivatives and lipids, potentially altering the overall membrane-protein-lipid interaction landscape.[57,58] Adjustments in pH, for example, can modify the charge on protein side chains or SMA functional groups, leading to different interaction strengths and shifts in the EPR spectra. High ionic strength environments may screen electrostatic interactions, thereby reducing the influence of charge-based interactions and lead to spectra that reflects more hydrophobic interactions within the membrane system.

Additionally, the presence of other components in the system, such as lipids or detergents, can also influence the interactions between the polymer belt and proteins during nanodisc formation. Depending on the position of the spin-label, interactions with the lipid headgroups could also significantly influence the EPR spectra.[57,58] Prior structural studies using EPR spectroscopy show that gp28 embeds into lipid bilayers with variable mobility depending on bilayer composition, whereas pinholins exhibit oligomerization-dependent pore formation dynamics.[44,55] The diversity and complexity of interactions

between SMA derivatives, membrane protein systems, and lipid environments fundamentally dictate the characteristics of CW-EPR spectra in nitroxide spin-labeled samples. Each component plays a pivotal role; SMA derivatives modulate the protein's lipid association, protein charge and structure determine interaction dynamics, and lipid composition influences the overall membrane context. A thorough understanding of these interdependencies is crucial for accurately interpreting EPR data and for the rational design of experiments that aim to elucidate membrane protein functionality. We agree with the conclusion of Ravula et al that the compatibility between polymer and highly charged proteins should be carefully considered when planning structural studies.[29] Membrane proteins such as KCNE1 can be solubilized efficiently by SMA copolymers, if the hydrophobic interactions between the protein and the lipid discs are favorable. These findings highlight how the inherent chemical properties of the selected polymer, which enable the formation of nanodiscs, can significantly influence the successful reconstitution of functional proteins. Overall, understanding the interplay between polymer belt charge and protein charges is crucial for optimizing nanodisc assembly and functionality, particularly in applications where precise control over protein encapsulation and interactions within the nanodiscs are desired.

3.5 Conclusion

The ability of the three SMADs to solubilize and stabilize gp28 and pinholin membrane peptides without detergents offers a distinct advantage in maintaining the native environment of the proteins, which is often disrupted by traditional detergent-based methods. All the SMA derivatives were reconstituted with peptide vesicles to form SMADLPs of varying sizes and a correlation was observed between the net polymer charge and the sizes of particles formed. SMA-Pos forms smaller nanodiscs compared to SMA-Glu and SMA-Neut. In CW-EPR studies, SMA-Pos was found to be incompatible with the pinholin mutants in comparison to SMA-Neut and SMA-Glu. For gp28 system, the CW-EPR spectra with the SMADs mimetic system line shows no perturbation thus confirming the incorporation of membrane-bound peptide with the nanodiscs, suggesting that the SMADLPs preserved a conducive environment for gp28 vesicles to achieve their native conformations. The native-like membrane environment was preserved in gp28 mutants. We conclude that the charge of styrene maleic acid derivatives plays a pivotal role in interactions with membrane proteins and systems. Whether dealing with positive, neutral, or negative charges, each scenario presents unique challenges and opportunities.

We observe that the use of SMA derivatives with the gp28 peptide and pinholin peptides can offer a versatile approach to membrane research. Further optimization and characterization of SMA derivatives will contribute to the development of innovative membrane-mimetic technologies with enhanced biocompatibility, stability, and functionality, benefiting scientific understanding and therapeutic applications. The ability of SMADs to solubilize, stabilize, and maintain the native environment of membrane proteins without detergents has revolutionized membrane protein research and holds promise for future innovations in biotechnology and pharmaceuticals.

Acknowledgments

Gary A. Lorigan would like to acknowledge support from NSF CHE – 2305834 grant and Miami University. Dr. Sahu would also like to acknowledge the support from National Science Foundation NSF MCB-2040917.

References

(1) Gatenby, R. A. The Role of Cell Membrane Information Reception, Processing, and Communication in the Structure and Function of Multicellular Tissue. Int J Mol Sci 2019, 20 (15), 3609. https://doi.org/10.3390/ijms20153609.

(2) Fletcher, A. The Cell Membrane and Receptors. Anaesthesia & Intensive Care Medicine 2023, 24 (5), 298–302. https://doi.org/10.1016/j.mpaic.2023.01.006.

(3) Rintz, E.; Gaffke, L.; Podlacha, M.; Brokowska, J.; Cyske, Z.; Węgrzyn, G.; Pierzynowska, K. Transcriptomic Changes Related to Cellular Processes with Particular Emphasis on Cell Activation in Lysosomal Storage Diseases from the Group of Mucopolysaccharidoses. Int J Mol Sci 2020, 21 (9), 3194. https://doi.org/10.3390/ijms21093194.

(4) Junge, F.; Schneider, B.; Reckel, S.; Schwarz, D.; Dötsch, V.; Bernhard, F. Large-Scale Production of Functional Membrane Proteins. Cellular and Molecular Life Sciences 2008, 65 (11), 1729–1755. https://doi.org/10.1007/s00018-008-8067-5.

(5) Hu, B.; Tan, C.; Wu, L.; Zheng, J.; Xia, J.; Gao, Z.; Liu, Z.; Wu, F.; Zhang, G.; Li, S. Z. Advances of Deep Learning in Protein Science: A Comprehensive Survey. 2024.

(6) Bernhofer, M.; Dallago, C.; Karl, T.; Satagopam, V.; Heinzinger, M.; Littmann, M.; Olenyi, T.; Qiu, J.; Schütze, K.; Yachdav, G.; Ashkenazy, H.; Ben-Tal, N.; Bromberg, Y.; Goldberg, T.; Kajan, L.; O'Donoghue, S.; Sander, C.; Schafferhans, A.; Schlessinger, A.; Vriend, G.; Mirdita, M.; Gawron, P.; Gu, W.; Jarosz, Y.; Trefois, C.; Steinegger, M.; Schneider, R.; Rost, B. PredictProtein - Predicting Protein Structure and Function for 29 Years. Nucleic Acids Res 2021, 49 (W1), W535–W540. https://doi.org/10.1093/nar/gkab354.

(7) Krishnarjuna, B.; Ramamoorthy, A. Detergent-Free Isolation of Membrane Proteins and Strategies to Study Them in a Near-Native Membrane Environment. Biomolecules 2022, 12 (8), 1076. https://doi.org/10.3390/biom12081076.

(8) le Maire, M.; Champeil, P.; Møller, J. V. Interaction of Membrane Proteins and Lipids with Solubilizing Detergents. Biochimica et Biophysica Acta (BBA) - Biomembranes 2000, 1508 (1–2), 86–111. https://doi.org/10.1016/S0304-4157(00)00010-1.

(9) Desuzinges Mandon, E.; Agez, M.; Pellegrin, R.; Igonet, S.; Jawhari, A. Novel Systematic Detergent Screening Method for Membrane Proteins Solubilization. Anal Biochem 2017, 517, 40–49. https://doi.org/10.1016/j.ab.2016.11.008.

(10) Demina, T.; Grozdova, I.; Krylova, O.; Zhirnov, A.; Istratov, V.; Frey, H.; Kautz, H.; Melik-Nubarov, N. Relationship between the Structure of Amphiphilic Copolymers and Their Ability To Disturb Lipid Bilayers. Biochemistry 2005, 44 (10), 4042–4054. https://doi.org/10.1021/bi048373q.

(11) Xue, M.; Cheng, L.; Faustino, I.; Guo, W.; Marrink, S. J. Molecular Mechanism of Lipid Nanodisk Formation by Styrene-Maleic Acid Copolymers. Biophys J 2018, 115 (3), 494–502. https://doi.org/10.1016/j.bpj.2018.06.018.

(12) Burridge, K. M.; Harding, B. D.; Sahu, I. D.; Kearns, M. M.; Stowe, R. B.; Dolan, M. T.; Edelmann, R. E.; Dabney-Smith, C.; Page, R. C.; Konkolewicz, D.; Lorigan, G. A. Simple Derivatization of RAFT-Synthesized Styrene–Maleic Anhydride Copolymers for Lipid Disk Formulations. Biomacromolecules 2020, 21 (3), 1274–1284. https://doi.org/10.1021/acs.biomac.0c00041.

(13) Bada Juarez, J. F.; Harper, A. J.; Judge, P. J.; Tonge, S. R.; Watts, A. From Polymer Chemistry to Structural Biology: The Development of SMA and Related Amphipathic Polymers for Membrane Protein

Extraction and Solubilisation. Chem Phys Lipids 2019, 221, 167–175. https://doi.org/10.1016/j.chemphyslip.2019.03.008.

(14) Unger, L.; Ronco-Campaña, A.; Kitchen, P.; Bill, R. M.; Rothnie, A. J. Biological Insights from SMA-Extracted Proteins. Biochem Soc Trans 2021, 49 (3), 1349–1359. https://doi.org/10.1042/BST20201067.

(15) Stroud, Z.; Hall, S. C. L.; Dafforn, T. R. Purification of Membrane Proteins Free from Conventional Detergents: SMA, New Polymers, New Opportunities and New Insights. Methods 2018, 147, 106–117. https://doi.org/10.1016/j.ymeth.2018.03.011.

(16) Overduin, M.; Esmaili, M. Structures and Interactions of Transmembrane Targets in Native Nanodiscs. SLAS Discovery 2019, 24 (10), 943–952. https://doi.org/10.1177/2472555219857691.

(17) Swainsbury, D. J. K.; Scheidelaar, S.; Foster, N.; van Grondelle, R.; Killian, J. A.; Jones, M. R. The Effectiveness of Styrene-Maleic Acid (SMA) Copolymers for Solubilisation of Integral Membrane Proteins from SMA-Accessible and SMA-Resistant Membranes. Biochim Biophys Acta Biomembr 2017, 1859 (10), 2133–2143. https://doi.org/10.1016/j.bbamem.2017.07.011.

(18) Knowles, T. J.; Finka, R.; Smith, C.; Lin, Y.-P.; Dafforn, T.; Overduin, M. Membrane Proteins Solubilized Intact in Lipid Containing Nanoparticles Bounded by Styrene Maleic Acid Copolymer. J Am Chem Soc 2009, 131 (22), 7484–7485. https://doi.org/10.1021/ja810046q.

(19) Zhang, G.; Odenkirk, M. T.; Janczak, C. M.; Lee, R.; Richardson, K.; Wang, Z.; Aspinwall, C. A.; Marty, M. T. Identifying Membrane Protein-Lipid Interactions with Lipidomic Lipid Exchange-Mass Spectrometry. June 3, 2023. https://doi.org/10.1101/2023.06.02.543293.

(20) Zhang, R.; Sahu, I. D.; Bali, A. P.; Dabney-Smith, C.; Lorigan, G. A. Characterization of the Structure of Lipodisq Nanoparticles in the Presence of KCNE1 by Dynamic Light Scattering and Transmission Electron Microscopy. Chem Phys Lipids 2017, 203, 19–23. https://doi.org/10.1016/j.chemphyslip.2016.12.003.

(21) Dörr, J. M.; Koorengevel, M. C.; Schäfer, M.; Prokofyev, A. V; Scheidelaar, S.; van der Cruijsen, E. A. W.; Dafforn, T. R.; Baldus, M.; Killian, J. A. Detergent-Free Isolation, Characterization, and

Functional Reconstitution of a Tetrameric K+ Channel: The Power of Native Nanodiscs. Proc Natl Acad Sci U S A 2014, 111 (52), 18607–18612. https://doi.org/10.1073/pnas.1416205112.

(22) Swainsbury, D. J. K.; Scheidelaar, S.; van Grondelle, R.; Killian, J. A.; Jones, M. R. Bacterial Reaction Centers Purified with Styrene Maleic Acid Copolymer Retain Native Membrane Functional Properties and Display Enhanced Stability. Angewandte Chemie International Edition 2014, 53 (44), 11803–11807. https://doi.org/10.1002/anie.201406412.

(23) Scheidelaar, S.; Koorengevel, M. C.; van Walree, C. A.; Dominguez, J. J.; Dörr, J. M.; Killian, J. A. Effect of Polymer Composition and PH on Membrane Solubilization by Styrene-Maleic Acid Copolymers. Biophys J 2016, 111 (9), 1974–1986. https://doi.org/10.1016/j.bpj.2016.09.025.

(24) Dörr, J. M.; Scheidelaar, S.; Koorengevel, M. C.; Dominguez, J. J.; Schäfer, M.; van Walree, C. A.; Killian, J. A. The Styrene–Maleic Acid Copolymer: A Versatile Tool in Membrane Research. European Biophysics Journal 2016, 45 (1), 3–21. https://doi.org/10.1007/s00249-015-1093-y.

(25) Orekhov, P. S.; Bozdaganyan, M. E.; Voskoboynikova, N.; Mulkidjanian, A. Y.; Karlova, M. G.; Yudenko, A.; Remeeva, A.; Ryzhykau, Y. L.; Gushchin, I.; Gordeliy, V. I.; Sokolova, O. S.; Steinhoff, H.-J.; Kirpichnikov, M. P.; Shaitan, K. V. Mechanisms of Formation, Structure, and Dynamics of Lipoprotein Discs Stabilized by Amphiphilic Copolymers: A Comprehensive Review. Nanomaterials (Basel) 2022, 12 (3). https://doi.org/10.3390/nano12030361.

(26) Kamilar, E.; Bariwal, J.; Zheng, W.; Ma, H.; Liang, H. SMALPs Are Not Simply Nanodiscs: The Polymer-to-Lipid Ratios of Fractionated SMALPs Underline Their Heterogeneous Nature. Biomacromolecules 2023, 24 (4), 1819–1838. https://doi.org/10.1021/acs.biomac.3c00034.

(27) Ujwal, R.; Bowie, J. U. Crystallizing Membrane Proteins Using Lipidic Bicelles. Methods 2011, 55 (4), 337–341. https://doi.org/10.1016/j.ymeth.2011.09.020.

(28) Newstead, S.; Ferrandon, S.; Iwata, S. Rationalizing A‐helical Membrane Protein Crystallization. Protein Science 2008, 17 (3), 466‐472. https://doi.org/10.1110/ps.073263108.

(29) Ravula, T.; Hardin, N. Z.; Bai, J.; Im, S.-C.; Waskell, L.; Ramamoorthy, A. Effect of Polymer Charge on Functional Reconstitution of Membrane Proteins in Polymer Nanodiscs. Chemical Communications 2018, 54 (69), 9615–9618. https://doi.org/10.1039/C8CC04184A.

(30) Drulis-Kawa, Z.; Majkowska-Skrobek, G.; Maciejewska, B.; Delattre, A.-S.; Lavigne, R. Learning from Bacteriophages - Advantages and Limitations of Phage and Phage-Encoded Protein Applications. Curr Protein Pept Sci 2012, 13 (8), 699–722. https://doi.org/10.2174/138920312804871193.

(31) Samir, S. Molecular Machinery of the Triad Holin, Endolysin, and Spanin: Key Players Orchestrating Bacteriophage-Induced Cell Lysis and Their Therapeutic Applications. Protein Pept Lett 2024, 31 (2), 85–96. https://doi.org/10.2174/0109298665181166231212051621.

(32) Abeysekera, G. S.; Love, M. J.; Manners, S. H.; Billington, C.; Dobson, R. C. J. Bacteriophage-Encoded Lethal Membrane Disruptors: Advances in Understanding and Potential Applications. Front Microbiol 2022, 13. https://doi.org/10.3389/fmicb.2022.1044143.

(33) Young, R. Phage Lysis: Three Steps, Three Choices, One Outcome. Journal of Microbiology 2014, 52 (3), 243–258. https://doi.org/10.1007/s12275-014-4087-z.

(34) Cahill, J.; Young, R. Phage Lysis: Multiple Genes for Multiple Barriers; 2019; pp 33–70. https://doi.org/10.1016/bs.aivir.2018.09.003.

(35) Wang, I.-N.; Smith, D. L.; Young, R. Holins: The Protein Clocks of Bacteriophage Infections. Annu Rev Microbiol 2000, 54 (1), 799–825. https://doi.org/10.1146/annurev.micro.54.1.799.

(36) Pimentel, M. Genetics of Phage Lysis. Microbiol Spectr 2014, 2 (1). https://doi.org/10.1128/microbiolspec.MGM2-0017-2013.

(37) Pang, T.; Park, T.; Young, R. Mutational Analysis of the S21 Pinholin. Mol Microbiol 2010, 76 (1), 68–77. https://doi.org/10.1111/j.1365-2958.2010.07080.x.

(38) Khan, M. R. H. Probing the Structural Topology, Dynamics, Conformation, and Secondary Structure of Pinholin S21 and Gp28, Bacteriophage Lytic Proteins, Using Electron Paramagnetic Resonance Spectroscopy. 2023. http://rave.ohiolink.edu/etdc/view?acc_num=miami1697138966748718 (accessed 2025-05-08).

(39) Ahammad, T. Probing the Structural Dynamics, Conformational Change, and Topology of Pinholin S21, a Bacteriophage Lytic Protein, Using Electron Paramagnetic Resonance Spectroscopy. 2020. http://rave.ohiolink.edu/etdc/view?acc_num=miami1595598100557068 (accessed 2025-05-08).

(40) Drew, D. L. Probing Structure and Dynamics of Transmembrane Alpha Helices of the S21 Pinholin Protein Using Electron Paramagnetic Resonance Spectroscopy. Biophys J 2016, 110 (3), 228a. https://doi.org/10.1016/j.bpj.2015.11.1261.

(41) Boeckaerts, D.; Stock, M.; Ferriol-González, C.; Oteo-Iglesias, J.; Sanjuán, R.; Domingo-Calap, P.; De Baets, B.; Briers, Y. Prediction of Klebsiella Phage-Host Specificity at the Strain Level. Nat Commun 2024, 15 (1), 4355. https://doi.org/10.1038/s41467-024-48675-6.

(42) Wilkinson, R. C.; Thomas, N. E.; Bhatti, A.; Burton, M. R.; Joyce, N.; Jenkins, R. E. Phage-Encoded Antimicrobial Peptide Gp28 Demonstrates LL-37-Like Antimicrobial Activity Against Multidrug-Resistant Pseudomonas Aeruginosa. PHAGE 2025, 6 (1), 12–19. https://doi.org/10.1089/phage.2024.0009.

(43) Rotich, N. C.; Khan, R. H.; Morris, A.; McCarrick, R.; Baral, B.; Okorafor, E. A.; Faul, E.; Wardrip, L.; Sahu, I. D.; Lorigan, G. A. Probing the Secondary Structure of Membrane-Bound Gp28 Using Electron Spin Echo Envelope Modulation (ESEEM) Spectroscopy. J Phys Chem B 2025, 129 (10), 2659–2667. https://doi.org/10.1021/acs.jpcb.4c08270.

(44) Khan, R. H.; Rotich, N. C.; Morris, A.; Ahammad, T.; Baral, B.; Sahu, I. D.; Lorigan, G. A. Probing the Structural Topology and Dynamic Properties of Gp28 Using Continuous Wave Electron Paramagnetic Resonance Spectroscopy. J Phys Chem B 2023, 127 (43), 9236–9247. https://doi.org/10.1021/acs.jpcb.3c03679.

(45) Holt, A.; Cahill, J.; Ramsey, J.; Martin, C.; O'Leary, C.; Moreland, R.; Maddox, L. T.; Galbadage, T.; Sharan, R.; Sule, P.; Cirillo, J. D.; Young, R. Phage-Encoded Cationic Antimicrobial Peptide Required for Lysis. J Bacteriol 2022, 204 (1). https://doi.org/10.1128/JB.00214-21.

(46) McCoy, M. T.; Jayanthi, S.; Cadet, J. L. Potassium Channels and Their Potential Roles in Substance Use Disorders. Int J Mol Sci 2021, 22 (3), 1249. https://doi.org/10.3390/ijms22031249.

(47) Splawski, I.; Shen, J.; Timothy, K. W.; Lehmann, M. H.; Priori, S.; Robinson, J. L.; Moss, A. J.; Schwartz, P. J.; Towbin, J. A.; Vincent, G. M.; Keating, M. T. Spectrum of Mutations in Long-QT Syndrome Genes. Circulation 2000, 102 (10), 1178–1185. https://doi.org/10.1161/01.CIR.102.10.1178.

(48) Stowe, R. A Spectroscopic and Biochemical Study of Protein Interactions and Membrane Mimetic Systems. 2023. http://rave.ohiolink.edu/etdc/view?acc_num=miami1687365132621403 (accessed 2025-05-08).

(49) Farrelly, M. D.; Martin, L. L.; Thang, S. H. Polymer Nanodiscs and Their Bioanalytical Potential. Chemistry – A European Journal 2021, 27 (51), 12922–12939. https://doi.org/10.1002/chem.202101572.

(50) Shah, M. Z.; Rotich, N. C.; Okorafor, E. A.; Oestreicher, Z.; Demidovich, G.; Eapen, J.; Henoch, Q.; Kilbey, J.; Prempeh, G.; Bates, A.; Page, R. C.; Lorigan, G. A.; Konkolewicz, D. Vinyl Ether Maleic Acid Polymers: Tunable Polymers for Self-Assembled Lipid Nanodiscs and Environments for Membrane Proteins. Biomacromolecules 2024. https://doi.org/10.1021/acs.biomac.4c00772.

(51) Sahu, I. D.; Zhang, R.; Dunagan, M. M.; Craig, A. F.; Lorigan, G. A. Characterization of KCNE1 inside Lipodisq Nanoparticles for EPR Spectroscopic Studies of Membrane Proteins. J Phys Chem B 2017, 121 (21), 5312–5321. https://doi.org/10.1021/acs.jpcb.7b01705.

(52) Hubbell, W. L.; Mchaourab, H. S.; Altenbach, C.; Lietzow, M. A. Watching Proteins Move Using Site-Directed Spin Labeling. Structure 1996, 4 (7), 779–783. https://doi.org/10.1016/S0969-2126(96)00085-8.

(53) Bodratti, A. M.; Alexandridis, P. Amphiphilic Block Copolymers in Drug Delivery: Advances in Formulation Structure and Performance. Expert Opin Drug Deliv 2018, 15 (11), 1085–1104. https://doi.org/10.1080/17425247.2018.1529756.

(54) Sligar, S. G.; Denisov, I. G. Nanodiscs: A Toolkit for Membrane Protein Science. Protein Science 2021, 30 (2), 297–315. https://doi.org/10.1002/pro.3994.

(55) Ahammad, T.; Khan, R. H.; Sahu, I. D.; Drew, D. L.; Faul, E.; Li, T.; McCarrick, R. M.; Lorigan, G. A. Pinholin S21 Mutations Induce Structural Topology and Conformational Changes. Biochim Biophys Acta Biomembr 2021, 1863 (12), 183771. https://doi.org/10.1016/j.bbamem.2021.183771.

(56) Sahu, I. D.; Lorigan, G. A. Site-Directed Spin Labeling EPR for Studying Membrane Proteins. Biomed Res Int 2018, 2018, 1–13. https://doi.org/10.1155/2018/3248289.

(57) Ravula, T.; Hardin, N. Z.; Ramamoorthy, A. Polymer Nanodiscs: Advantages and Limitations. Chem Phys Lipids 2019, 219, 45–49. https://doi.org/10.1016/j.chemphyslip.2019.01.010.

(58) Okorafor, E. A.; Rotich, N. C.; Lorigan, G. A. BPS2025 - Effect of Charged Polymers and Charged Lipids on the Biophysical Studies of Membrane Proteins. Biophys J 2025, 124 (3), 264a–265a. https://doi.org/10.1016/j.bpj.2024.11.1439.

(59) Karin, M. NF‐κB and Cancer: Mechanisms and Targets. Mol Carcinog 2006, 45 (6), 355‐361. https://doi.org/10.1002/mc.20217.

(60) Okorafor, E. A.; Gordon, E. A.; Sahu, I. D.; Shah, M. Z.; Konkolewicz, D.; Lorigan, G. Influence of Lipid Saturation on the Structural Properties of Styrene Maleic Acid Lipid Nanoparticles (SMALPs). Biochimica et Biophysica Acta (BBA) - Biomembranes 2025, 184424. https://doi.org/10.1016/j.bbamem.2025.184424.

(61) Zhou H, Lutkenhaus J. Membrane binding by MinD involves insertion of hydrophobic residues within the C-terminal amphipathic helix into the bilayer. J Bacteriol. 2003 Aug;185(15):4326-35. doi: 10.1128/JB.185.15.4326-4335.2003. PMID: 12867440; PMCID: PMC165746.

Chapter 4

Vinyl Ether Maleic Acid Polymers: Tunable Polymers for Self-assembled Lipid Nanodiscs and Environments for Membrane Proteins

Muhammad Zeeshan Shah,[a] Nancy C. Rotich,[a] Evelyn A. Okorafor,[a] Zachery Oestreicher,[b] Gabrielle Demidovich,[a] Jeremy Eapen,[a] Quinton Henoch,[a] Julia Kilbey,[a] Godfred Prempeh,[a] Alison Bates,[a] Richard C. Page,[a] Gary A. Lorigan,[a] Dominik Konkolewicz [a]

[a] Department of Chemistry and Biochemistry, Miami University, 651 E High St, Oxford, OH, 45056, USA

[b] Center for Advanced Microscopy and Imaging, Miami University, Oxford, OH, 45056, USA

This work has been published in Biomacromolecules Journal: Vinyl Ether Maleic Acid Polymers: Tunable Polymers for Self-Assembled Lipid Nanodiscs and Environments for Membrane Proteins. Biomacromolecules. 2024 Oct 14;25(10):6611-6623. doi: 10.1021/acs.biomac.4c00772. Epub 2024 Sep 16. PMID: 39283997; PMCID: PMC11473226. Reproduced in part with permission.

N.C.R., participated in the polymer bio-application experimental design, data acquisition, formal analysis, manuscript writing and editing. M.Z.S., participated in designing polymer synthesis experiments, data acquisition, data analysis, manuscript writing and editing.

4.0 Abstract

Lipid bilayer mimetics, including amphiphilic polymers, play an essential role in facilitating the solubilization of membrane-bound peptides and proteins. Copolymers composed of vinyl ether monomers and maleic anhydride engineered via reversible addition-fragmentation chain transfer polymerization are expected to provide precise control over molecular weights and hydrophobicity. The copolymerization of vinyl ether and maleic anhydride occurs in a nearly alternating fashion, resulting in alternating hydrophilic maleic acid units and hydrophobic vinyl ether units along the backbone upon hydrolysis. The copolymers self-assemble with lipids, generating vinyl ether-maleic acid lipid particles (VEMALPs) with adjustable sizes dictated by either the vinyl ether hydrophobicity or polymer molecular weight. The generated VEMALPs were characterized by dynamic light scattering (DLS) and transmission electron microscopy (TEM). The ability of VEMALPs to support membrane proteins was evaluated using Continuous Wave Electron Paramagnetic Resonance (CW-EPR) Spectroscopy. These VEMALPs demonstrated the capacity to accommodate the membrane bound protein (KCNE1) as well as gp28 peptide thus introducing a novel category of lipid bilayer mimetics. Overall, the study indicates that efficient self-assembly with lipids is possible and that the generated VEMALPs can support membrane bound proteins and peptides.

4.1 Introduction

Membrane proteins (MPs) are essential for various functions in both eukaryotic and prokaryotic cells, with approximately 30% of an organism's genome dedicated to coding for these proteins.[1,2] Given their critical roles and connection to pathogenic bacteria and viruses, around 70% of pharmaceuticals target MPs.[3,4] To develop drugs that effectively interact with MPs, understanding their structure and function is crucial; however, this has been challenging due to the difficulty in recreating their natural lipid environments.[5-7] Traditional methods like Magnetic Resonance Spectroscopy (MRS) are not applicable for studying MPs in vitro under these conditions.[8,9] Detergents have often been employed to extract MPs along with some lipid bilayers creating large liposomes in solutions.[10] However, these liposomes are not compatible with many analytical techniques used for protein study, such as MRS, chromatography, and optical spectroscopy. The use of detergents is particularly problematic because they do not accurately mimic the native environment of MPs and can lead to protein denaturation over time.[12,13]

Recent advancements have introduced lipid bicelles and nanodisc systems as alternatives for studying MPs.[14.15] Each system has its drawbacks; bicelle systems are limited by their lipid composition which may affect peptide functionality, while nanodiscs can alter the absorbance properties of certain proteins due to the loss of scaffolding proteins during preparation.[6,16] Detergents are still necessary when preparing proteins for nanodiscs. To overcome these challenges, a novel system was devised that solubilizes MPs while generating particles that closely resemble the native lipid environment.[4,8,13,17] The Styrene-Maleic Anhydride (SMA) copolymer system has emerged as the preferred option for extracting MPs and lipids from bilayers without relying on detergents.[5,18-20]

The synthesis of SMA occurs via conventional radical polymerization (FRP) resulting in polymers with dispersity values (2.0-2.5), indicating variability in molecular weight due to conventional radical polymerization methods.[21-23]Reversible addition-fragmentation chain-transfer (RAFT) polymerization, RAFT have substantially narrower molecular weight distributions, with dispersity in the order of 1.3-1.4.[24–26] This control over polymer structure in RAFT facilitates structure property correlations, while also allowing detailed investigation of the polymer composition along the chain.[8,23,27] While styrene-maleic anhydride lipid particles (SMALPs) offer advantages over traditional detergents, they possess a significant limitation: the inability to utilize ultraviolet-visible (UV-Vis) light spectroscopy effectively for

quantifying MP amounts within nanodisc systems.[28] Common amino acids like phenylalanine, tyrosine, and tryptophan contain aromatic rings that absorb UV light at similar wavelengths as SMALPs due to their styrene content further complicating far-UV circular dichroism (CD analyses.[7,11,28,30] A potential solution involves substituting styrene with non-aromatic hydrophobic compounds within the polymer system to resemble lipids that have no aromatic rings.[32] This study aims to replace styrene in SMA with aliphatic vinyl ethers such as dodecyl vinyl ether (DVE) and butyl vinyl ether (BVE) through copolymerization with maleic anhydride (MA) to create an amphiphilic copolymer expected to impart comparable hydrophobicity.[11,31-37] Similarly to styrene and α-olefins,[23,32] vinyl ether monomers have a strong tendency to alternate with MAn.[36–39] This has been studied primarily in FRP, where charge transfer complexes between the MAn and various VE monomers and efficient near alternating copolymerization has been found.[40–42] However, the controlled polymerization of a wide variety of alkyl vinyl ethers with maleic anhydride by RAFT has not been explored to the best of our knowledge, with studies only in one monomer, divinyl ether.[43] Use of vinyl ether-maleic anhydride based copolymers to make self-assembled lipid nanodiscs has not been studied.

Model membrane-bound proteins and peptides are needed to evaluate the effectiveness of lipid bilayer mimetics. KCNE1, KCNE4, and gp28, serve as excellent model proteins and peptides as they are small to moderate in size and can be studied in various lipids.[44] The KCNE family modulates voltage-gated potassium (Kv) channels such as Kv1.1, Kv1.3, Kv2.1, and Kv7.1.[45,46] Incorrect modulation of these channels has been linked to several diseases such as long Q1 syndrome, allergic rhinitis, and acute lymphoblastic leukemia.[47] KCNE1, modulates the function of KCNQ1.[48,49] KCNE1 is a single-pass transmembrane protein of 129 amino acids at a size of 15 kDa.[50,51] When KCNE1 interacts with KCNQ1 (Kv7.1), it forms the slow-delayed rectifier channel which is responsible for repolarization of the cardiac action potential.[45,47,47] KCNE4 is a single-pass transmembrane protein of 170 amino acids at a size of 24 kDa.[50] Relatively little is known about the structure of KCNE4; however, current predictions indicate that there is an alpha helix within the transmembrane region (residues 37-56) and likely additional helices within the C-terminal intracellular region.[52,53] KCNE4 has four leucine residues in a row, (residues 69-72), which has been linked to protein-protein interactions.[53–55] The known structural and functional information of KCNE1 and the importance of gaining structural insights into KCNE4 make them excellent systems for MP studies.[56,57] Gp28 is a 56-residue cationic antimicrobial peptide (CAMP), capable of disrupting the outer membranes of bacteria. This peptide represents a distinct category of phage-encoded lysis proteins.[58,59] The cationic nature of gp28, characterized by its +7 positive charge, underscores its

significance in the realm of antimicrobial peptides.[44,60] The unique charge and lipid interaction ability of gp28 makes it an important peptide for lipid interaction studies.

KCNE1, KCNE4, and gp28 were used to explore VE-MAn polymers for nanodisc formation. It was expected that the addition of dodecyl vinyl ether (DVE) and butyl vinyl ether (BVE) in the new copolymer will incorporate hydrophobic units similar to styrene in SMA, although with the hydrophobicity of the polymer easily tuned by the ratio of DVE to BVE used, and the possibility of generating well-controlled polymers with molecular weights tuned between ~5,000 to ~40,000. This newly developed DVE-BVE-MA copolymer was evaluated against different lipids and membrane proteins to form nanodiscs capable of supporting membrane-bound proteins and peptides. Self-assembled nanodiscs between the DVE-BVE-MA copolymer and lipids are termed vinyl ether maleic acid lipid particles or VEMALPs.

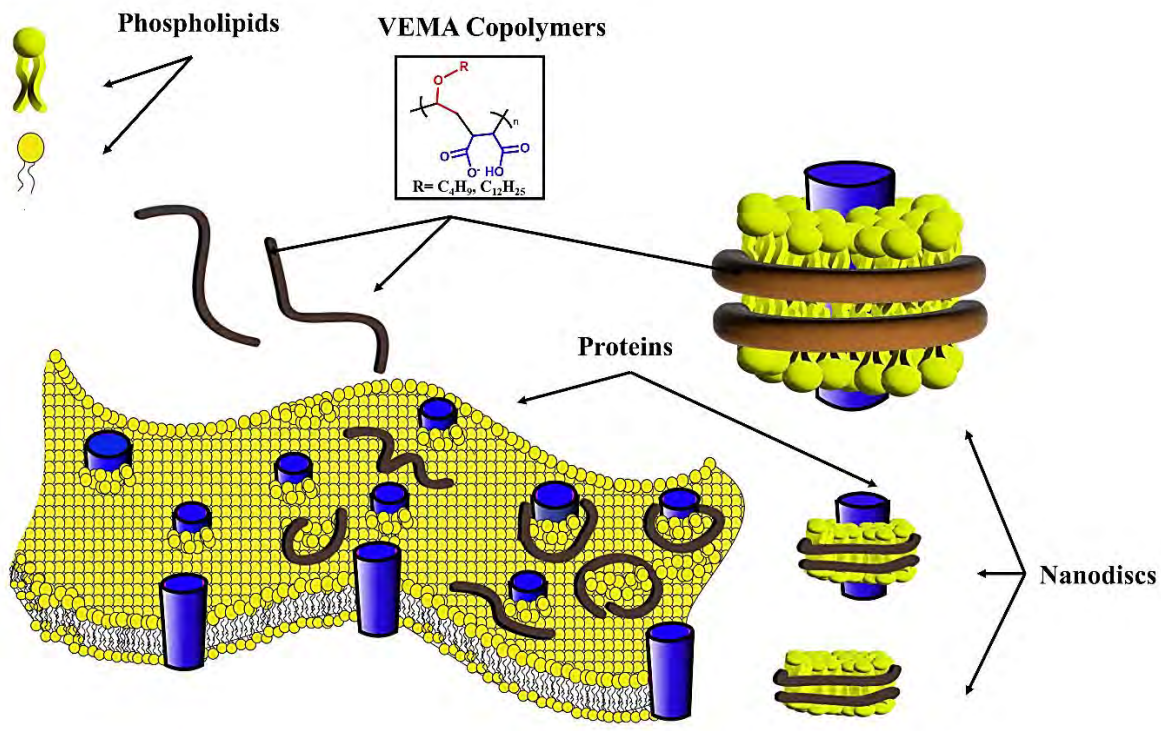

Figure 4. 1: Structure of VEMA copolymers and their proposed interactions with lipids to form nanodiscs containing membrane proteins.

The VE-MAn polymers were subsequently hydrolyzed to give amphiphilic polymers capable of forming VEMALPs through self-assembly with lipids. The generated VEMALPs were characterized by dynamic light scattering (DLS) and transmission electron microscopy (TEM). The ability of VEMALPs to support

membrane proteins was evaluated using Continuous Wave Electron Paramagnetic Resonance (CW-EPR) Spectroscopy. Overall, the studies indicate that efficient self-assembly with lipids is possible, the generated VEMALPs can support membrane bound proteins and peptides. This is highlighted in **Figure 4.1.**

4.2 Experimental

4.2.1 Synthesis of gp28

Fmoc solid-phase peptide synthesis (Fmoc-SPPS) was used to synthesize gp28 spin-labeled peptides with an introduced cysteine mutation at various positions. A nitroxide spin label, MTSL (*S*-(1-oxyl-2,2,5,5-tetramethyl-2,5-dihydro-1*H*-pyrrol-3-yl)methylethanesulfonothioate), was site-specifically attached to the cysteine using site-directed spin labeling (SDSL).

4.2.2 Preparation of KCNE1

KCNE1 mutant T58C was overexpressed in BL21 *Escherichia coli* cells grown in TB minimal medium with 50 μg/mL of chloramphenicol and 75 μg/mL of ampicillin. The cell cultures were grown until an OD_{600} of 0.4–0.8 was reached, and then the cells were induced with 1 mM isopropyl-1-thio-d-galactopyranoside. Purification was completed using the previously described protocol although the protein was eluted with 0.5% dodecylphosphocholine (DPC) detergent rather than 1-myristoyl-2-hydroxy-*sn*-glycero-3-phospho-(1′-rac-glycerol) (LMPG) detergent.[46] The protein was concentrated with an ultracel regenerated cellulose membrane concentrator (3 kDa molecular cutoff; Millipore Sigma), and protein purity was confirmed using sodium dodecyl sulfate-polyacrylamide gel electrophoresis (SDS-PAGE).

4.2.3 Preparation of KCNE4

KCNE4 mutant S9C was overexpressed in BL21 *E. coli* cells grown in TB minimal medium with 50 μg/mL of chloramphenicol and 75 μg/mL of ampicillin. The cell cultures were grown until an OD_{600} of 0.4–0.8 was reached, and then the cells were induced with 1 mM isopropyl-1-thio-d-galactopyranoside. The cells were suspended by end-over-end mixing in 40 mL of lysis buffer (70 mM tris-HCl pH 8.0, 300 mM NaCl), supplemented with 140 μL of LDR stock (100 mg/mL lysozyme, 10 mg/mL DNase, 10 mg/mL RNase), 1.75 mM of TCEP, and 0.4 mM of $Mg(Ac)_2$ at 4 °C for 1 h. The cell suspension was sonicated on ice with 5 s on/off pulse for 8.5 min at 40% amplitude (Fisher Scientific Sonic

Dismembrator Model 500). The lysate was centrifuged at 13,000 RCF and 4 °C for 30 min to recover inclusion bodies.

Inclusion bodies were suspended until smooth in 20 mL of inclusion body wash buffer (70 mM tris-HCl pH 8.0, 300 mM NaCl, 12.5% sucrose, and 1% Triton X-100) and centrifuged at 40,000 RCF and 4 °C for 10 min. The supernatant was discarded, and the inclusion bodies were subjected to a second wash treatment and centrifuged at 40,000 RCF and 4 °C for 10 min. To remove excess Triton X-100, the inclusion bodies were rinsed three times; the pellet was resuspended in 40 mL of cold water and centrifuged at 40,000 RCF and 4 °C for 10 min each time. The final inclusion body pellet was solubilized overnight at room temperature (RT) in a solution of 20 mL of urea-TS (8 M urea, 20 mM tris pH 8.0, and 150 mM NaCl), 1 mM TCEP, and 0.2% SDS.

Solubilized inclusion bodies were centrifuged at 14,000 RCF for 30 min at RT to remove insoluble material. The supernatant was incubated with 3 mL of a 100% pre-equilibrated Ni(II)-NTA superflow resin (Qiagen) at RT overnight. After incubation, the resin–protein mixture was settled and then suspended in 30 mL of 20 mM tris pH 8.0, 150 mM NaCl, and 0.1% 1-myristoyl-2-hydroxyl-*sn*-glycero-3-phospho-(1′-rac-glycerol) (LMPG) (Anatrace). The resin pellet was suspended in 30 mL of 20 mM tris pH 8.0, 150 mM NaCl, 50 mM imidazole, and 0.1% LMPG. The protein was eluted from the resin using 4 mL of 20 mM tris pH 8.0, 150 mM NaCl, 250 mM imidazole, and 0.1% LMPG. Buffer exchange was achieved by centrifugation of the solutions through an ultracel regenerated cellulose membrane concentrator (3 kDa molecular cutoff; Millipore Sigma) with 50 mM phosphate buffer pH 7 and 0.05% *n*-dodecylphosphocholine (DPC) (Anatrace) at 4284 RCF at 4 °C for 30 min, 3 times.

4.2.4 MTSL Spin Labeling

MTSL (250 mM stock, DMSO) (Toronto Research Chemicals) was added directly to concentrated His_{6x}-E4 protein in 50 mM phosphate buffer, pH 7.0, and 0.05% DPC at a 10:1 MTSL/protein molar ratio. The solution reacted overnight at room temperature with shaking. The mixture was placed on an ultracel regenerated cellulose membrane, 3 kDa molecular cutoff, (Millipore Sigma) for centrifugal filtering with 50 mM phosphate buffer, pH 7, and 0.05% DPC at 4284 RCF at 4 °C for 30 min, 3 times, followed by incubation with 3 mL of pre-equilibrated Ni(II)-NTA superflow resin overnight at 4 °C. The resin was washed with 300 mL of 50 mM phosphate buffer, pH 7.0, and 0.05% DPC. The protein was eluted with 4 mL of 50 mM phosphate buffer, pH 7.0, 250 mM imidazole, and 0.5% DPC.

4.2.5 Vesicle Reconstitution

Vesicle samples were composed of a 3:1 molar ratio of 1-palmitoyl-2-oleoyl-*sn*-glycero-3-phosphocholine (POPC) and 1-palmitoyl-2-oleoyl-*sn*-glycero-3-phospho-(1′-rac-glycerol) (sodium salt) (POPG) (Avanti Polar Lipids). The powdered lipids were dissolved in chloroform and evaporated to form a thin film on the side of a pear-shaped flask. The sample was dried overnight in a vacuum desiccator. The thin film was suspended in 50 mM phosphate buffer at pH 7 to a final concentration of 100 mM lipid. The proteoliposomes were generated by mixing the protein and lipid solution at a ratio of 1:400 and subjecting them to three freeze–thaw cycles. All vesicles were prepared with a protein concentration of approximately 100 μM. Excess detergent was removed via dialysis with spectrum spectra/Por 4 RC dialysis membrane tubing 12–14 kDa MWCO (Fisher Scientific) for 72 h in 100 mM imidazole and 2 mM EDTA pH 7 changed roughly every 12 h. The dialysate is concentrated by ultracentrifugation at 300,000*g* for 35 min. The proteoliposome pellet was thoroughly resuspended in 100 μL of 50 mM phosphate buffer at pH 7 and immediately used for spectroscopic measurements.

4.2.6 Preparation of POPC Vesicles

A previously published procedure was used to prepare the POPC and POPG vehicles.[5] Given that the phosphatidylcholine headgroup is the most abundant headgroup in eukaryotic cell membranes, POPC was chosen as our main lipid system. Powdered POPC and POPG lipids were dissolved in chloroform and evaporated to form a thin film on the sides of a heart-shaped flask. The sample was then dried overnight in a vacuum desiccator. The lipid film was suspended in a buffer containing 100 mM NaCl and 20 mM *N*-(2-hydroxyethyl)piperazine-*N*′-ethanesulfonic acid (HEPES) at pH 7.0 to a final concentration of 100 mM. The solution was vortexed vigorously to mix completely, resulting in a homogeneous milky solution after 5 freeze/sonication cycles. Vesicle solutions were then placed in a freezer overnight (−20 °C). Dynamic light scattering (DLS) experiments were used to confirm the size and homogeneity of the vesicles.

4.2.7 BVE and Vesicle Mixing Protocol

VEMA samples were dissolved in a buffer (20 mM HEPES, 100 mM NaCl pH 7) at an approximate concentration of 5% (m/v) and sonicated for about 25–30 min. The lipid nanoparticles (LPs) were formed by adding the polymer solution dropwise to the POPC vesicles at a volume ratio of 1/2 lipid to the polymer. Samples were then equilibrated via five freeze/sonication cycles. Samples were allowed to

mix and equilibrate overnight in a freezer overnight (−4 °C). The mixture was then centrifuged at 25k rpm for 30 min before making the DLS measurement.

4.2.8 pH Stability of SMALPs vs VEMALPs

SMA polymer at a 1:3 ratio of MA to S was synthesized as outlined in the literature.[63] SMALPs and VEMALPs were formed by mixing together SMA (MA:S = 1:3, M_n = 11,000, M_w/M_n = 1.34) and VEMA (MA:BVE:DVE = 50:53:13, M_n = 10,000, M_w/M_n = 1.51) polymers (5% w/v) and POPC vesicles (20 mM) at a 2:1 v/v ratio followed by five freeze–thaw cycles and rotated at 4 °C overnight. Then, the turbidity of solutions of varying pH values was measured in a 96-well plate. The SMA and VEMA solutions (20 μL) were combined with 120 μL of 0.1 M NaCl with 0.1 M buffer–pH 3 HEPES, pH 5 acetate, pH 7 HEPES, and pH 9 CHES. The optical density at 620 nm was used to measure turbidity using a Biotek Synergy multimode reader.[63]

4.2.9 Stability of SMALPs vs VEMALPs against Mg^{2+}

SMALPs and VEMALPs were prepared as described in the previous section. In a 96-well plate, 20 μL of the solutions were combined with Mg^{2+} containing buffer for a final volume of 150 μL at the desired [Mg^{2+}] up to 1000 mM. All points were run baselined against a solution of SMALPs and VEMALPs at 0 mM Mg^{2+}. The optical density at 620 nm was used to measure turbidity using a Biotek Synergy multimode reader.[63]

4.3 Synthesis of VEMA Polymer

To generate amphiphilic polymers, the maleic anhydride unit was hydrolyzed by adapting published protocols for S-MAn hydrolysis to the newly synthesized VE-MAn polymers.[68] Amphiphilic vinyl ether-maleic acid (VEMA) polymers were generated by RAFT using the ratios MA:BVE = 50:66, MA:BVE:DVE = 50:53:13, and MA:BVE:DVE = 50:44:22 and evaluated on their ability of these polymers to self-assemble with lipids and form nanodiscs with the lipids 1-palmitoyl-2-oleoyl-sn-glycero-3-phosphocholine (POPC) or 1-palmitoyl-2-oleoyl-sn-glycero-3-phospho-(1'-rac-glycerol) (sodium salt) (POPG). In all cases, the polymer was added to prepared lipid vesicles followed by incubation. The generated self-assembled polymer lipid nanoparticles are termed vinyl ether maleic acid lipid particles or VEMALPs.

4.4 Results and Discussion

When comparing the different polymer compositions for their ability to self-assemble with lipids and form nanodiscs visual inspection of the MA:BVE:DVE = 50:53:13 and MA:BVE:DVE = 50:44:22 upon mixing with POPC lipids converted the milky POPC vesicle solution to an essentially clear solution. In contrast, the MA:BVE = 50:66 polymer did not form a clear solution upon being mixed with POPC lipids. These visual observations were confirmed with DLS in **Figure 4.2A**. The POPC vesicles had a size in the order of 1000 nm, MA:BVE:DVE = 50:53:13 polymer gave nanoparticles in the range of ~10 nm, while MA:BVE:DVE = 50:44:22 polymer yielded nanoparticles in the range of ~20 nm. In contrast, MA:BVE = 50:66 had limited ability to form self-assembled nanoparticles, since the size of POPC vesicles mixed with BVE was ~500 nm. Interestingly the data in **Figure 4.2A** indicates that there is an optimal hydrophilic-lipophilic balance to form narrowly distributed small disc through polymer-lipid self-assembly.

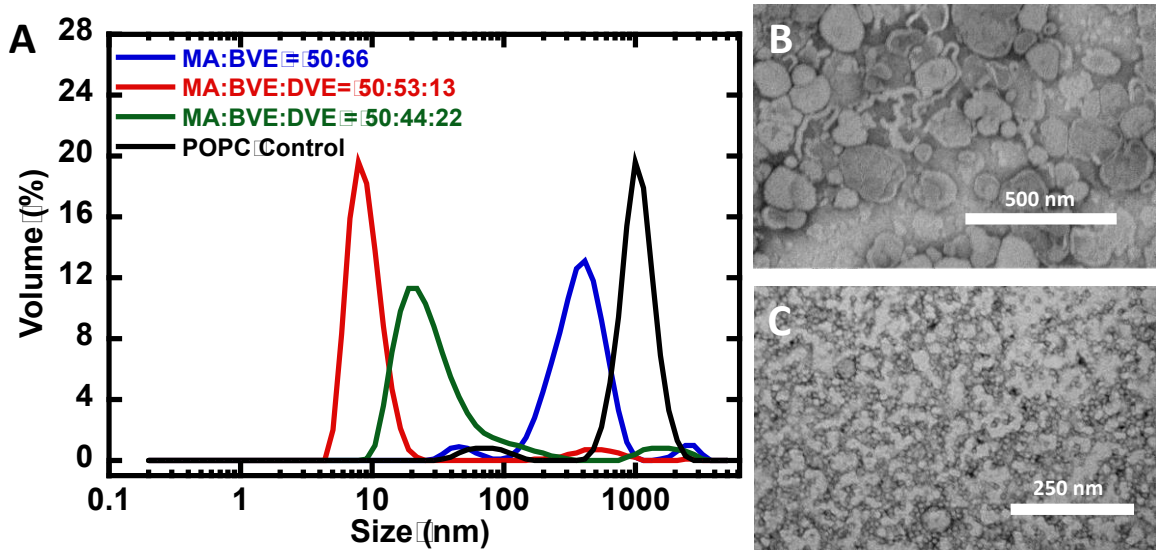

Figure 4. 2: A) DLS size (diameter) distribution of POPC vesicles (black), VEMALPs generated from self-assembly of POPC lipids with polymers of MA:BVE = 50:66 (blue), MA:BVE:DVE = 50:53:13 (orange) and MA:BVE:DVE = 50:44:22 (green). B) TEM image of POPC vesicles. C) VEMALPs generated via self-assembly of POPC lipids with MA:BVE:DVE = 50:53:13 polymers.

BVE is substantially less lipophilic than DVE. When using polymers with only BVE, the interactions with the hydrophobic tails of the lipids appear to be limited and large nanoparticles are formed. The composition MA:BVE:DVE = 50:53:13 gave the best defined and smallest nanoparticles, consistent with this being an optimal hydrophilic-lipophilic balance with sufficient hydrophilicity to stabilize the nanodiscs but enough hydrophobic dodecyl chains to interact with the lipid alkyl chains. Finally,

MA:BVE:DVE = 50:44:22 gave larger nanoparticles and was substantially more hydrophobic. This is similar to earlier work with SMA polymers, where an optimal ratio of styrene to maleic anhydride gave the best defined nanodiscs.[69]

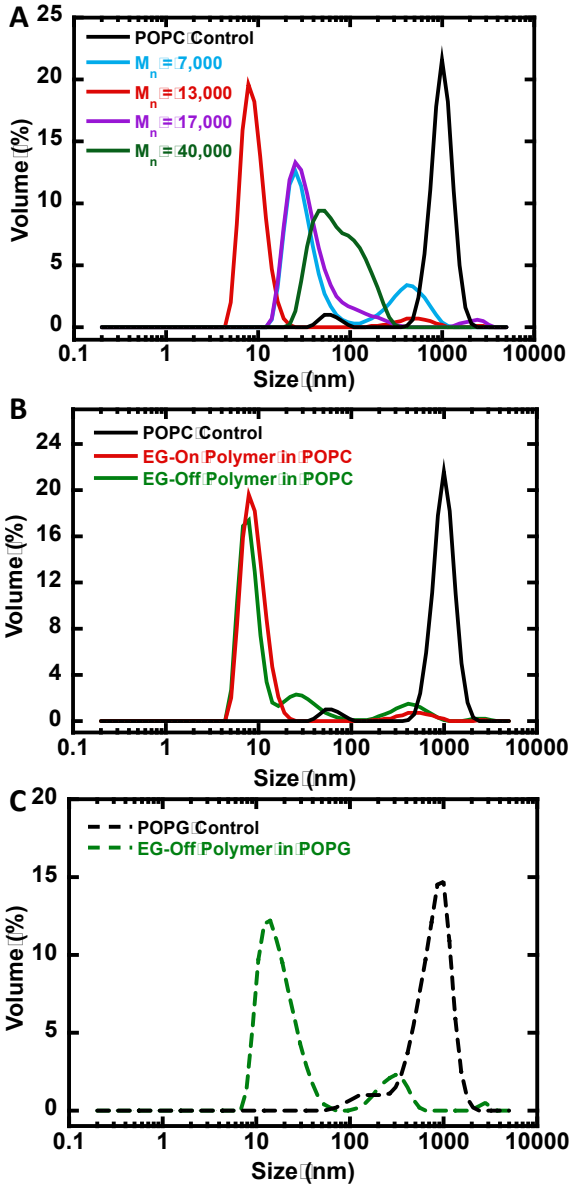

Figure 4. 3: A) DLS size distribution of POPC vesicles (black) and VEMALPs using lipid:BVE ratio of 1:2 v/v with different molecular weights of polymers with ratios [MA]:[BVE]:[DVE] = 50:53:13. B) Size distribution of POPC vesicles and VEMALPs from polymer of M_n = 13,000, [MA]:[BVE]:[DVE] = 50:53:13 with and without end-group removed. C) Size distribution of POPG vesicles and VEMALPs from polymer of M_n = 13,000, [MA]:[BVE]:[DVE] = 50:53:13 with end-group removed.

TEM was used to confirm the well-defined self-assembled VEMALPs between POPC lipids and the MA:BVE:DVE = 50:53:13 copolymers. **Figure 4.2B** shows the large vesicles of POPC, which appear

smaller than measured by DLS, plausibly due to the drying and vacuum methods needed in TEM analysis. As seen in **Figure 4.2C**, TEM results show round lipid discs formation in 10-30 nm range MA:BVE:DVE = 50:53:13 copolymers, consistent with the formation of well-defined VEMALPs. This size range of 10-30 nm is promising for downstream applications of VEMALPs in membrane protein research as already reported in literature for SMALPs.[5,30,70] To observe the effect of different polymer sizes, the hydrophobically optimized ratio of MA:BVE:DVE = 50:53:13 was tested with polymers of different molecular weights in **Figure 4.3A**. Polymers of relatively low or high molecular weight were less efficient at forming VEMALPs in the order of 10 nm. With lower molecular weights in the order of 7,000 high the size of nano-discs was in the order of 20 nm, which could be due to a higher solubility of the smaller polymer in the aqueous medium, decreasing its ability to self-assemble with lipids. Polymers of M_n ~ 10,000-13,000 gave the smallest diameter nanodiscs near 10 nm diameter. Higher ratios M_n of 17,000 gave similar, albeit slightly larger discs of 20 nm, while the very large polymer of M_n ~ 40,000 gave larger and less uniform VEMALPs of diameter ~50 nm. The higher molecular weight polymers appeared to have poor self-assembly, possibly due to lower solubility in the aqueous phase, which could inhibit the exchange needed to form uniform discs. Additionally, as highlighted in **Figure 4.1**, the RAFT end group can be removed through reaction with lauroyl peroxide (LPO) combined with AIBN.[71] The RAFT end group absorbs strongly near 300 nm,[72] which can interfere with the quantification of proteins by UV-Vis spectroscopy. As seen in **Figure 4.3B** the VEMALPs generated by self-assembling the MA:BVE:DVE = 50:53:13 polymer with POPC is essentially the same for EG-On or EG-Off.

Continuous wave-electron paramagnetic resonance (CW-EPR) line shape analysis was used to confirm that the VEMALPs are able to support complex membrane interacting or membrane-bound proteins and peptides. Insights into the structural and dynamic characteristics of membrane proteins can be gleaned by line shape analysis in CW-EPR spectra of spin-labeled molecules within various membrane-mimicking environments.[74] The CW-EPR line shapes evident in the respective spectra mirror the dynamics of the spin label.[75] The presence of three equally spaced, sharp lines of comparable intensity is indicative of an unrestrained reorientational motion of the nitroxide spin label. In this study, VEMALPs were employed as a model system to mimic membranes, allowing for the exploration of the structural and dynamic features of two distinct entities: the integral membrane proteins KCNE1, KCNE4, and the phage-encoded cationic antimicrobial peptide, gp28. Site-directed spin labeling coupled with EPR spectroscopy, was employed. A lipid bilayer composed of a POPC:POPG (3:1) ratio was selected to simulate the phospholipid composition commonly encountered in mammalian membranes. The CW-EPR data are

shown in **Figure 4.4**. This lipid bilayer served a dual purpose, acting not only as a representative model, but also as the basis for the control CW-EPR line shapes.

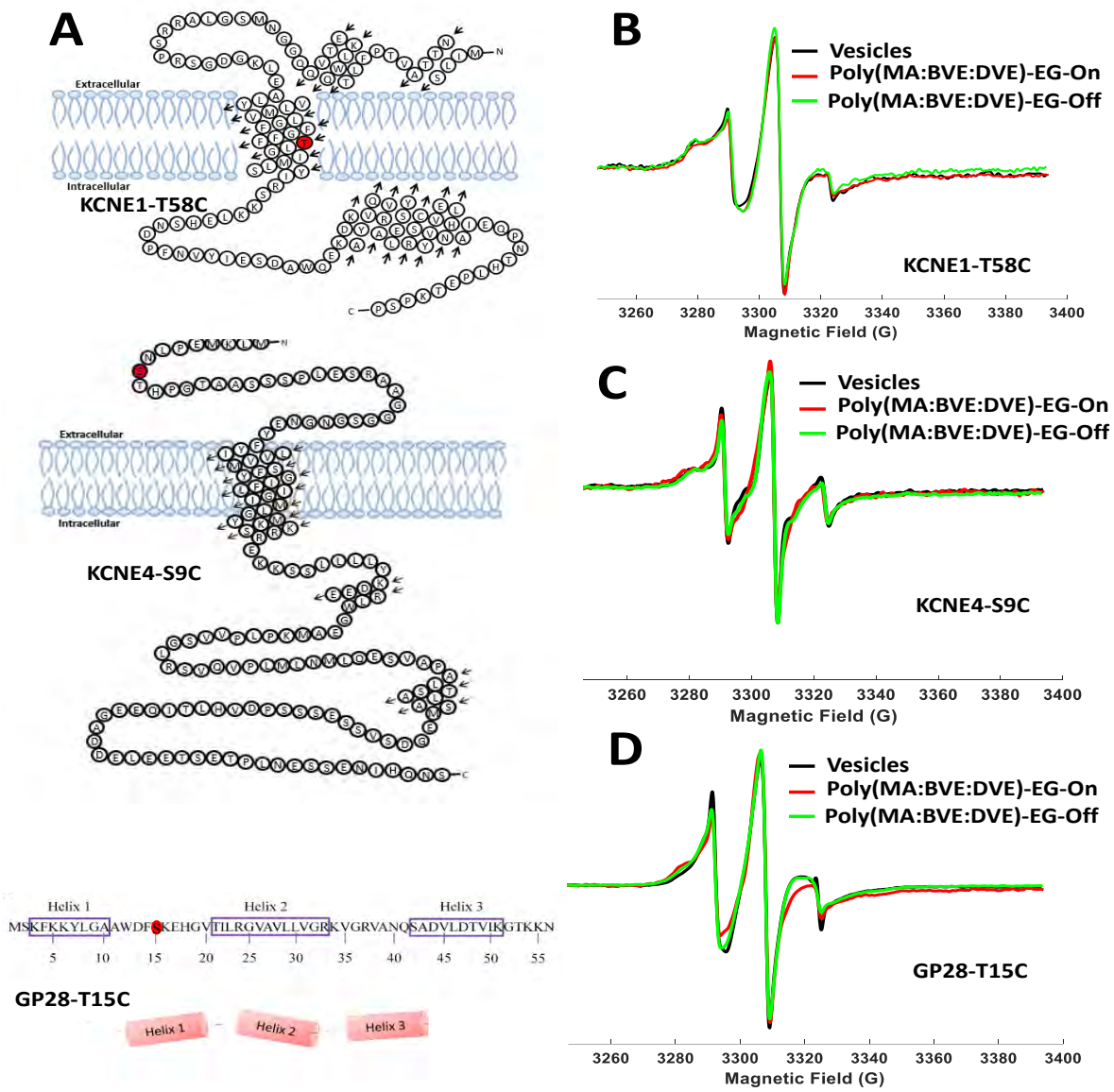

Figure 4. 4: A) Structures of KNCE1, KCNE4 and gp28 including location of spin labels. B) CW-EPR spectra of KCNE1 T58C spin labelled system in different lipid bilayer mimetics. C) CW-EPR spectra of KCNE4 S9C spin labelled system in different lipid bilayer mimetics. D) CW-EPR spectra of gp28 T15C spin labelled system in different lipid bilayer mimetics.

KCNE1 was selected as the primary model system for examining the behavior of the VEMALPs and their variations, especially the end group removed derivative. This choice was based on the extensive prior research on KCNE1, and the consistent alignment of the CW-EPR results with the solution nuclear magnetic resonance (NMR) structure of the protein.[43,76] KCNE1 T58C mutant was chosen as the control

given that its EPR line shape has been thoroughly substantiated through comparison with the existing literature.[68,75] The CW line shapes of KCNE1 have been comprehensively characterized within both lipid bilayers and in the context of soluble membrane-like nanodiscs such as SMALPs.[70] This makes KNCE1 an appealing model system for subsequent analysis. A complementary albeit larger protein in the KCNE family is KCNE4.[51,52] Although KCNE4 is less studied than KCNE1, it is beneficial to apply new membrane mimetics to alternative proteins to ensure they are broadly useful. Finally, a fifty-six residue peptide, gp28 disrupts bacterial membranes, hence its interaction with the lipid membrane mimetics through CW line shape analysis can provide insights into the impact of various mimetics. The sequence of KNCE1, KCNE4 and gp28 are given in **Figure 4.4A**. The site at which the spin label is attached is also highlighted.

The proteins were incorporated into POPC:POPG=3:1 lipids and were combined with polymers of MA:BVE:DVE = 50:53:13 with a M_n of 13,000. The CW-EPR data in **Figures 4.4B** and **4.4C** revealed essentially no notable distinctions in the EPR spectral lineshape and the corresponding inverse central line width between spin-labeled residues of KCNE1/E4, which indicates no major changes in the structure or dynamics of these proteins. Both the EG-On and EG-Off systems behaved similarly. In cases where spectral clarity is needed deep into the UV, the EG-Off system could be used, while the synthetic ease of synthesizing the EG-On sample is appealing when UV-Vis analysis is not needed. The data on KCNE1 and KCNE4 is highly encouraging and indicates that the VEMA polymers are able to make lipid membrane mimetics capable of supporting complex membrane bound proteins and can be used in future studies. However, as seen in **Figure 4.4D**, the peptide gp28 does lead to some slight differences in line shape between the POPC: POPG vesicles and the VEMALPs. Given that gp28 is a fifty-six amino acid peptide hence smaller in size compared to the KCNE1/4 membrane protein system, the side chain motion is more sensitive hence the minor shifts/ changes were detectable. Importantly, however, the line shapes of gp28 in the VEMALPs were essentially the same for the EG-On and the EG-Off system. Therefore, changes in the dynamics and line shape arise from the nature of the self-assembled VEMALPs, not the end group of the polymer.

4.6 Conclusion

The controlled RAFT copolymerization of vinyl ether monomers with maleic anhydride was investigated. The polymers could self-assemble with lipids forming VEMALPs, the vinyl ether analogues of SMALPs,

with size tuned by both the molecular weight of the polymer and the hydrophilic/lipophilic balance of the polymers. VEMA polymers with and without the end group were able to solubilize both membrane proteins and cationic antimicrobial peptides like gp28. CW-EPR line shape agreement of spin-labeled peptides and proteins in the lipid vesicle system and the VEMA systems reflect the native membrane environment and serve as a robust confirmation of the effectiveness of VEMA polymers. The demonstrated efficacy of VEMA polymers in facilitating the study of these biomolecules broadens the methodological repertoire available to investigators in this field, contributing to advancements in our understanding of these complex biological entities without the limitations of SMALPs from competitive UV-Vis absorbance, especially in the end-group removed system. Further, the ease of tuning the hydrophobicity and hydrophilicity is an advantage of the VEMALPs system compared to SMALPs or DIBMALPs, and as demonstrated here, the molecular weight of the VEMA system can be controlled, which is an advantage over the current maleic acid α-olefin based system.

Author Contributions

M.Z.S., participated in designing the experiments, data acquisition, data analysis, manuscript writing and editing. N.C.R., and E.O. participated in experimental design, data acquisition, formal analysis, writing and editing. Q.H participated in data acquisition, analysis and writing. Z.O. participated in data acquisition, formal analysis, and editing. G.D., J.E., G.A.P., and J.K., participated in data collection. A.B., participated in data collection and editing. R.C.P., participated in conceptualization, editing and formal analysis of data. G.A.L., participated in conceptualization, experimental design, formal analysis, and editing. D.K. participated in conceptualization, experimental design, formal analysis, and writing and editing.

Acknowledgements

We acknowledge Anne Carroll for support in the ^{1}H-NMR acquisition. DK acknowledges support from NIGMS/NIH under award number R15GM144907 for polymer synthesis, kinetics, and characterization. GAL acknowledges generous support by a NIGMS/NIH Maximizing Investigator's Research Award (MIRA) R35 GM126935 for membrane protein and lipid biochemistry. RCP acknowledges support from NIGMS/NIH R35 GM128595 for protein biophysics.

References

(1) Chen, A.; Majdinasab, E. J.; Fiori, M. C.; Liang, H.; Altenberg, G. A. Polymer-Encased Nanodiscs and Polymer Nanodiscs: New Platforms for Membrane Protein Research and Applications. *Front. Bioeng. Biotechnol.* **2020**, *8*, 598450. https://doi.org/10.3389/fbioe.2020.598450.

(2) Dürr, U. H. N.; Gildenberg, M.; Ramamoorthy, A. The Magic of Bicelles Lights Up Membrane Protein Structure. *Chem. Rev.* **2012**, *112* (11), 6054–6074. https://doi.org/10.1021/cr300061w.

(3) Ravula, T.; Hardin, N. Z.; Ramamoorthy, A. Polymer Nanodiscs: Advantages and Limitations. *Chem. Phys. Lipids* **2019**, *219*, 45–49. https://doi.org/10.1016/j.chemphyslip.2019.01.010.

(4) Cournia, Z.; Allen, T. W.; Andricioaei, I.; Antonny, B.; Baum, D.; Brannigan, G.; Buchete, N.-V.; Deckman, J. T.; Delemotte, L.; del Val, C.; Friedman, R.; Gkeka, P.; Hege, H.-C.; Hénin, J.; Kasimova, M. A.; Kolocouris, A.; Klein, M. L.; Khalid, S.; Lemieux, M. J.; Lindow, N.; Roy, M.; Selent, J.; Tarek, M.; Tofoleanu, F.; Vanni, S.; Urban, S.; Wales, D. J.; Smith, J. C.; Bondar, A.-N. Membrane Protein Structure, Function, and Dynamics: A Perspective from Experiments and Theory. *J. Membr. Biol.* **2015**, *248* (4), 611–640. https://doi.org/10.1007/s00232-015-9802-0.

(5) Gordon, E. A.; Richardson, Y. B.; Shah, M. Z.; Burridge, K. M.; Konkolewicz, D.; Lorigan, G. A. Formation of Styrene Maleic Acid Lipid Nanoparticles (SMALPs) Using SMA Thin Film on a Substrate. *Anal. Biochem.* **2022**, *647*, 114692. https://doi.org/10.1016/j.ab.2022.114692.

(6) Raschle, T.; Hiller, S.; Etzkorn, M.; Wagner, G. Nonmicellar Systems for Solution NMR Spectroscopy of Membrane Proteins. *Curr. Opin. Struct. Biol.* **2010**, *20* (4), 471–479. https://doi.org/10.1016/j.sbi.2010.05.006.

(7) Nestorow, S. A.; Dafforn, T. R.; Frasca, V. Biophysical Characterisation of SMALPs. *Biochem. Soc. Trans.* **2021**, *49* (5), 2037–2050. https://doi.org/10.1042/BST20201088.

(8) Craig, A. F.; Clark, E. E.; Sahu, I. D.; Zhang, R.; Frantz, N. D.; Al-Abdul-Wahid, M. S.; Dabney-Smith, C.; Konkolewicz, D.; Lorigan, G. A. Tuning the Size of Styrene-Maleic Acid Copolymer-Lipid Nanoparticles (SMALPs) Using RAFT Polymerization for Biophysical Studies. *Biochim. Biophys. Acta BBA - Biomembr.* **2016**, *1858* (11), 2931–2939. https://doi.org/10.1016/j.bbamem.2016.08.004.

(9) Henry, G. D.; Sykes, B. D. Methods to Study Membrane Protein Structure in Solution. In *Methods in Enzymology*; Elsevier, 1994; Vol. 239, pp 515–535. https://doi.org/10.1016/S0076-6879(94)39020-7.

(10) Privé, G. G. Detergents for the Stabilization and Crystallization of Membrane Proteins. *Methods* **2007**, *41* (4), 388–397. https://doi.org/10.1016/j.ymeth.2007.01.007.

(11) Oluwole, A. O.; Danielczak, B.; Meister, A.; Babalola, J. O.; Vargas, C.; Keller, S. Solubilization of Membrane Proteins into Functional Lipid-Bilayer Nanodiscs Using a Diisobutylene/Maleic Acid Copolymer. *Angew. Chem. Int. Ed.* **2017**, *56* (7), 1919–1924. https://doi.org/10.1002/anie.201610778.

(12) Seddon, A. M.; Curnow, P.; Booth, P. J. Membrane Proteins, Lipids and Detergents: Not Just a Soap Opera. *Biochim. Biophys. Acta BBA - Biomembr.* **2004**, *1666* (1–2), 105–117. https://doi.org/10.1016/j.bbamem.2004.04.011.

(13) Bada Juarez, J. F.; Harper, A. J.; Judge, P. J.; Tonge, S. R.; Watts, A. From Polymer Chemistry to Structural Biology: The Development of SMA and Related Amphipathic Polymers for Membrane Protein Extraction and Solubilisation. *Chem. Phys. Lipids* **2019**, *221*, 167–175. https://doi.org/10.1016/j.chemphyslip.2019.03.008.

(14) Ujwal, R.; Bowie, J. U. Crystallizing Membrane Proteins Using Lipidic Bicelles. *Methods* **2011**, *55* (4), 337–341. https://doi.org/10.1016/j.ymeth.2011.09.020.

(15) Denisov, I. G.; Sligar, S. G. Nanodiscs for Structural and Functional Studies of Membrane Proteins. *Nat. Struct. Mol. Biol.* **2016**, *23* (6), 481–486. https://doi.org/10.1038/nsmb.3195.

(16) Frey, L.; Lakomek, N.; Riek, R.; Bibow, S. Micelles, Bicelles, and Nanodiscs: Comparing the Impact of Membrane Mimetics on Membrane Protein Backbone Dynamics. *Angew. Chem. Int. Ed.* **2017**, *56* (1), 380–383. https://doi.org/10.1002/anie.201608246.

(17) Katzen, F.; Peterson, T. C.; Kudlicki, W. Membrane Protein Expression: No Cells Required. *Trends Biotechnol.* **2009**, *27* (8), 455–460. https://doi.org/10.1016/j.tibtech.2009.05.005.

(18) Stroud, Z.; Hall, S. C. L.; Dafforn, T. R. Purification of Membrane Proteins Free from Conventional Detergents: SMA, New Polymers, New Opportunities and New Insights. *Methods* **2018**, *147*, 106–117. https://doi.org/10.1016/j.ymeth.2018.03.011.

(19) Hawkins, O. P.; Jahromi, C. P. T.; Gulamhussein, A. A.; Nestorow, S.; Bahra, T.; Shelton, C.; Owusu-Mensah, Q. K.; Mohiddin, N.; O'Rourke, H.; Ajmal, M.; Byrnes, K.; Khan, M.; Nahar, N. N.; Lim, A.; Harris, C.; Healy, H.; Hasan, S. W.; Ahmed, A.; Evans, L.; Vaitsopoulou, A.; Akram, A.; Williams, C.; Binding, J.; Thandi, R. K.; Joby, A.; Guest, A.; Tariq, M. Z.; Rasool, F.; Cavanagh, L.; Kang, S.; Asparuhov, B.; Jestin, A.; Dafforn, T. R.; Simms, J.; Bill, R. M.; Goddard, A. D.; Rothnie, A. J. Membrane Protein Extraction and Purification Using Partially-Esterified SMA Polymers. *Biochim. Biophys. Acta BBA - Biomembr.* **2021**, *1863* (12), 183758. https://doi.org/10.1016/j.bbamem.2021.183758.

(20) Hesketh, S. J.; Klebl, D. P.; Higgins, A. J.; Thomsen, M.; Pickles, I. B.; Sobott, F.; Sivaprasadarao, A.; Postis, V. L. G.; Muench, S. P. Styrene Maleic-Acid Lipid Particles (SMALPs) into Detergent or Amphipols: An Exchange Protocol for Membrane Protein Characterisation. *Biochim. Biophys. Acta BBA - Biomembr.* **2020**, *1862* (5), 183192. https://doi.org/10.1016/j.bbamem.2020.183192.

(21) Yao, Z.; Zhang, J.-S.; Chen, M.-L.; Li, B.-J.; Lu, Y.-Y.; Cao, K. Preparation of Well-Defined Block Copolymer Having One Polystyrene Segment and Another Poly(Styrene-Alt-Maleic Anhydride) Segment with RAFT Polymerization. *J. Appl. Polym. Sci.* **2011**, *121* (3), 1740–1746. https://doi.org/10.1002/app.33816.

(22) Neville, G. M.; Edler, K. J.; Price, G. J. Fluorescent Styrene Maleic Acid Copolymers to Facilitate Membrane Protein Studies in Lipid Nanodiscs. *Nanoscale* **2022**, *14* (15), 5689–5693. https://doi.org/10.1039/D1NR07230G.

(23) Smith, A. A. A.; Autzen, H. E.; Laursen, T.; Wu, V.; Yen, M.; Hall, A.; Hansen, S. D.; Cheng, Y.; Xu, T. Controlling Styrene Maleic Acid Lipid Particles through RAFT. *Biomacromolecules* **2017**, *18* (11), 3706–3713. https://doi.org/10.1021/acs.biomac.7b01136.

(24) Bali, A. P.; Sahu, I. D.; Craig, A. F.; Clark, E. E.; Burridge, K. M.; Dolan, M. T.; Dabney-Smith, C.; Konkolewicz, D.; Lorigan, G. A. Structural Characterization of Styrene-Maleic Acid Copolymer-Lipid Nanoparticles (SMALPs) Using EPR Spectroscopy. *Chem. Phys. Lipids* **2019**, *220*, 6–13. https://doi.org/10.1016/j.chemphyslip.2019.02.003.

(25) Dörr, J. M.; Scheidelaar, S.; Koorengevel, M. C.; Dominguez, J. J.; Schäfer, M.; van Walree, C. A.; Killian, J. A. The Styrene–Maleic Acid Copolymer: A Versatile Tool in Membrane Research. *Eur. Biophys. J.* **2016**, *45* (1), 3–21. https://doi.org/10.1007/s00249-015-1093-y.

(26) Baruah, S. D.; Laskar, N. C. Styrene-Maleic Anhydride Copolymers: Synthesis, Characterization, and Thermal Properties. *J. Appl. Polym. Sci.* **1996**, *60* (5), 649–656. https://doi.org/10.1002/(SICI)1097-4628(19960502)60:5<649:AID-APP1>3.0.CO;2-Q.

(27) Burridge, K. M.; Rahman, M. S.; De Alwis Watuthanthrige, N.; Gordon, E.; Shah, M. Z.; Chandrarathne, B. M.; Lorigan, G. A.; Page, R. C.; Konkolewicz, D. Network Polymers Incorporating Lipid-Bilayer Disrupting Polymers: Towards Antiviral Functionality. *Polym. Chem.* **2022**, *13* (31), 4547–4556. https://doi.org/10.1039/D2PY00602B.

(28) Durchschlag, H.; Tiefenbach, K.-J.; Gebauer, S.; Jaenicke, R. Spectroscopic Investigations of Detergents and Protein–Detergent Complexes. *J. Mol. Struct.* **2001**, *563–564*, 449–455. https://doi.org/10.1016/S0022-2860(00)00890-5.

(29) Lee, S. C.; Knowles, T. J.; Postis, V. L. G.; Jamshad, M.; Parslow, R. A.; Lin, Y.; Goldman, A.; Sridhar, P.; Overduin, M.; Muench, S. P.; Dafforn, T. R. A Method for Detergent-Free Isolation of Membrane Proteins in Their Local Lipid Environment. *Nat. Protoc.* **2016**, *11* (7), 1149–1162. https://doi.org/10.1038/nprot.2016.070.

(30) Simon, K. S.; Pollock, N. L.; Lee, S. C. Membrane Protein Nanoparticles: The Shape of Things to Come. *Biochem. Soc. Trans.* **2018**, *46* (6), 1495–1504. https://doi.org/10.1042/BST20180139.

(31) Oluwole, A. O.; Klingler, J.; Danielczak, B.; Babalola, J. O.; Vargas, C.; Pabst, G.; Keller, S. Formation of Lipid-Bilayer Nanodiscs by Diisobutylene/Maleic Acid (DIBMA) Copolymer. *Langmuir* **2017**, *33* (50), 14378–14388. https://doi.org/10.1021/acs.langmuir.7b03742.

(32) Workman, C. E.; Bag, P.; Cawthon, B.; Ali, F. H.; Brady, N. G.; Bruce, B. D.; Long, B. K. Alternatives to Styrene- and Diisobutylene-Based Copolymers for Membrane Protein Solubilization via Nanodisc Formation. *Angew. Chem. Int. Ed.* **2023**, *62* (43), e202306572. https://doi.org/10.1002/anie.202306572.

(33) Barniol-Xicota, M.; Verhelst, S. H. L. Stable and Functional Rhomboid Proteases in Lipid Nanodiscs by Using Diisobutylene/Maleic Acid Copolymers. *J. Am. Chem. Soc.* **2018**, *140* (44), 14557–14561. https://doi.org/10.1021/jacs.8b08441.

(34) Gulamhussein, A. A.; Uddin, R.; Tighe, B. J.; Poyner, D. R.; Rothnie, A. J. A Comparison of SMA (Styrene Maleic Acid) and DIBMA (Di-Isobutylene Maleic Acid) for Membrane Protein Purification. *Biochim. Biophys. Acta BBA - Biomembr.* **2020**, *1862* (7), 183281. https://doi.org/10.1016/j.bbamem.2020.183281.

(35) Voskoboynikova, N.; Orekhov, P.; Bozdaganyan, M.; Kodde, F.; Rademacher, M.; Schowe, M.; Budke-Gieseking, A.; Brickwedde, B.; Psathaki, O.-E.; Mulkidjanian, A. Y.; Cosentino, K.; Shaitan, K. V.; Steinhoff, H.-J. Lipid Dynamics in Diisobutylene-Maleic Acid (DIBMA) Lipid Particles in Presence of Sensory Rhodopsin II. *Int. J. Mol. Sci.* **2021**, *22* (5), 2548. https://doi.org/10.3390/ijms22052548.

(36) Plochocka, K.; Liu, X.; Tallon, M. A.; Musa, O. M. The Quintessential Alternating Copolymer Family: Alkyl Vinyl Ether Co-Maleic Anhydride Copolymers. In *Handbook of Maleic Anhydride Based Materials*; Musa, O. M., Ed.; Springer International Publishing: Cham, 2016; pp 211–250. https://doi.org/10.1007/978-3-319-29454-4_4.

(37) Fujimori, K.; Organ, P. P.; Costigan, M. J.; Craven, I. E. Relative Reactivity of Free Monomers and Donor-Acceptor Complex in Alternating Copolymerization of Isobutyl Vinyl Ether with Maleic Anhydride from the Rate of Polymerization. *J. Macromol. Sci. Part - Chem.* **1986**, *23* (5), 647–655. https://doi.org/10.1080/00222338608058502.

(38) Suzuki, T.; Tomono, T. Syntheses of Monomethoxy Polyethyleneglycol Vinyl Ether Macromonomers and Their Radical Copolymerization with Maleic Anhydride. *J. Polym. Sci. Polym. Chem. Ed.* **1984**, *22* (11), 2829–2839. https://doi.org/10.1002/pol.1984.170221109.

(39) Fleš, D.; Vuković, R.; Kurešević, V.; Radičevic, R. The Influence of Steric Factors on the Mechanism of Copolymerization of Phenylvinyl Alkyl Ethers and Maleic Anhydride. *J. Polym. Sci. Polym. Chem. Ed.* **1981**, *19* (1), 35–43. https://doi.org/10.1002/pol.1981.170190104.

(40) Serbin, A. V.; Karaseva, E. N.; Dunaeva, I. V.; Krut'ko, E. B.; Talyzenkov, Yu. A.; Filatova, M. P.; Chernikova, E. V. Controlled Free-Radical Copolymerization of Maleic Anhydride and Divinyl Ether

in the Presence of Reversible Addition-Fragmentation Chain-Transfer Agents. *Polym. Sci. Ser. B* **2011**, *53* (3–4), 116–124. https://doi.org/10.1134/S1560090411030079.

(41) Khan, R. H.; Rotich, N. C.; Morris, A.; Ahammad, T.; Baral, B.; Sahu, I. D.; Lorigan, G. A. Probing the Structural Topology and Dynamic Properties of Gp28 Using Continuous Wave Electron Paramagnetic Resonance Spectroscopy. *J. Phys. Chem. B* **2023**, *127* (43), 9236–9247. https://doi.org/10.1021/acs.jpcb.3c03679.

(42) Kang, C.; Tian, C.; Sönnichsen, F. D.; Smith, J. A.; Meiler, J.; George, A. L.; Vanoye, C. G.; Kim, H. J.; Sanders, C. R. Structure of KCNE1 and Implications for How It Modulates the KCNQ1 Potassium Channel. *Biochemistry* **2008**, *47* (31), 7999–8006. https://doi.org/10.1021/bi800875q.

(43) Coey, A. T.; Sahu, I. D.; Gunasekera, T. S.; Troxel, K. R.; Hawn, J. M.; Swartz, M. S.; Wickenheiser, M. R.; Reid, R.; Welch, R. C.; Vanoye, C. G.; Kang, C.; Sanders, C. R.; Lorigan, G. A. Reconstitution of KCNE1 into Lipid Bilayers: Comparing the Structural, Dynamic, and Activity Differences in Micelle and Vesicle Environments. *Biochemistry* **2011**, *50* (50), 10851–10859. https://doi.org/10.1021/bi2009294.

(44) Kuenze, G.; Vanoye, C. G.; Desai, R. R.; Adusumilli, S.; Brewer, K. R.; Woods, H.; McDonald, E. F.; Sanders, C. R.; George, A. L.; Meiler, J. Allosteric Mechanism for KCNE1 Modulation of KCNQ1 Potassium Channel Activation. *eLife* **2020**, *9*, e57680. https://doi.org/10.7554/eLife.57680.

(45) Wu, X.; Perez, M. E.; Noskov, S. Y.; Larsson, H. P. A General Mechanism of KCNE1 Modulation of KCNQ1 Channels Involving Non-Canonical VSD-PD Coupling. *Commun. Biol.* **2021**, *4* (1), 887. https://doi.org/10.1038/s42003-021-02418-1.

(46) Bohnen, M. S.; Peng, G.; Robey, S. H.; Terrenoire, C.; Iyer, V.; Sampson, K. J.; Kass, R. S. Molecular Pathophysiology of Congenital Long QT Syndrome. *Physiol. Rev.* **2017**, *97* (1), 89–134. https://doi.org/10.1152/physrev.00008.2016.

(47) Teng, S.; Ma, L.; Zhen, Y.; Lin, C.; Bähring, R.; Vardanyan, V.; Pongs, O.; Hui, R. Novel Gene hKCNE4 Slows the Activation of the KCNQ1 Channel. *Biochem. Biophys. Res. Commun.* **2003**, *303* (3), 808–813. https://doi.org/10.1016/S0006-291X(03)00433-9.

(48) Gofman, Y.; Shats, S.; Attali, B.; Haliloglu, T.; Ben-Tal, N. How Does KCNE1 Regulate the Kv7.1 Potassium Channel? Model-Structure, Mutations, and Dynamics of the Kv7.1-KCNE1 Complex. *Structure* **2012**, *20* (8), 1343–1352. https://doi.org/10.1016/j.str.2012.05.016.

(49) Roig, S. R.; Solé, L.; Cassinelli, S.; Colomer-Molera, M.; Sastre, D.; Serrano-Novillo, C.; Serrano-Albarrás, A.; Lillo, M. P.; Tamkun, M. M.; Felipe, A. Calmodulin-Dependent KCNE4 Dimerization Controls Membrane Targeting. *Sci. Rep.* **2021**, *11* (1), 14046. https://doi.org/10.1038/s41598-021-93562-5.

(50) KCNE4 - Potassium Voltage-Gated Channel Subfamily E Member 4 - Homo Sapiens (Human) - KCNE4 Gene & Protein. https://www.uniprot.org/uniprot/Q8WWG9 (accessed 2021-07-15).

(51) Manderfield, L. J.; Daniels, M. A.; Vanoye, C. G.; George Jr, A. L. KCNE4 Domains Required for Inhibition of KCNQ1. *J. Physiol.* **2009**, *587* (2), 303–314. https://doi.org/10.1113/jphysiol.2008.161281.

(52) Grunnet, M.; Rasmussen, H. B.; Hay-Schmidt, A.; Rosenstierne, M.; Klaerke, D. A.; Olesen, S.-P.; Jespersen, T. KCNE4 Is an Inhibitory Subunit to Kv1.1 and Kv1.3 Potassium Channels. *Biophys. J.* **2003**, *85* (3), 1525–1537. https://doi.org/10.1016/S0006-3495(03)74585-8.

(53) Wang, Y.; Eldstrom, J.; Fedida, D. Gating and Regulation of KCNQ1 and KCNQ1 + KCNE1 Channel Complexes. *Front. Physiol.* **2020**, *11*, 504. https://doi.org/10.3389/fphys.2020.00504.

(54) Lvov, A.; Gage, S. D.; Berrios, V. M.; Kobertz, W. R. Identification of a Protein–Protein Interaction between KCNE1 and the Activation Gate Machinery of KCNQ1. *J. Gen. Physiol.* **2010**, *135* (6), 607–618. https://doi.org/10.1085/jgp.200910386.

(55) Holt, A.; Cahill, J.; Ramsey, J.; Martin, C.; O'Leary, C.; Moreland, R.; Maddox, L. T.; Galbadage, T.; Sharan, R.; Sule, P.; Cirillo, J. D.; Young, R. Phage-Encoded Cationic Antimicrobial Peptide Required for Lysis. *J. Bacteriol.* **2022**, *204* (1), e00214-21. https://doi.org/10.1128/JB.00214-21.

(56) Thennarasu, S.; Tan, A.; Penumatchu, R.; Shelburne, C. E.; Heyl, D. L.; Ramamoorthy, A. Antimicrobial and Membrane Disrupting Activities of a Peptide Derived from the Human Cathelicidin Antimicrobial Peptide LL37. *Biophys. J.* **2010**, *98* (2), 248–257. https://doi.org/10.1016/j.bpj.2009.09.060.

(57) Kuppusamy; Willcox; Black; Kumar. Short Cationic Peptidomimetic Antimicrobials. *Antibiotics* **2019**, *8* (2), 44. https://doi.org/10.3390/antibiotics8020044.

(58) Perrier, S. *50th Anniversary Perspective* : RAFT Polymerization—A User Guide. *Macromolecules* **2017**, *50* (19), 7433–7447. https://doi.org/10.1021/acs.macromol.7b00767.

(59) Phiri, M. M.; Hadasha, W.; Pfukwa, R.; Klumperman, B. Synthesis and Characterization of Liquid Molecular Brush Binder for Coating Applications. *Eur. Polym. J.* **2018**, *102*, 178–186. https://doi.org/10.1016/j.eurpolymj.2018.03.023.

(60) Seymour, R. B.; Harris, F. F.; Branum, I. Copolymers of Vinyl Compounds and Maleic Anhydride. *Ind. Eng. Chem.* **1949**, *41* (7), 1509–1513.

(61) Moad, G. A Critical Assessment of the Kinetics and Mechanism of Initiation of Radical Polymerization with Commercially Available Dialkyldiazene Initiators. *Prog. Polym. Sci.* **2019**, *88*, 130–188. https://doi.org/10.1016/j.progpolymsci.2018.08.003.

(62) Fugimori, K.; Wickramasinghe, N. A. The Alternating Copolymerization of N-Butyl Vinyl Ether with Maleic Anhydride. **1979**.

(63) Denizli, B. K.; Can, H. K.; Rzaev, Z. M. O.; Güner, A. Synthesis of Copolymers of *Tert* -butyl Vinyl Ether with Maleic and Citraconic Anhydrides. *J. Appl. Polym. Sci.* **2006**, *100* (3), 2455–2463. https://doi.org/10.1002/app.23577.

(64) Harrisson, S.; Wooley, K. L. Shell-Crosslinked Nanostructures from Amphiphilic AB and ABA Block Copolymers of Styrene-Alt-(Maleic Anhydride) and Styrene: Polymerization, Assembly and Stabilization in One Pot. *Chem. Commun.* **2005**, No. 26, 3259. https://doi.org/10.1039/b504313a.

(65) Barb, W. G. Effect of Nonterminal Monomer Units on the Reactivity of Polymeric Free Radicals. *J. Polym. Sci.* **1953**, *11* (2), 117–126. https://doi.org/10.1002/pol.1953.120110202.

(66) Heuts, J. P. A.; Gilbert, R. G.; Maxwell, I. A. Penultimate Unit Effect in Free-Radical Copolymerization. *Macromolecules* **1997**, *30* (4), 726–736. https://doi.org/10.1021/ma960704m.

(67) Fukuda, T.; Ma, Y. D.; Inagaki, H.; Kubo, K. Penultimate-Unit Effects in Free-Radical Copolymerization. *Macromolecules* **1991**, *24* (2), 370–375. https://doi.org/10.1021/ma00002a005.

(68) Burridge, K. M.; Harding, B. D.; Sahu, I. D.; Kearns, M. M.; Stowe, R. B.; Dolan, M. T.; Edelmann, R. E.; Dabney-Smith, C.; Page, R. C.; Konkolewicz, D.; Lorigan, G. A. Simple Derivatization of RAFT-Synthesized Styrene–Maleic Anhydride Copolymers for Lipid Disk Formulations. *Biomacromolecules* **2020**, *21* (3), 1274–1284. https://doi.org/10.1021/acs.biomac.0c00041.

(69) Kuo, Y.-M.; Henry, R. A.; Andrews, A. J. Measuring Specificity in Multi-Substrate/Product Systems as a Tool to Investigate Selectivity in Vivo. *Biochim. Biophys. Acta BBA - Proteins Proteomics* **2016**, *1864* (1), 70–76. https://doi.org/10.1016/j.bbapap.2015.08.011.

(70) Harding, B. D.; Dixit, G.; Burridge, K. M.; Sahu, I. D.; Dabney-Smith, C.; Edelmann, R. E.; Konkolewicz, D.; Lorigan, G. A. Characterizing the Structure of Styrene-Maleic Acid Copolymer-Lipid Nanoparticles (SMALPs) Using RAFT Polymerization for Membrane Protein Spectroscopic Studies. *Chem. Phys. Lipids* **2019**, *218*, 65–72. https://doi.org/10.1016/j.chemphyslip.2018.12.002.

(71) Chen, M.; Moad, G.; Rizzardo, E. Thiocarbonylthio End Group Removal from RAFT-synthesized Polymers by a Radical-induced Process. *J. Polym. Sci. Part Polym. Chem.* **2009**, *47* (23), 6704–6714. https://doi.org/10.1002/pola.23711.

(72) Skrabania, K.; Miasnikova, A.; Bivigou-Koumba, A. M.; Zehm, D.; Laschewsky, A. Examining the UV-Vis Absorption of RAFT Chain Transfer Agents and Their Use for Polymer Analysis. *Polym. Chem.* **2011**, *2* (9), 2074. https://doi.org/10.1039/c1py00173f.

(73) Noble, J. E.; Bailey, M. J. A. Chapter 8 Quantitation of Protein. In *Methods in Enzymology*; Elsevier, 2009; Vol. 463, pp 73–95. https://doi.org/10.1016/S0076-6879(09)63008-1.

(74) Klug, C. S.; Feix, J. B. Methods and Applications of Site-Directed Spin Labeling EPR Spectroscopy. In *Methods in Cell Biology*; Elsevier, 2008; Vol. 84, pp 617–658. https://doi.org/10.1016/S0091-679X(07)84020-9.

(75) Sahu, I. D.; Lorigan, G. A. Electron Paramagnetic Resonance as a Tool for Studying Membrane Proteins. *Biomolecules* **2020**, *10* (5), 763. https://doi.org/10.3390/biom10050763.

(76) Sahu, I. D.; Zhang, R.; Dunagan, M. M.; Craig, A. F.; Lorigan, G. A. Characterization of KCNE1 inside Lipodisq Nanoparticles for EPR Spectroscopic Studies of Membrane Proteins. *J. Phys. Chem. B* **2017**, *121* (21), 5312–5321.

Chapter 5

Probing the Structural Topology of the Voltage-Sensor-Like Domain in TRPV1 Using Site-Directed Mutagenesis and EPR Spectroscopy

Nancy C. Rotich[1], Rebecca B. Stowe[1], Evelyn Okorafor[1], Ben Dubin[1], Chaymae Younes[1], Aerial Owens[2], Andrew K. Morris[1], Wade Van Horn[2], Carole Dabney-Smith[1], Gary A. Lorigan[1]

1. Department of Chemistry and Biochemistry, Miami University, Oxford Ohio 45056

2. School of Molecular Sciences, Arizona State University, Tempe, AZ 85287

Sample preparation and data collection by N.C.R. Dr. Stowe provided training on instrumentation. Data analysis by N.C.R. and A.K.M. Manuscript written by N.C.R. Manuscript edited by G.A.L and N.C.R.

5.0 Abstract

Transient receptor potential vanilloid 1 (TRPV1) is a key member of the TRP channel family, playing a crucial role in detecting noxious heat and contributing to pain sensation. Its activation by stimuli such as heat, protons, and capsaicin makes it an important target for pain management therapies. Understanding the structural dynamics of TRPV1 is essential for developing modulators that can effectively alleviate chronic pain while minimizing adverse effects. TRP channels share a similar architecture with voltage-gated ion channels (VGICs), featuring six transmembrane helices. In VGICs, the first four helices (S1-S4) form the voltage-sensing domain (VSD), analogous to the voltage sensor-like domain (VSLD) in TRP channels. A cysteine-less TRPV1 mutant was engineered to introduce targeted cysteine substitutions across the VSLD, allowing precise investigation of residue-specific mobility and topology using continuous-wave (CW) EPR and power saturation (PS) techniques. Using electron paramagnetic resonance (EPR) spectroscopy combined with site-directed spin labeling, we have successfully mapped and confirmed the structural topology and dynamics of the four transmembrane helices within the TRPV1 VSLD. The results provide crucial insights into the conformational landscape of the VSLD, offering a deeper understanding of its role in TRPV1 activation. These findings contribute to the broader effort of elucidating TRPV1's structural mechanisms which may aid in the development of targeted pain therapeutics.

5.1 Introduction

In the ever-evolving field of biochemistry, understanding the structural and functional dynamics of membrane proteins stands as a critical challenge.[1,2] These proteins, which are essential for numerous cellular processes such as signaling, structural integrity, and transport, engage in intricate interactions with their lipid environments, which consist of various types of lipids that form membranes, modify protein function, and influence cellular dynamics.[2] The complexity of these interactions often presents significant challenges for researchers, as they must consider the diverse roles that lipids play in modulating protein behavior, stability, and function.[3] Consequently, investigating these relationships requires sophisticated experimental and computational techniques, making the study of protein-lipid interactions a highly complex endeavor that demands a multidisciplinary approach.[4]

Transient receptor potential (TRP) channels are a group of ion channels located in the cell membrane.[5] TRP channels are divided into several subfamilies, such as TRPV, TRPC, TRPM, TRPA, and TRPN, each with distinct functions and activation mechanisms. Within the animal kingdom all senses, including vision, smell, taste, hearing, and touch, appear mediated by TRP channels.[6] They can be activated by various stimuli, including thermal changes, mechanical stress, and chemical agents. TRP channels are involved in numerous physiological processes and have been implicated in various pathologies, making them potential targets for therapeutic interventions.[7,8] Mutations in many of about 27 human TRP have been associated with a large variety of diseases ranging from episodic pain syndrome (TRPA1), stationary night blindness (TRPM1), kidney diseases (TRPP2 and TRPC6), hypomagnesemia and hypocalcemia (TRPM6), skeletal diseases and neuropathies (TRPV4), cardiac disease (TRPM4) and neurodegenerative disorders (TRPM2 and TRPML1).[9] In the last 20 years, interest in TRP channels has grown exponentially until reaching its peak in 2021 with the awarding of the Nobel Prize in Physiology or Medicine to David Julius for the discovery of the capsaicin receptor TRPV1 in 1997. [10,11]

Transient receptor potential vanilloid 1 (TRPV1) is a polymodal ion channel implicated in nociception and thermosensation.[13] All six channels have distinct properties and react to several endogenous ligands as well as different gating stimuli such as heat, pH, mechanical stress, or osmotic changes. In many tissues they serve as sensors for different pain stimuli (heat, pressure,

pH) and contribute to the homeostasis of electrolytes and the maintenance of barrier functions.[14] Their fundamental role in various physiological and pathophysiological processes is significant. TRPV1 channels are promising targets for drug development. However, drugs targeting specific TRPV1 channels, which are suitable for drug therapy, are rare.[15] Moreover, selective and potent compounds for further research at TRPV1 channels are often lacking. While its pore-forming and ligand-binding domains have been extensively studied, the structural and functional roles of its voltage-sensor-like domain (VSLD) remain less well understood.[9] The VSLD, comprising transmembrane segments S1–S4, shares topological similarity with classical voltage-sensor domains, but lacks canonical gating charges and shows unique modulatory features.[14] To gain mechanistic insight into the VSLD's structural organization and potential conformational changes during gating, we employed a combination of site-directed spin labeling (SDSL) and electron paramagnetic resonance (EPR) spectroscopy. This approach enables direct measurement of residue accessibility, thereby providing a dynamic picture of VSLD topology.[17,18]

Exploring protein structures and their complex functions is a fundamental aspect of contemporary biochemistry and molecular biology. Understanding the structural topology of proteins allows for insights into their roles in cellular processes, mechanisms of action, and potential as drug targets. In this context, site-directed spin labeling (SDSL) combined with electron paramagnetic resonance (EPR) spectroscopic techniques offers a formidable approach to elucidate the dynamic structures of proteins.

5.2 Materials and Methods

5.2.1 Site-Directed Mutagenesis

Site-Directed Mutagenesis was performed on the human TRPV1 VSLD in a pET-16b vector using pfuUltra II High Fidelity DNA Polymerase (Agilent) according to manufacturer's instructions. Primers were designed using A plasmid Editor (ApE) (University of Utah, Salt Lake City, UT). Purified plasmid DNA was extracted from transformed XL-Gold competent cell with a QIAprep Spin Miniprep Kit (Qiagen). Mutagenesis was confirmed with Sanger Sequencing (Genewiz).

5.2.2 Expression and Purification

Human TRPV1 VSLD in pET-16b vector was transformed into BL21-Codon Plus DE3-RP competent cells (Agilent). Cells were grown in LB Media (Fisher Scientific) with 50 µg/mL

Kanamycin. The cultures were shaken at 250 rpm and maintained at 18°C until they achieved an OD600 of 0.6, after which they were induced with 100 mM isopropyl D-thiogalactopyranoside (IPTG). Cells were cultured overnight with shaking at 250 rpm and at 25 °C to allow for protein overexpression. The cells were harvested by centrifugation at 11000 xg for 10 minutes at 4 °C. Cell pellets were resuspended in 10x excess lysis buffer (75 mM Tris, 300 mM NaCl, 0.2 mM EDTA, pH 7.5) with 10x w/v excess of LDR stock (100 mg/mL lysozyme,10 mg/mL DNAse, 10 mg/mL RNAse), PMSF (20 mg/mL), and Magnesium Acetate (0.1 M). The cells were rotated for 30 minutes at room temperature to resuspend the pellet fully. Cell lysis was carried out with a Fisher Scientific Sonicator with the pulse set to 5 s on and 5 s off at 40% amplitude and a 1/4" tip. The cells were subjected to sonication twice for 7 ½ minutes and once for 5 minutes. After sonication, the lysed cells were rotated at 4 °C with 3% Empigen BB detergent for 40 minutes to an hour. The solubilized portion was then fractionated from the insoluble portion by centrifugation at 17000 x g and 4 °C for 30 minutes. The supernatant was stirred and allowed to incubate overnight with Ni^{2+}-NTA resin to facilitate the binding of proteins. The resin and supernatant mixture were centrifuged at 2700 x g to separate the resin from the supernatant, and the resin was then transferred to a gravity column for protein purification. The TRPV1 VSLD protein was purified by a rinse of Buffer A (40 mM HEPES and 300 mM NaCl, pH 7.5) with 2 mM tris(2-carboxyethyl) phosphine (TCEP) and 1.5% empigen BB detergent. The column was washed with Buffer A, containing 2 mM TCEP, 1.5% empigen BB detergent, and 50 mM imidazole, in order to eliminate any proteins that were bound nonspecifically. The column was treated with a detergent exchange buffer containing 25 mM phosphate pH 7.0, 2 mM TCEP, and 0.05% 1-palmitoyl-2-hydroxy-*sn*-glycero-3-phospho-(1′-*rac*-glycerol) (LPPG), then the purified TRPV1 VSLD protein was eluted with 25 mM phosphate pH 7.0, 2 mM TCEP, 0.1% LPPG, and 250 mM imidazole. The purified protein was concentrated with an Amicon spin filter that has a molecular weight cutoff of 10,000 Da, and its purity was verified using SDS PAGE.

5.2.3 Site-Directed Spin Labeling (SDSL)

A tenfold excess of dithiothreitol (DTT) was introduced to the purified TRPV1 VSLD protein, and the resulting mixture was flushed with nitrogen gas for one minute. DTT maintains all accessible cysteine residues in their reduced state, preventing the formation of intra or intermolecular disulfide bonds. This ensures that only the target cysteine(s) at the designated site(s) are available for labeling. The mixture was then shaken and allowed to incubate at room temperature for 24

hours to facilitate the reduction of disulfide bonds. A 250 mM stock of S-(1-oxyl-2,2,5,5-tetramethyl-2,5-dihydro-1H-pyrrol-3-yl)methyl methanesulfonothioate (MTSL) (Toronto Research Chemicals) was prepared in methanol and added directly to the purified TRPV1 VSLD protein at a 20x molar excess. The solution was kept at room temperature for 30 minutes, followed by incubation at 37°C while shaking for 3 hours, and finally, it was shaken at room temperature for the rest of the 24 hours. The labeled protein was then buffer exchanged into 25 mM phosphate pH 7.0 and 0.05% LPPG by three rounds of centrifugation at 6000 xg in Amicon spin filter tubes (10000 Da molecular weight cutoff). During each round of centrifugation, 7 mL of 25 mM phosphate, pH 7.0 + 0.05% LPPG, was added to the filter, allowing for the removal of excess spin label. After the third round of centrifugation the protein was incubated with pre-equilibrated Ni2+-NTA resin overnight. The resin was transferred to a gravity column and washed with 300 mL of 25 mM phosphate pH 7.0 + 0.05% LPPG to ensure total removal of unreacted spin label, then the protein was eluted in 25 mM phosphate pH 7.0, 0.1% LPPG, and 250 mM imidazole.

5.2.5 Vesicle Reconstitution

Vesicle samples were composed of a 3:1 molar ratio of 1-Palmitoyl-2-Oleoyl-sn-Glycero-3-Phosphocholine (POPC) and 1-palmitoyl-2-oleoyl-sn-glycero-3-phospho-(1'-rac-glycerol) (sodium salt) (POPG) (Avanti Polar Lipids). The powdered lipids were dissolved in chloroform and then evaporated to create a thin film along the inner surface of a pear-shaped flask. The sample was then left to dry overnight in a vacuum desiccator. Later, the thin film was reconstituted in 50 mM phosphate buffer at pH 7 to achieve a final lipid concentration of 100 mM. The TRPV1 VSLD protein was mixed with the lipid solution in a 1:400 ratio to produce proteoliposomes, which were then subjected to three freeze-thaw cycles. All vesicles were prepared with a protein concentration of approximately 100 μM. Excess detergent was removed via dialysis with a dialysis membrane tubing of 12 to 14 kDa MWCO (Fisher Scientific) for 72 hrs in 100 Mm imidazole and 2 mM EDTA pH 7 changed roughly every 12 hours. The dialysate was pelleted by ultracentrifugation at 300000 RCF for 35 mins. The proteoliposomes pellet was thoroughly resuspended in 100 μL of 50 mM phosphate buffer at pH 7 and immediately used for EPR spectroscopic measurements.

5.2.6 CW-EPR Spectroscopy

CW-EPR spectroscopy measurements were collected on a Bruker EMX X-Band spectrometer with a Premium X bridge and ER4119-HS cavity. All measurements were conducted at room

temperature with a center field of G, a 150 G sweep width, 100 kHz modulation frequency, 1 G modulation amplitude, and a 10.02 mW microwave power.[19]

5.2.7 Power Saturation

Verification of proper insertion of TRPV1 VSLD into 3:1 POPC: POPG lipid bilayers were confirmed using the CW-EPR power saturation technique at X-band frequency. Power saturation experiments were performed on a Bruker X-band CW-EPR spectrometer consisting of an ER041X microwave bridge coupled with an ER4119-HS resonator (Bruker BioSpin). Samples were loaded into gas permeable TPX capillary tubes with a total volume of 3-4 µL at a concentration of 90-110 µM. EPR data were collected using a modulation amplitude of 1 G and a starting microwave power of 159 mW with 2 dB power reduction between 17 points. The final spectra were obtained by signal averaging 4 scans per each attenuation step. This method works on the principle that under non-saturating conditions, the height of the spectral lines is linearly proportional to the square root of the incident microwave power. If the microwave power is subsequently increased, the increase in signal amplitude becomes less linear with $P_{1/2}$, and signal height starts to decrease as the sample saturates. Power saturation curves were obtained under three conditions: (1) equilibrated with nitrogen as a control, (2) equilibrated with a lipid-soluble paramagnetic reagent, 21% oxygen (air), and (3) equilibrated with nitrogen in the presence of a water-soluble paramagnetic reagent, NiEDDA (2 mM) as described previously. The samples were purged with a steady stream of either air or nitrogen gas for 1 hour to bring the sample to equilibrium before each measurement was taken. The resonator remained connected to the gas during all measurements, and experiments were performed at RT. Peak-to-peak amplitudes (A) of the first derivative ($m_I = 0$) resonance lines were plotted against the square root of incident microwave power. The data points were then fitted according to equation 1.[19,20]

$$A = I\sqrt{P}\left[1 + \frac{\left(2^{\frac{1}{\varepsilon}} - 1\right)P}{P_{1/2}}\right]^{-\varepsilon} \quad \text{..... (1)}$$

Here, 'I' is a scaling factor, $P_{1/2}$ represents the power where the first derivative amplitude is reduced to half of its unsaturated value, and ε is a measure of the homogeneity of saturation of the resonance line. For the homogeneous and inhomogeneous saturation limits, ε = 1.5 and ε = 0.5, respectively. Using equation 2, the corresponding depth parameters were calculated.[19,21]

$$\Phi = ln\left[\frac{\Delta P_{\frac{1}{2}}(O_2)}{\Delta P_{\frac{1}{2}}(NiEDDA)}\right] \quad \text{..... (2)}$$

Here, $\Delta P_{1/2}$(NiEDDA) is the difference in the $P_{1/2}$ values for NiEDDA and nitrogen equilibriums and $\Delta P_{1/2}(O_2)$ is the difference in the $P_{1/2}$ values for oxygen and nitrogen equilibriums.

5.3 Results and Discussion

To better understand the structural topology and dynamics of the TRPV1-VSLD using CW-EPR spectroscopy, single cysteine mutants were generated from the Cys-less vector. Achieving site-specific spin labeling is essential, and it requires that all native cysteines in the protein of interest be replaced with alternative amino acids while keeping structural integrity intact.[17] In the case of TRPV1 VSLD, the strategic alteration of the single native cysteine, C443A, to alanine opens such possibilities. Once the Cys-less C443A was successfully expressed, other sites in the protein were explored by substituting the native amino acids with cysteines. So far, 20 mutants have been designed across the four transmembrane domains of TRPV1-VSLD and the surrounding loops or linker regions.

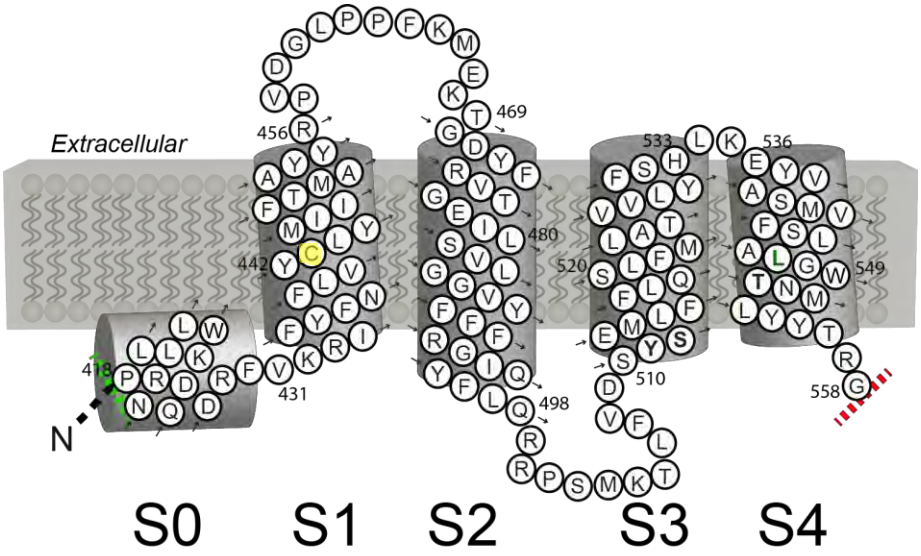

Figure 5.1: *Predicted Membrane topology diagram of TRPV1 VSLD. Yellow residue indicates the native cysteine C443.*[22]

15 mutants were successfully expressed and purified, while additional mutants are still being explored. TRPV1 VSLD sites, as indicated in Table 5.1, were substituted with cysteines to allow spin label attachment to examine the dynamic properties as a report of the local environment, as well as to determine their depth in the membrane.

Table 5.1: *List of TRPV1 VSLD cysteine variants used in this study.*

TRPV1 Cysteine Mutant	Predicted Cellular Location	Site Location
L422C	Intracellular	S0
D425C	Intracellular	S0
A452C	Transmembrane	S1
V458C	Extracellular	S1-S2 linker
L461C	Extracellular	S1-S2 linker
G470C	Extracellular	S1-S2 linker
V475C	Transmembrane	S2
L481C	Transmembrane	S2
K504C	Intracellular	S2-S3 linker
D509C	Intracellular	S2-S3 linker
L521C	Transmembrane	S3
L534C	Extracellular	S3-S4 linker
A539C	Transmembrane	S4
G548C	Transmembrane	S4

Previous studies have used Cryo-EM to determine the structure of TRPV1, providing a detailed topology of the channel, including the VSLD.[22] Based on this structural predictions as well as other predictions of TRPV1 VSLD topology from sequence alignments, AlphaFold models, and molecular simulations it is expected that S1-S2 and S3-S4 linkers are located in the extracellular region, S0 to S4 are buried inside the membrane, and S0-S1 and S2-S3 linkers are in the intracellular region. This structural information is crucial for designing SDSL-EPR experiments to probe specific regions of the VSLD.

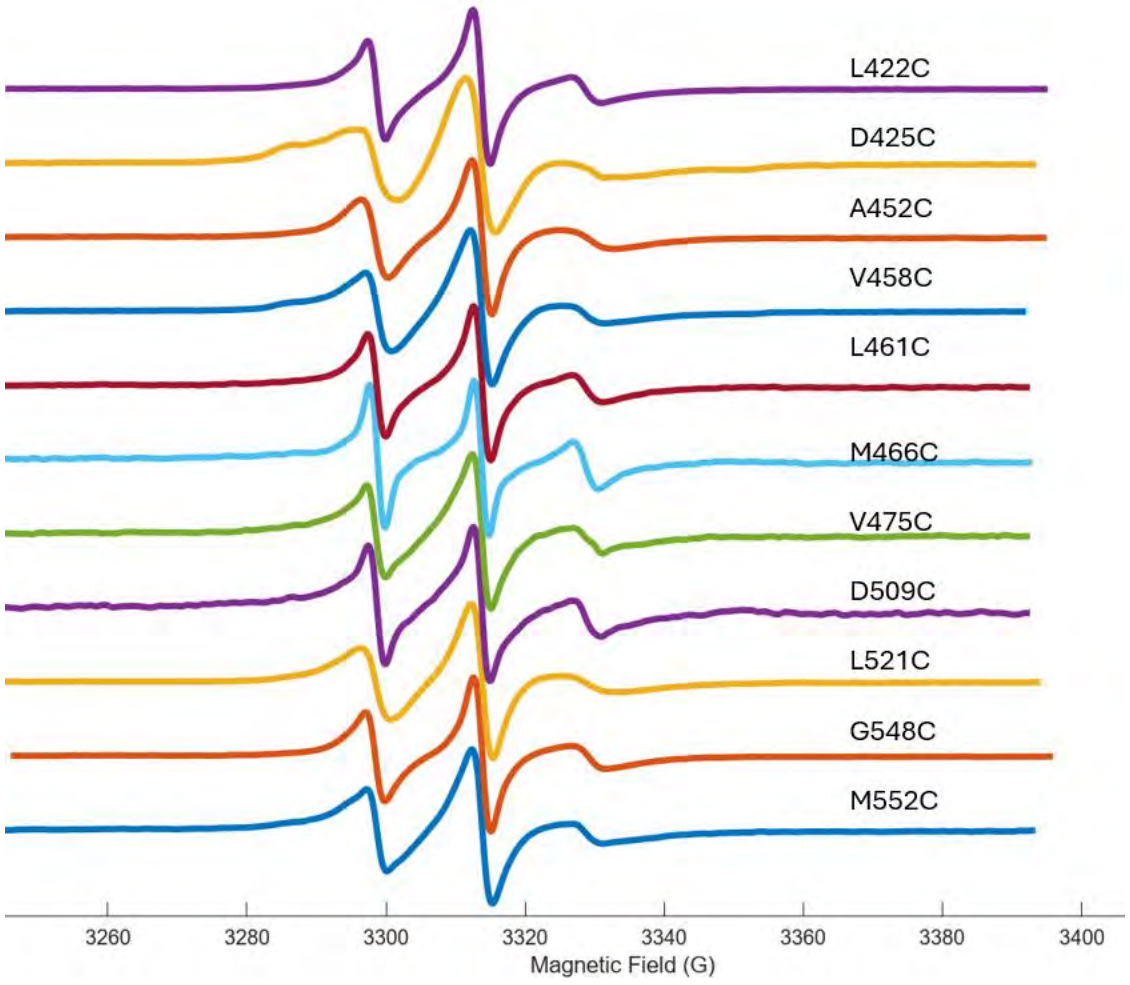

***Figure 5.2**: Site-specific dynamic information of the protein was explored using CW-EPR spectroscopy. This shows the CW-EPR spectra for each cysteine variant in 3:1 POPC:POPG vesicles.*

CW-EPR spectroscopic methods were employed to investigate the site-specific dynamic characteristics of the mutants listed in Table 5.1. The application of the power saturation method

enabled the determination of membrane depth parameters at these positions, thereby enhancing our understanding of the protein's topology and its interaction within the lipid bilayer. CW-EPR spectra were collected on 15 spin-labeled TRPV1-VLSD mutants, and the results are shown in **Figure 5.2**. The CW-EPR spectra of the M466C and D509C samples exhibit increased motion of the spin label, evidenced by the presence of sharper linewidths as shown in **Figure 5.3**. This phenomenon is indicative of a reduced rotational correlation time which quantitatively suggests that the motion of these spin labels is more dynamic indicating that this region of the protein is solvent accessible.

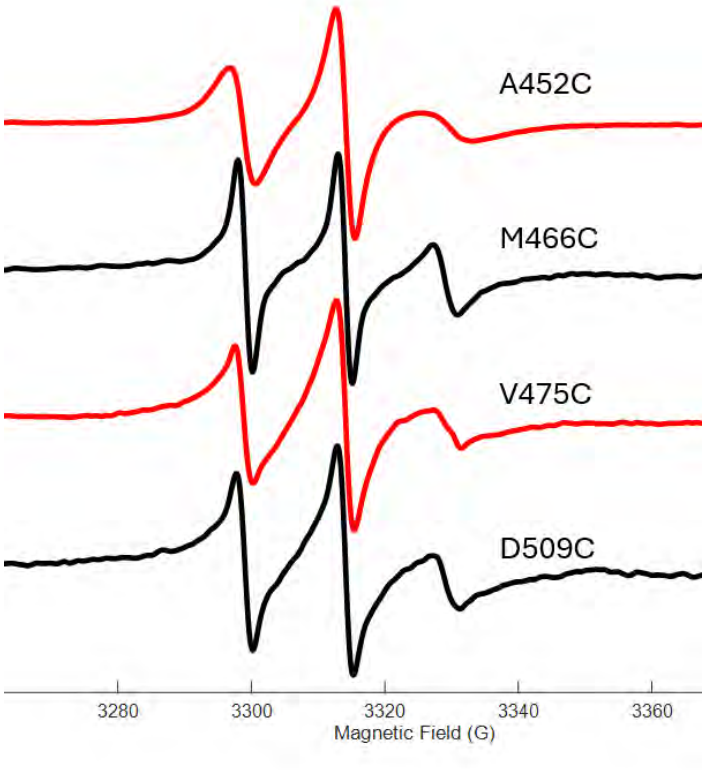

***Figure 5.3**: CW-EPR spectra of TRPV1 cysteine variants in 3:1 POPC:POPG vesicles. All cysteine variants were labeled with 10:1 MTSL:protein molar ratio at approximately 100 μ M. The sharper hyperfine splitting represents the extracellular cysteine variants as shown in black (M466C and D509C) whereas the rigid or transmembrane cysteine variants are in red (A452C and V475C).*

The observed sharper linewidths can be directly correlated with enhanced flexibility in the region surrounding these labels. This interpretation is consistent with prior structural data, which indicates

that the M466C and D509C sites are located in the extracellular domain of the protein.[22] Such localization suggests that the spin labels are less hindered by nearby structural constraints, allowing for greater freedom of movement and alignment with the surrounding molecular environment. In contrast, the spectra of amino acids in the S1/S2/S3/S4, such as A452C or V475C, are expected to be located in the transmembrane region and have broader linewidths and larger rotational correlation times and this was observed in **Figure 5.3.** These linewidths are like those of other buried transmembrane regions of other membrane proteins when in 3:1 POPC: POPG vesicles.

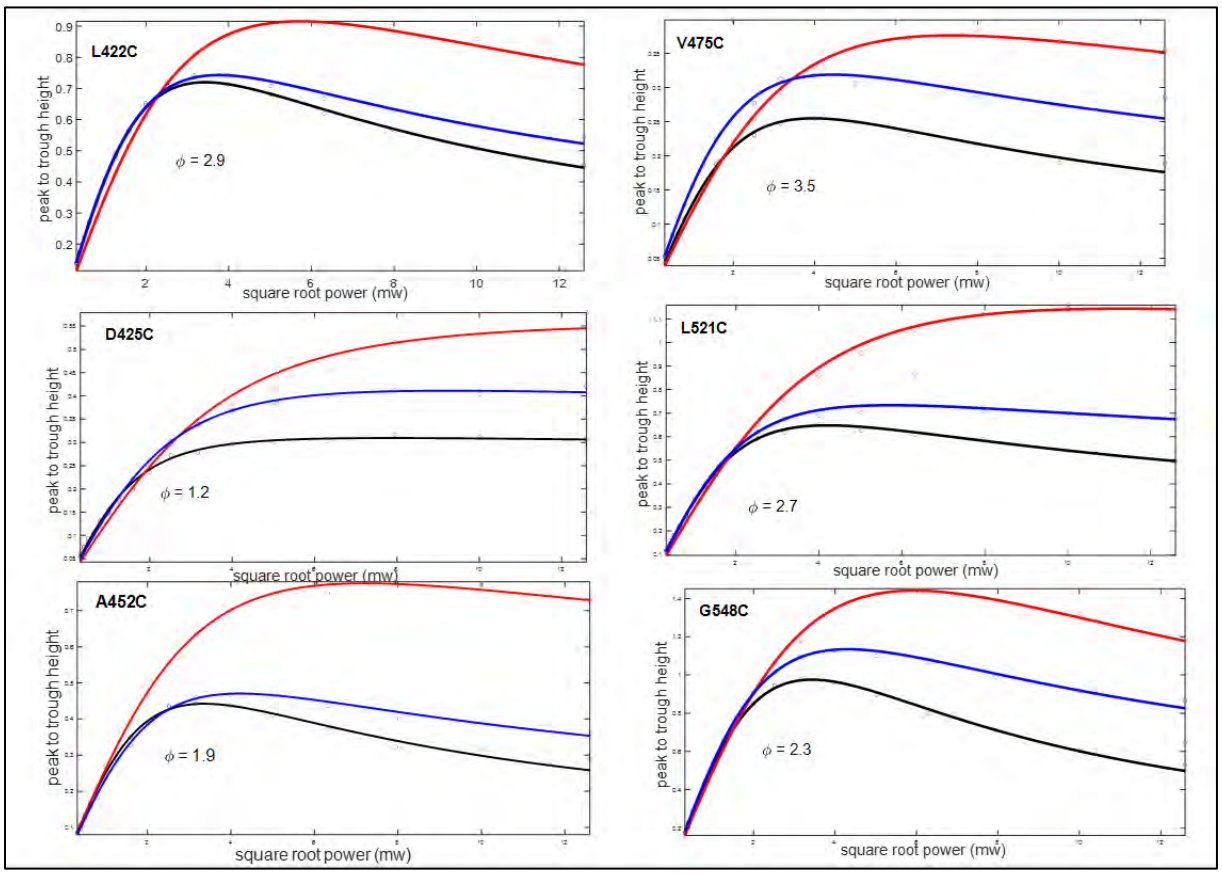

***Figure 5.4**: CW-EPR Power Saturation PS curves for different spin-labelled sites of TRPV1 VSLD.*

When studying the structural dynamics of membrane proteins, EPR spectroscopy reveals how different regions of a protein move in relation to each other and how these movements are

influenced by external factors such as ligand binding, changes in the lipid environment, or alterations in pH. CW-EPR power saturation experiments measure the interactions between spin labels and paramagnetic reagents to determine depth parameters, providing a reliable method to gain insights into the intricate dynamics of these interactions, leading to more precise measurements.[20] A positive value for the depth parameter suggests that the residues are embedded within the membrane, whereas a negative value indicates that the residues are accessible to the solvent. For membrane proteins, a transition from negative values in the extracellular region to positive values in the transmembrane region, followed by a return to negative values in the intracellular region, is expected. The Φ for L422C was 3.0, D425C was 2.0, A452C was 1.9, V458C was 0.5, L521C was 3.3, and G548C was 1.2 as shown in **Figure 5.4 and Figure 5.5.**

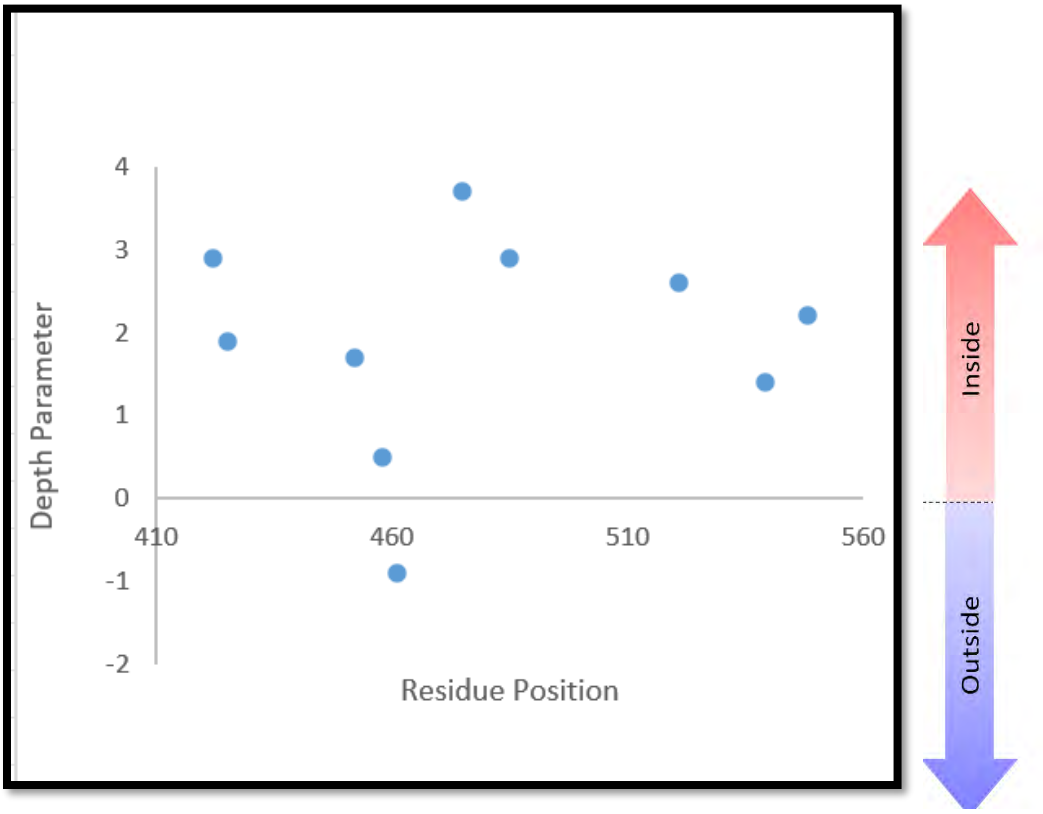

Figure 5.5 *Calculated depth parameter (φ) for different positions of TRPV1-VSLD as a function of residue positions in POPC/POPG proteoliposomes. Positive (φ) values indicate that the R1 side chains are embedded inside the lipid bilayer and negative (φ) values indicate that the R1 side chains are solvent-exposed.*

Our data reveal that out of 10 residues investigated using power saturation EPR in this study, the highest Φ value was 3.5 from residue V475C in the S2 region indicating that this region is

exposed to the hydrophobic core and may be deeply buried in the center of the lipid bilayer. The residues with less positive Φ values, such as V458C reported as 0.5 might be closer to the surface of the membrane. We expect that more CW-EPR spectra will reveal differential mobility and solvent accessibility across the VSLD, consistent with the helical architecture and membrane embedding of the S1–S4 segments. Power saturation parameters allow the distinguishing of intra- and extracellularly facing residues and estimation of their depth within the membrane. These data will help with the refinement of the topological map of the VSLD and may identify previously unresolved extracellular loops or lipid-accessible sites that could play crucial roles in channel function.

5.4 Conclusions

In this study, CW-EPR spectra from several strategically placed spin labels within the TRPV1 voltage-sensor-like domain (VSLD) was successfully collected. The resulting data shows clear differences in spectral features from site to site, which align well with the anticipated differences in their local structural environments. Additional CW-EPR power saturation experiments will provide further insight that will reveal patterns of accessibility between the extracellular regions and the transmembrane domains. It is expected that these observations will support the hypothesis that TRPV1-VSLD undergoes site-specific conformational changes with extracellular portions displaying greater flexibility or solvent exposure compared to the more rigid transmembrane segments. Overall, these findings offer valuable preliminary evidence for dynamic behavior within the TRPV1-VSLD and lay the groundwork for future studies aimed at understanding its structural role in TRPV1 function. While site-directed mutagenesis challenges remain, ongoing methodological advancements promise to provide increasingly detailed insights into TRPV1 function and gating mechanisms. These insights are invaluable for understanding the mechanisms of protein function and can guide the design of therapeutic agents targeting these proteins. SDSL and EPR spectroscopy have emerged as powerful techniques for studying the structural dynamics and topology of membrane proteins, including the voltage-sensing domain (VSD) of TRPV1 channels. This study examines how these methods have been applied to investigate TRPV1 VSD structure and function.

References

(1) Kim, S.; Ga, S.; Bae, H.; Sluyter, R.; Konstantinov, K.; Shrestha, L. K.; Kim, Y. H.; Kim, J. H.; Ariga, K. Multidisciplinary Approaches for Enzyme Biocatalysis in Pharmaceuticals: Protein Engineering, Computational Biology, and Nanoarchitectonics. EES Catalysis 2024, 2 (1), 14–48. https://doi.org/10.1039/D3EY00239J.

(2) Levental, I.; Lyman, E. Regulation of Membrane Protein Structure and Function by Their Lipid Nano-Environment. Nature Reviews Molecular Cell Biology. 2023. https://doi.org/10.1038/s41580-022-00524-4.

(3) Corradi, V.; Sejdiu, B. I.; Mesa-Galloso, H.; Abdizadeh, H.; Noskov, S. Yu.; Marrink, S. J.; Tieleman, D. P. Emerging Diversity in Lipid–Protein Interactions. Chem Rev 2019, 119 (9), 5775–5848. https://doi.org/10.1021/acs.chemrev.8b00451.

(4) Gong, J.; Chen, Y.; Pu, F.; Sun, P.; He, F.; Zhang, L.; Li, Y.; Ma, Z.; Wang, H. Understanding Membrane Protein Drug Targets in Computational Perspective. Curr Drug Targets 2019, 20 (5), 551–564. https://doi.org/10.2174/1389450120666181204164721.

(5) Nilius, B.; Owsianik, G. The Transient Receptor Potential Family of Ion Channels. Genome Biol 2011, 12 (3), 218. https://doi.org/10.1186/gb-2011-12-3-218.

(6) Zhang, Q.; Cherezov, V. Chemical Tools for Membrane Protein Structural Biology. Curr Opin Struct Biol 2019, 58, 278–285. https://doi.org/10.1016/j.sbi.2019.06.002.

(7) Trevisani, M.; Szallasi, A. Targeting TRPV1: Challenges and Issues in Pain Management. Open Drug Discov J 2010, 2 (1), 37–49. https://doi.org/10.2174/1877381801002010037.

(8) Pedersen, S. F.; Owsianik, G.; Nilius, B. TRP Channels: An Overview. Cell Calcium 2005, 38 (3–4), 233–252. https://doi.org/10.1016/j.ceca.2005.06.028.

(9) Moran, M. M.; McAlexander, M. A.; Bíró, T.; Szallasi, A. Transient Receptor Potential Channels as Therapeutic Targets. Nat Rev Drug Discov 2011, 10 (8), 601–620. https://doi.org/10.1038/nrd3456.

(10) Kaneko, Y.; Szallasi, A. Transient Receptor Potential (<scp>TRP</Scp>) Channels: A Clinical Perspective. Br J Pharmacol 2014, 171 (10), 2474–2507. https://doi.org/10.1111/bph.12414.

(11) Logan, D. W. Hot to Touch: The Story of the 2021 Nobel Prize in Physiology or Medicine. Dis Model Mech 2021, 14 (10). https://doi.org/10.1242/dmm.049352.

(12) Sterner, E. Analyses of the 2021 Nobel Prize in Physiology or Medicine: Receptors for Temperature and Touch. Sci Technol Libr (New York, NY) 2022, 41 (1), 24–41. https://doi.org/10.1080/0194262X.2022.2028700.

(13) Caterina, M. J. Transient Receptor Potential Ion Channels as Participants in Thermosensation and Thermoregulation. American Journal of Physiology-Regulatory, Integrative and Comparative Physiology 2007, 292 (1), R64–R76. https://doi.org/10.1152/ajpregu.00446.2006.

(14) Dhaka, A.; Viswanath, V.; Patapoutian, A. TRP Ion Channels and Temperature Sensation. Annu Rev Neurosci 2006, 29 (1), 135–161. https://doi.org/10.1146/annurev.neuro.29.051605.112958.

(15) Carnevale, V.; Rohacs, T. TRPV1: A Target for Rational Drug Design. Pharmaceuticals 2016, 9 (3), 52. https://doi.org/10.3390/ph9030052.

(16) Zhang, M.; Ma, Y.; Ye, X.; Zhang, N.; Pan, L.; Wang, B. TRP (Transient Receptor Potential) Ion Channel Family: Structures, Biological Functions and Therapeutic Interventions for Diseases. Signal Transduct Target Ther 2023, 8 (1), 261. https://doi.org/10.1038/s41392-023-01464-x.

(17) Klare, J. P. Site-Directed Spin Labeling EPR Spectroscopy in Protein Research. bchm 2013, 394 (10), 1281–1300. https://doi.org/10.1515/hsz-2013-0155.

(18) Li, H.; Pan, Y.; Yang, Z.; Rao, J.; Chen, B. Emerging Applications of Site-Directed Spin Labeling Electron Paramagnetic Resonance (SDSL-EPR) to Study Food Protein Structure, Dynamics, and Interaction. Trends Food Sci Technol 2021, 109, 37–50. https://doi.org/10.1016/j.tifs.2021.01.022.

(19) Bates, A.; Miller, I.; Travis, E. M.; Sahu, I. D.; Morris, A.; McCarrick, R. M.; Dabney-Smith, C.; Lorigan, G. A. The Expression, Purification, Spectroscopic Characterization, and Membrane Topology Classification of KCNE4 from Recombinant E. Coli. J Phys Chem B 2025, 129 (1), 228–237. https://doi.org/10.1021/acs.jpcb.4c06665.

(20) Altenbach, C.; Greenhalgh, D. A.; Khorana, H. G.; Hubbell, W. L. A Collision Gradient Method to Determine the Immersion Depth of Nitroxides in Lipid Bilayers: Application to Spin-Labeled Mutants of Bacteriorhodopsin. Proc Natl Acad Sci U S A 1994, 91 (5), 1667–1671. https://doi.org/10.1073/pnas.91.5.1667.

(21) Klug, C. S.; Su, W.; Feix, J. B. Mapping of the Residues Involved in a Proposed β-Strand Located in the Ferric Enterobactin Receptor FepA Using Site-Directed Spin-Labeling. Biochemistry 1997, 36 (42), 13027–13033. https://doi.org/10.1021/bi971232m.

(22) Liao, M.; Cao, E.; Julius, D.; Cheng, Y. Structure of the TRPV1 Ion Channel Determined by Electron Cryo-Microscopy. Nature 2013, 504 (7478), 107–112. https://doi.org/10.1038/nature12822.

Chapter 6

Conclusion and Future Directions

The work in this dissertation made use of biophysical techniques to further the understanding of protein-protein interactions as well as the development and application of novel membrane mimetic systems. These contributions help address fundamental questions about how proteins behave and interact in membrane environments, which are often inaccessible to traditional structural methods. [1,2] A key theme throughout this work is the evolution of membrane mimetic systems. While traditional detergent-based methods enabled early progress in membrane protein purification and stabilization, this study embraced more advanced and physiologically relevant systems including lipid vesicles and polymer-based platforms such as Styrene Maleic Acid copolymers and their derivatives.[3,4] These next-generation mimetics more accurately replicate the complexity of native lipid bilayers and are critical for preserving the structural and functional integrity of membrane proteins during biophysical analysis.[5]

In Chapter 2, the study employed Electron Spin Echo Envelope Modulation (ESEEM) spectroscopy to probe the local secondary structure of gp28, a phage-derived lytic membrane protein essential for bacteriophage release in systems lacking spanins. Synthesized gp28 constructs were first characterized using circular dichroism (CD) spectroscopy to validate their global secondary structure.[6,7] ESEEM measurements were then focused on predicted alpha-helical regions within the protein. The resulting modulation patterns and their Fourier-transformed spectra were consistent with hallmark features of alpha helices, including characteristic periodicities. Analysis of normalized frequency intensities in membrane vesicle systems further supported these findings, revealing turn-specific modulation patterns indicative of helical structure.[8] This work confirmed the presence of alpha helices at all three predicted regions within gp28, in agreement with earlier computational models and experimental evidence reported by the Ry Young group.[9] These findings not only reinforce the structural predictions for gp28 but also demonstrate the effectiveness of ESEEM spectroscopy as a powerful method for resolving local secondary structures in membrane proteins.[10,11]

In Chapter 3, the application of three distinct SMA derivatives; SMA-Glu, SMA-Neut, and SMA-Pos were evaluated for their ability to solubilize and stabilize membrane-associated peptides, specifically gp28 and pinholin, without the use of traditional detergents.[12] These polymer-based membrane mimetics

offer a significant advantage in preserving the native-like lipid environment, which is often compromised by detergent-based solubilization methods.[13] Each SMA derivative was successfully reconstituted with peptide vesicles to form SMA-derived lipid particles (SMADLPs) of varying sizes. CW-EPR spectroscopic studies revealed that SMA-Pos was incompatible with spin-labeled pinholin mutants, potentially due to charge-based interactions or structural disruption, whereas SMA-Glu and SMA-Neut supported stable incorporation. In contrast, for the gp28 system, CW-EPR spectra showed no significant perturbation across all SMADs evaluated, confirming the successful incorporation of gp28 into nanodiscs and suggesting that the SMADLP environment supports its native conformation.

Chapter 4 presents the development of Vinyl Ether Maleic Acid (VEMA) copolymers as a versatile and tunable platform for membrane protein studies. Through controlled RAFT polymerization of vinyl ether and maleic anhydride monomers, polymers with defined molecular weights and adjustable hydrophilic-lipophilic balance were synthesized. Upon hydrolysis, these polymers formed VEMALPs nanodiscs capable of the reconstitution of membrane proteins and peptides like gp28 in place of lipids.[14] EPR spectroscopy confirmed that VEMALPs preserve a native-like lipid environment, making them effective tools for structural and functional analysis. Unlike traditional SMALPs, VEMA systems offer enhanced compatibility and greater control over polymer properties.[15] In future **studies,** the focus will be on applying VEMALPs to a broader range of membrane proteins, integrating them with high-resolution structural techniques, and optimizing polymer design for targeted biophysical or therapeutic applications. This system offers a powerful alternative for membrane protein reconstitution and analysis, advancing the field of detergent-free structural biology.

Chapter 5 explores the successful use of continuous-wave EPR spectroscopy to investigate the structural dynamics of the TRPV1 voltage-sensor-like domain (VSLD) through site-directed spin labeling. The spectral diversity observed across labeled sites indicates unique local environments and reinforces the hypothesis of conformational variability within the domain.[16,17] Notably, extracellular regions exhibited features indicative of higher mobility or solvent accessibility compared to the more constrained transmembrane helices, suggesting functional flexibility across the VSLD. These preliminary findings lay important groundwork for further exploring the dynamic behavior of TRPV1 and its potential role in gating.[18]

This dissertation highlights the power of combining site-directed spin labeling with EPR spectroscopy to explore the structural topology and conformational dynamics of membrane proteins, specifically gp28

and the TRPV1 voltage-sensor-like domain (VSLD). Through strategic labeling and the application of techniques such as CW-EPR, power saturation, and ESEEM, distinct and site-specific structural features were revealed. These findings have provided valuable insights into the conformational flexibility, local environment, and membrane-associated behavior of these proteins advancing our understanding of their potential roles in gating and membrane interactions. These findings also demonstrate that SMA derivatives and VEMA polymer-based mimetic systems can be tailored to support membrane protein stability and conformational integrity, opening new possibilities for detergent-free biophysical studies.

Continued refinement of these experimental approaches, paired with complementary techniques such as molecular dynamics simulations and Double Electron-Electron Resonance (DEER), will enable a more in-depth understanding of membrane protein dynamics, including conformational changes in response to ligands, temperature, and membrane composition.[19,20] This integrated approach is especially promising for identifying pharmacologically relevant conformations and lipid-protein interactions central to function. This work underscores the value of multidisciplinary strategies in membrane protein research and paves the way for new developments in structural biology, drug discovery, and the broader life sciences.[18] Several avenues will enhance our mechanistic understanding of the TRPV1-VSLD. Temperature-dependent EPR measurements will be used to assess the thermal stability of individual segments, helping to determine how environmental conditions influence structural integrity. Incorporating molecular dynamics (MD) simulations alongside EPR spectroscopic data will provide atomic-level insight into the interaction between the S1–S4 helices and the surrounding lipid bilayer which are critical for understanding how membrane curvature and lipid composition affect VSLD conformation.[19-21] Furthermore, DEER spectroscopy between strategically selected residue pairs will reveal intradomain distance changes and conformational flexibility under resting and activated conditions, such as exposure to capsaicin, altered pH, or elevated temperatures. Shifts in DEER distance distributions will serve as direct evidence for ligand or stimulus-induced structural rearrangements. All these approaches will enable the development of refined models of the TRPV1-VSLD in different functional states and provide experimentally anchored insights into TRPV1 gating mechanisms. This knowledge can be expanded to aid in identifying pharmacologically targetable conformations of the channel.[22] More broadly, these studies contribute to our understanding of voltage-sensing and membrane protein regulation, offering potential pathways toward novel treatments for disorders associated with TRP channel dysfunction.[22,23]

References

(1) Palomar-Alonso, N.; Lee, M.; Kim, M. Exosomes: Membrane-Associated Proteins, Challenges and Perspectives. *Biochemistry and Biophysics Reports*. 2024. https://doi.org/10.1016/j.bbrep.2023.101599.

(2) Escribá, P. V.; González-Ros, J. M.; Goñi, F. M.; Kinnunen, P. K. J.; Vigh, L.; Sánchez-Magraner, L.; Fernández, A. M.; Busquets, X.; Horváth, I.; Barceló-Coblijn, G. Membranes: A Meeting Point for Lipids, Proteins and Therapies. *J Cell Mol Med* 2008, *12* (3), 829–875. https://doi.org/10.1111/j.1582-4934.2008.00281.x.

(3) Kopf, A. H.; Koorengevel, M. C.; van Walree, C. A.; Dafforn, T. R.; Killian, J. A. A Simple and Convenient Method for the Hydrolysis of Styrene-Maleic Anhydride Copolymers to Styrene-Maleic Acid Copolymers. *Chem Phys Lipids* 2019, *218*. https://doi.org/10.1016/j.chemphyslip.2018.11.011.

(4) Schmidt, V.; Sturgis, J. N. Modifying Styrene-Maleic Acid Co-Polymer for Studying Lipid Nanodiscs. *Biochim Biophys Acta Biomembr* 2018, *1860* (3). https://doi.org/10.1016/j.bbamem.2017.12.012.

(5) Swainsbury, D. J. K.; Scheidelaar, S.; Foster, N.; van Grondelle, R.; Killian, J. A.; Jones, M. R. The Effectiveness of Styrene-Maleic Acid (SMA) Copolymers for Solubilisation of Integral Membrane Proteins from SMA-Accessible and SMA-Resistant Membranes. *Biochim Biophys Acta Biomembr* 2017, *1859* (10). https://doi.org/10.1016/j.bbamem.2017.07.011.

(6) Khan R. H.; Probing the Structural Topology, Dynamics, Conformation, And Secondary Structure of Pinholin S21 And gp28 Bacteriophage Lytic Proteins using Electron Paramagnetic Resonance Spectroscopy.

(7) Khan, R. H.; Rotich, N. C.; Morris, A.; Ahammad, T.; Baral, B.; Sahu, I. D.; Lorigan, G. A. Probing the Structural Topology and Dynamic Properties of Gp28 Using Continuous Wave Electron Paramagnetic Resonance Spectroscopy. *J Phys Chem B* 2023, *127* (43), 9236–9247. https://doi.org/10.1021/acs.jpcb.3c03679.

(8) Rotich, N. C.; Khan, R. H.; Morris, A.; McCarrick, R.; Baral, B.; Okorafor, E. A.; Faul, E.; Wardrip, L.; Sahu, I. D.; Lorigan, G. A. Probing the Secondary Structure of Membrane-Bound Gp28 Using Electron Spin Echo Envelope Modulation (ESEEM) Spectroscopy. *J Phys Chem B* 2025, *129* (10), 2659–2667. https://doi.org/10.1021/acs.jpcb.4c08270.

(9) Holt, A.; Cahill, J.; Ramsey, J.; Martin, C.; O'Leary, C.; Moreland, R.; Maddox, L. T.; Galbadage, T.; Sharan, R.; Sule, P.; Cirillo, J. D.; Young, R. Phage-Encoded Cationic Antimicrobial Peptide Required for Lysis. *J Bacteriol* 2022, *204* (1). https://doi.org/10.1128/JB.00214-21.

(10) Dzuba, S. A.; Marsh, D. Chapter 5. ESEEM of Spin Labels to Study Intermolecular Interactions, Molecular Assembly and Conformation; 2014; pp 102–121. https://doi.org/10.1039/9781782620280-00102.

(11) Åhrling, K. A.; Evans, M. C. W.; Nugent, J. H. A.; Ball, R. J.; Pace, R. J. ESEEM Studies of Substrate Water and Small Alcohol Binding to the Oxygen-Evolving Complex of Photosystem II during Functional Turnover. *Biochemistry* 2006, *45* (23), 7069–7082. https://doi.org/10.1021/bi052146m.

(12) Burridge, K. M.; Harding, B. D.; Sahu, I. D.; Kearns, M. M.; Stowe, R. B.; Dolan, M. T.; Edelmann, R. E.; Dabney-Smith, C.; Page, R. C.; Konkolewicz, D.; Lorigan, G. A. Simple Derivatization of RAFT-Synthesized Styrene-Maleic Anhydride Copolymers for Lipid Disk Formulations. *Biomacromolecules* 2020, *21* (3). https://doi.org/10.1021/acs.biomac.0c00041.

(13) Scheidelaar, S.; Koorengevel, M. C.; van Walree, C. A.; Dominguez, J. J.; Dörr, J. M.; Killian, J. A. Effect of Polymer Composition and PH on Membrane Solubilization by Styrene-Maleic Acid Copolymers. *Biophys J* 2016, *111* (9). https://doi.org/10.1016/j.bpj.2016.09.025.

(14) Craig, A. F.; Clark, E. E.; Sahu, I. D.; Zhang, R.; Frantz, N. D.; Al-Abdul-Wahid, M. S.; Dabney-Smith, C.; Konkolewicz, D.; Lorigan, G. A. Tuning the Size of Styrene-Maleic Acid Copolymer-Lipid Nanoparticles (SMALPs) Using RAFT Polymerization for Biophysical Studies. *Biochim Biophys Acta Biomembr* 2016, *1858* (11). https://doi.org/10.1016/j.bbamem.2016.08.004.

(15) Shah, M. Z.; Rotich, N. C.; Okorafor, E. A.; Oestreicher, Z.; Demidovich, G.; Eapen, J.; Henoch, Q.; Kilbey, J.; Prempeh, G.; Bates, A.; Page, R. C.; Lorigan, G. A.; Konkolewicz, D. Vinyl Ether Maleic Acid Polymers: Tunable Polymers for Self-Assembled Lipid Nanodiscs and Environments for Membrane Proteins. *Biomacromolecules* 2024, *25* (10), 6611–6623. https://doi.org/10.1021/acs.biomac.4c00772.

(16) Torricella, F.; Pierro, A.; Mileo, E.; Belle, V.; Bonucci, A. Nitroxide Spin Labels and EPR Spectroscopy: A Powerful Association for Protein Dynamics Studies. *Biochimica et Biophysica Acta*

(BBA) - Proteins and Proteomics 2021, *1869* (7), 140653. https://doi.org/10.1016/j.bbapap.2021.140653.

(17) Malmberg, N. J.; Falke, J. J. Use of EPR Power Saturation to Analyze the Membrane-Docking Geometries of Peripheral Proteins: Applications to C2 Domains. *Annu Rev Biophys Biomol Struct* 2005, *34* (1), 71–90. https://doi.org/10.1146/annurev.biophys.34.040204.144534.

(18) Shuba, Y. M. Beyond Neuronal Heat Sensing: Diversity of TRPV1 Heat-Capsaicin Receptor-Channel Functions. *Front Cell Neurosci* 2021, *14*. https://doi.org/10.3389/fncel.2020.612480.

(19) LINDAHL, E.; SANSOM, M. Membrane Proteins: Molecular Dynamics Simulations. *Curr Opin Struct Biol* 2008, *18* (4), 425–431. https://doi.org/10.1016/j.sbi.2008.02.003.

(20) Zhou, A.; Abu-Baker, S.; Sahu, I. D.; Liu, L.; McCarrick, R. M.; Dabney-Smith, C.; Lorigan, G. A. Determining α-Helical and β-Sheet Secondary Structures via Pulsed Electron Spin Resonance Spectroscopy. *Biochemistry* 2012, *51* (38). https://doi.org/10.1021/bi3010736.

(21) Marsh, D. Lateral Pressure Profile, Spontaneous Curvature Frustration, and the Incorporation and Conformation of Proteins in Membranes. *Biophys J* 2007, *93* (11). https://doi.org/10.1529/biophysj.107.107938.

(22) Straub, R. H. TRPV1, TRPA1, and TRPM8 Channels in Inflammation, Energy Redirection, and Water Retention: Role in Chronic Inflammatory Diseases with an Evolutionary Perspective. *J Mol Med* 2014, *92* (9), 925–937. https://doi.org/10.1007/s00109-014-1175-9.

(23) Iftinca, M.; Defaye, M.; Altier, C. TRPV1-Targeted Drugs in Development for Human Pain Conditions. *Drugs* 2021, *81* (1), 7–27. https://doi.org/10.1007/s40265-020-01429-2.